https://doi.org/10.15388/vu.thesis.599
https://orcid.org/0000-0001-6088-9495

VILNIUS UNIVERSITY

Evelina Kazlauskė

Cellular Uptake and Accumulation Studies of Functionalized Upconverting Nanoparticles

DOCTORAL DISSERTATION

Natural Sciences,
Biophysics (N 011)

VILNIUS 2024

This dissertation was written between 2019 and 2023 at Vilnius University Life Sciences Center Institute of Bioscences.
Experiments were conducted at the National Cancer Institute, Biomedical Physics Laboratory.
Scholarships from Research Council of Lithuania were granted for academic achievemements and for doctoral student trips in 2023.
Scientific fund of National Cancer Institute supported the research.

Academic supervisor:
Prof. Habil. Dr. Ričardas Rotomskis (Vilnius University, Natural Sciences, Biophysics – N 011).
Academic consultant:
Dr. Vitalijus Karabanovas (National Cancer Institute, Natural Sciences, Biophysics – N 011).

This doctoral dissertation will be defended in a public meeting of the Dissertation Defence Panel:
Chairman – **Prof. Dr. Osvaldas Rukšėnas** (Vilnius University, Natural Sciences, Biophysics – N 011).
Members:
Prof. Dr. Aidas Alaburda (Vilnius University, Natural Sciences, Biophysics – N 011),
Dr. Agata Mlynska (National Cancer Institute, Natural Sciences, Biology – N 010),
Dr. Lina Mikoliūnaitė (Vilnius University, Natural Sciences, Chemistry – N 003),
Dr. Vladimir Sivakov (Leibniz Institute of Photonic Technology, Natural Sciences, Biophysics – N 011).

The dissertation shall be defended at a public meeting of the Dissertation Defence Panel at 10 h on 14 th of May 2024 in the meeting room R-401 of Vilnius University Life Sciences Center.
Address: Saulėtekio al. 7, LT-10527, Vilnius, Lithuania.
Tel. +37052234420; e-mail: info@gmc.vu.lt

The text of this dissertation can be accessed at the libraries of Vilnius University as well as on the website of Vilnius University:
www.vu.lt/lt/naujienos/ivykiu-kalendorius

https://doi.org/10.15388/vu.thesis.599
https://orcid.org/0000-0001-2345-6789

VILNIAUS UNIVERSITETAS

Evelina Kazlauskė

Funkcionalizuotų apkonvertuojančių nanodalelių kaupimosi ir pasiskirstymo ląstelėse tyrimai

DAKTARO DISERTACIJA

Gamtos mokslai,
Biofizika (N 011)

VILNIUS 2024

Disertacija rengta 2019–2023 metais Vilniaus universiteto Gyvybės mokslų centro Biomokslų institute.
Eksperimentiniai darbai atlikti Nacionalinio vėžio instituto Biomedicininės fizikos laboratorijoje.
Iš Lietuvos mokslo tarybos 2023 metais gautos stipendijos už doktorantūros studijų rezultatus ir doktorantų akademinėms išvykoms.
Tyrimus rėmė ir Nacionalinio vėžio instituto Mokslo fondas.

Mokslinis vadovas:
prof. habil. dr. Ričardas Rotomskis (Vilniaus universitetas, gamtos mokslai, biofizika – N 011).
Mokslinis konsultantas:
dr. Vitalijus Karabanovas (Nacionalinis vėžio insitutas, gamtos mokslai, biofizika – N 011).

Gynimo taryba:
Pirmininkas – **prof. dr. Osvaldas Rukšėnas** (Vilniaus universitetas, gamtos mokslai, biofizika – N 011).
Nariai:
prof. dr. Aidas Alaburda (Vilniaus universietetas, gamtos mokslai, biofizika – N 011),
dr. Agata Mlynska (Nacionalinis vėžio institutas, gamtos mokslai, biologija – N 010),
dr. Lina Mikoliūnaitė (Vilniaus universitetas, gamtos mokslai, chemija – N 003),
dr. Vladimir Sivakov (Leibnico fotoninių technologijų institutas, gamtos mokslai, biofizika – N 011).

Disertacija ginama viešame Gynimo tarybos posėdyje 2024 m. gegužės mėn. 14 d. 10 val. Vilniaus universiteto Gyvybės mokslų centro R-401 auditorijoje ir/arba nuotoliniu būdu.
Adresas: Saulėtekio al. 7, LT-10257, Vilnius, Lietuva.
Tel. +37052234420; el. paštas: info@gmc.vu.lt

Disertaciją galima peržiūrėti Vilniaus universiteto bibliotekoje ir VU interneto svetainėje adresu:
https://www.vu.lt/naujienos/ivykiu-kalendorius

Have no fear of perfection:

you‘ll never reach it.

MARIE CURIE

CONTENTS

ABBREVIATIONS

A2M – α-2-macroglobulin;
AP-2 – Adaptor protein-2;
ApoAX – Apolipoprotein A, X stands for ApoA number as 1 or 4;
BBB – Blood-brain barrier;
CAP1 – Cyclase-associated protein 1;
Chlor – Chlorpromazine;
CM – Cellular membrane;
CME – Clathrin-mediated endocytosis;
CR – Cross-relaxation;
CVME – Caveolin-mediated endocytosis;
DI – Deionized water;
DLS – Dynamic light scattering;
DMEM – Dulbecco's modified eagle medium;
DSPE-PEG-FA – 1,2-distearoyl-sn-glycero-3-phosphoethanolamine-N-[folate (polyethylene glycol)-2000];
DSPE-PEG-N3 – 1,2-distearoyl-sn-glycero-3-phosphoethanolamine-N-[azido (polyethylene glycol)-2000];
EGF – Epidermal growth factor;
EIPA – 5-(N-ethyl-N-isopropyl)amiloride;
ER – Estrogen receptor;
ESA – Excited state absorption;
ETU – Energy transfer upconversion;
F5 – Coagulation factor V;
FBS – Fetal bovine serum;
HER2 – Human epidermal growth factor 2 receptor;
Ho-1 – Heme oxygenase-1;
LDH – Lactate dehydrogenase;
LRP – Low-density lipoprotein receptor-related protein;
LSCM – Laser scanning confocal microscopy;
MP – Macropinocytosis;
MPS – Mononuclear phagocyte system;
NIR – Near-infrared;
NM – Nanomedicine;
Nys – Nystatin;
Noc – Nocodazole;
NPs – Nanoparticles;
PBS – Phosphate buffered saline;
PC – Protein corona;

PCC – Pearson's correlation coefficient;
PdI – Polydispersity index;
PEG – Polyethylene glycol;
PhNPs – Photoluminescent NPs;
PR – Progesterone receptor;
PS – Photosensitizer;
PVP – Polyvinylpyrrolidone;
QDs – Quantum dots;
RBCs – Red blood cells;
RE – Rare-earth;
ROS – Reactive oxygen species;
SA-PEG-Ner-UCNPs – Streptavidin-polyethylene glycol and neridronate-coated UCNPs;
Tf – Transferrin;
THBS1 – Thrombospondin-I;
TNBC – Triple-negative breast cancer;
UC(L) – Upconversion (luminescence);
UCNPs – Upconverting nanoparticles;
ULISA – Upconversion-linked immunosorbent assay;
UV – Ultraviolet;
VIS – Visible;
XTT – 3′-[1- (phenylaminocarbonyl)- 3,4- tetrazolium]-bis (4-methoxy6-nitro) benzene sulfonic acid hydrate.

1. INTRODUCTION

The effective utilization of nanoparticles (NPs) for biomedical purposes depends on both the efficient uptake by cells and the suitability of NPs themselves as theranostic[1] agents. Efficient cellular uptake refers to the ability of a drug or therapeutic agent to enter cells effectively. This process is pivotal in drug delivery and targeting because it determines how readily a drug can reach its intended site of action within the body. Drug targeting refers to the precise release of drugs at a particular physiological location, organ, tissue, or cell where a specific pharmacological effect is needed. Nanocarriers play a key role in achieving cell targeting. Here, drugs are transported to the target organ/cell based on the extended circulation of the pharmaceutical carrier in the bloodstream, leading to the accumulation of the drug-loaded nano delivery system at the desired site. Efficient drug delivery via this method usually depends on the outer layer of the drug/nanocarrier. Outer layer or coating of NPs plays a vital role in nanocarriers' intracellular localization. However, there is still scarcity in knowledge about what happens to NPs when they are introduced in the cell: where and how NPs are localized within the cell (Gnach et al., 2015). Usually, various types of biomolecules, mainly proteins in blood adsorb on NPs' surface forming additional layer of plasma proteins called "protein corona" (PC) (Docter et al., 2015). PC influences NPs' biodistribution, targeting, cellular accumulation and localization; however, sometimes PC can prevent from cellular uptake (Francia et al., 2019; W. Zhang et al., 2019). Also, it is known that PC mainly depends on NPs' size, shape, and surface composition (Docter et al., 2015; Fleischer & Payne, 2014; Francia et al., 2019). For successful therapy, surface compostion of the nanocarrier is only one aspect to look for. Another very important aspect is NPs themselves. Successful therapeutic nanocarrier should be biocompatible and favorably possess dual modality, that facilitates early detection and targeted treatment. The growing demand for multifunctionality in biomedical applications has driven the development of photoluminescent NPs (PhNPs), which can integrate imaging capabilities with targeted and customizable therapeutics. PhNPs usually are biocompatible, quickly taken up by cells, and proficient at delivering drugs to the intended site. However, many PhNPs exhibit limited functionality because their excitation and emission wavelengths are restricted to a narrow ultraviolet/visible (UV/VIS) spectral range (Damalakiene et al., 2013; Dreaden et al., 2012). Moreover, UV has low penetration depth into tissue, i.e., ~ 400 nm wavelength penetrates only

[1] Combination of therapy and diagnostics.

around 60 μm. Thus, for *in vivo* imaging it is essential to develop NPs that can be stimulated without the need for UV/VIS radiation. In the context of imaging, it's necessary for NPs to emit within the tissue optical transparency window (~650-1100 nm) (**Figure 1**), particularly in the near-infrared (NIR) spectral region. The optical window refers to a specific range of wavelengths in the electromagnetic spectrum where biological tissues exhibit minimal absorption and scattering of light, allowing for deeper penetration and clearer visualization of internal structures and processes. The utilization of NIR light for excitation offers several advantages, including enhanced penetration depth, reduced phototoxicity, minimal autofluorescence background, and decreased light scattering. One example of such innovative nanomaterials is the upconverting nanoparticles (UCNPs) containing rare-earth (RE) ions, whose absorption lies in the NIR radiation region are promising for deep lesion treatment (Jalani et al., 2018; Kobayashi et al., 2010; Yao et al., 2020).

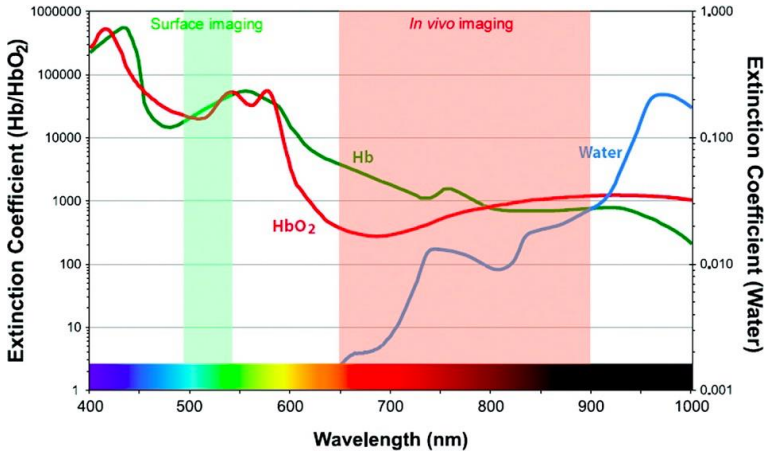

Figure 1. *A plot displaying the absorbance of water, oxyhemoglobin, and deoxyhemoglobin across a range of wavelengths from visible to near-infrared* (Kobayashi et al., 2010).

UCNPs are an example of NPs that convert two or more lower-energy photons (or NIR radiation) into one high energy photon (or higher-energy radiation) in a relatively wide spectral range spanning from UV to NIR. This UCNPs' energy "metamorphosis" is called the upconversion (UC) phenomenon that enables UCNPs to serve as next-generation biocompatible nanomaterials with high quantum yield (Auzel, 2004; Jalani et al., 2018). Also, UCNPs excitation by NIR lays into biological optical transparency window, which results in UCNPs' excitation deeper in a tissue and enhanced therapeutic processes (Skripka et al., 2019). However, UCNPs are typically

hydrophobic immediately after synthesis and need to be surface-modified with biocompatible coatings (Gnach & Bednarkiewicz, 2012). There are countless methods of surface modification in the literature, but optimal coatings are still being sought to ensure colloidal stability, biocompatibility, and selective accumulation of UCNPs in cells. Therapeutic efficiency of NPs mainly depends on cellular uptake efficacy and intracellular localization. Thus, it is important to research which uptake mechanism is used by the cell depending on NPs' surface modification (Oliveira et al., 2019).

1.1. Novelty and significance of the thesis

In the existing literature, studies on NPs and their interactions with cells are typically conducted separately. Remarkably, there is a lack of research dedicated to UCNPs and PC studies. According to the Web of Science database, between 2000 and 2022, only 14 research entries were found using the keywords "upconverting nanoparticles" and "protein corona".

The relevance of this research lies in the importance of maximizing NPs' penetration into cancer cells. The localization within cells is crucial from a therapeutic perspective. The crux of this dissertation revolves around how surface functionalization of UCNPs can aid in the formation of a suitable PC. This, in turn, enhances the colloidal stability of NPs and facilitates their delivery to cells through various endocytosis mechanisms, ensuring effective intracellular distribution. To achieve this, it is necessary to engineer NPs with appropriate surface coatings, leading to the formation of a specific PC, which, in turn, facilitates better penetration into cancer cells.

These studies were performed for the first time:

1. research focused on PC formation around differently coated UCNPs as well as cellular uptake mechanisms together with UCNPs' internalization dynamics based on these surface coatings;
2. investigation into how different PEG amount in UCNPs surface coatings influences colloidal stability of UCNPs and their access to cells.

1.2. The aim and objectives of the thesis

The aim of the research:

To explore how upconverting nanoparticles (UCNPs) with varying surface coatings interact with the biological surroundings, as well as to examine their accumulation mechanisms within cells.

Objectives of the research:

- to evaluate the impact of the biological environment on $LiYF_4$: Yb^{3+}, Tm^{3+} UCNPs coated with various coatings (citrate, phospholipids (PEG-DOPE:DOPC), SiO_2, copolymers (P_9MAA-25 low PEGylated and P_9MAA-75));
- to examine the cellular accumulation patterns of these UCNPs with various coatings;
- to evaluate possible toxicity of differently coated UCNPs to cells via various vability assays;
- to ascertain whether the entry of UCNPs into cells is influenced by the cell surface proteome and the surrounding protein corona (PC);
- to investigate the distinct pathways through which differently coated UCNPs enter into cells;
- to identify whether PEGylation density has impact on cellular accumulation.

1.3. Defense statements

I) Protein corona enhances colloidal stability of UCNPs regardless of their surface coating.

II) UCNPs' endocytic dynamics depend on surface coatings. Surface coatings change the cellular accumulation rates in cells. The MDA-MB-231 cell line exhibits the highest accumulation rate of cUCNPs.

III) UCNPs are biocompatible, not toxic to cells, and show no adverse impact on the viability of either MDA-MB-231 or MCF-7 cells.

IV) The cell surface proteome and PC influence the accumulation of UCNPs in cells. MDA-MB-231 demonstrates elevated integrin expression and, therefore, exhibits higher uptake rates of I-UCNPs due to THBS1 protein in its PC.

V) Small size of cUCNPs and their PC, rich in CAP1 and THBS1 proteins, result in clathrin-mediated endocytosis in MDA-MB-231 cells and caveolin-mediated endocytosis in MCF-7 cells. The highest PC-bearing sUCNPs with A2M and F5 proteins result in macropinocytosis in either cell line.

VI) The amount of PEG in the coatings of II-UCNPs influences cellular accumulation. Highly PEGylated UCNPs, such as 25-UCNPs, accumulate at higher rates in MDA-MB-231 cancer cells compared to their less PEGylated counterparts (75-UCNPs).

1.4. Author‘s contribution

The thesis author played a central role in implementing the research idea, as well as serving as the primary investigator for studies conducted on both cancer cell monolayers and the experiments with UCNPs. The author conducted experiments for UCNPs characterization, stability, investigated UCNPs’ biocompatibility and accumulation dynamics in cells, performed experiments to evaluate the internalization routes of UCNPs into cells as well as cellular localization studies.

The author took responsibility for analyzing, processing, and interpreting all the obtained results, presented the findings at scientific conferences and collaborated with co-authors to prepare publications based on the dissertation. Importantly, the author is credited as a co-author in two publications, one of which as first author, specifically focused on the topic of dissertation. Based on the work documented in the publications prepared during their doctoral studies, the author successfully completed dissertation manuscript.

The experimental research directions were formulated by the supervisor Prof. Dr. Ričardas Rotomskis who provided guidance on result interpretation, participated in the preparation of scientific publications, and contributed to conference materials, revised the thesis manuscript.

Dr. Vitalijus Karabanovas generated valuable ideas, advised on experiment planning and execution, analyzed the results, and collaborated on scientific publications and conference materials and revised the thesis manuscript. Prof. Dr. Fiorenzo Vetrone participated in supervising, article polishing and interpretation of results. Assoc. Prof. Dr. Artūras Katelnikovas was responsible for supervision, data accuracy, and article manuscript edition. Dr. Mindaugas Valius was responsible for supervision, data accuracy, and article manuscript edition.

Dr. Vaidas Klimkevičius performed coating of the UCNPs with brush-type polymers, made a portion of measurements on coated UCNPs’ characterization, contributed to the writing of the article and results interpretation. Dr. Artiom Skripka synthesized and evaluated UCNPs, was responsible for article manuscript writing.

Dr. Greta Jarockytė conducted confocal microscopy imaging, interpreted data. Dr. Marija Ger performed biochemical protein corona analysis and data interpretation. Dr. Algirdas Kaupinis was responsible for mass spectrometry. Dalius Kučiauskas performed cellular proteomics.

2. THEORETICAL BASIS

Nanoscale objects, when in contact with the cell, must overcome many barriers such as highly evolved and intricate cellular networks. These networks provide unique access and control over crucial biological processes and are often called as „bionano-scale identity“ and can be described as contextual property that pertains to what the cell perceives or "sees" in relation to the nanostructure (Behzadi et al., 2017; Walczyk et al., 2010). Intrinsic NP properties as shape, size, structure, surface modification, as well as extrinsic properties as cell type, nanomaterials‘ *in situ* environment play a crucial role in cellular uptake. Bio-nanoscale recognition mechanisms are quite universal, however, depending on the type of contact – cell (e.g., healthy, immune, damaged) or tissue (e.g., tumor, connective tissue), information gathered at each of them can differ.

Figure 2*. Projected shadows mainly from rubbish. Name of the work: "Self-imposed misery", year 2010. Rights belong to Tim Noble and Sue Webster.*

At the cellular level, the cell can insufficiently identify the exogenous material (as depicted in **Figure 2**) before engulfment. This projection of falsity is used by scientists and is called the "Trojan horse" concept. For instance, therapeutic NPs coated with cellular friendly material (Trojan horse exterior) can be taken up by the cell of the interest, distinguished as appropriate material, later the absorbed NPs can be "activated" inside the cell to destroy the malicious cell (as hidden soldiers in a Trojan horse legend) (Oliveira et al., 2019). Thus, acquiring a thorough comprehension of the interplay between NPs and biological systems is vital when designing and advancing clinical diagnostic and therapeutic applications. Also, data can

differ even between the research conditions. Despite promising results being obtained *in vitro*, they can be totally misleading when studies are performed *in vivo.* As an example, PC of gold NPs changes at *in vivo* conditions (Cox et al., 2018).

Acquiring accurate and dependable data regarding the characterization of NPs using suitable methodologies is crucial for achieving reliable results concerning their safety, therapeutic efficacy, and diagnostic potential (Mahmoudi, 2021). Through numerous published studies, it has become evident that upon introduction of NPs into biological tissues or fluids, a biomolecular corona spontaneously forms in less than 0.5 min (Cai & Chen, 2019). This corona primarily consists of various types of biomolecules, particularly proteins. The type, quantity, and structure of proteins adsorbed onto the surface of NPs play a pivotal role in regulating biocompatibility and, ultimately, determining the destiny of the nanomaterial, both *in vitro* and *in vivo* (Dawson & Yan, 2021). Also, PC can enable NPs to enter the cell through "Trojan horse" effect (Xue et al., 2018). Thus, it is pivotal to "construct" PC that is favorable for the cell to "see" the good (because the cell "sees" the PC not the pristine surface of the NP) and for the researchers to upload the nano-vehicle with the drug or gene "under" the PC cloud (Oliveira et al., 2019; Walczyk et al., 2010). On the other hand, it is also favorable to synthesize NPs with the appropriate surface modification which would attract proteins of interest and result in high cellular uptake rates.

Gaining a more comprehensive understanding of the interactions between NPs and their biological environments can enhance the safety and therapeutic effectiveness of nanomedicine (NM) technologies, as well as accelerate their use in clinics.

2.1. Photoluminescent nanoparticles for biomedical research

2.1.1. Upconverting nanoparticles

UCNPs or RE-doped NPs are a promising new class of PhNPs. UCNPs synthesis uses lanthanides with electronic configuration $4f^n5s^25p^6$ (n = 0-14). The fully unfilled 4f orbital provides energy levels for the UV, visible, and NIR light spectra. The advantage of these NPs compared to "traditional" NPs (QDs, silica NPs, semiconductor nanocrystals, etc.) is that UCNPs can convert low energy photons into higher energy ones during the multiphoton process called UC (Auzel, 2004; Jalani et al., 2018).

UC is a nonlinear optical process in which two or more photons are absorbed in a ladder-like principle stepwise, resulting in the emission of light

with a shorter wavelength than the excitation wavelength of the radiation. In other words, lower-energy radiation, such as NIR, is converted into higher-energy radiation, such as UV, visible light, or even shorter-wavelength NIR (Haase & Schäfer, 2011; Rodriguez Burbano et al., 2015). The concept of UC was first proposed by physicist Nicolaas Bloembergen in 1959, who suggested recording IR radiation using RE metal or transition metal ions embedded in crystalline materials (Bloembergen, 1959). UC was first observed in 1966 with advancements in laser and optical technologies in Francois Auzel's experiment (Auzel, 2004). At that time, it was not believed to have biomedical applications. However, with the development of new NP synthesis methods, the potential for wider use of this phenomenon emerged (B. Zhou et al., 2015). One of the significant properties of UCNPs that they can be stimulated with inexpensive, continuous-wave lasers with a power of about 1 W, resulting in a strong emission signal (Hirai et al., 2002). Moreover, no damage in cells is observed even after 3000 higher power excitations. For instance, in Nam and coworkers work Trypan blue did not stain cells after 980 nm irradiation (**Figure 3**) (Nam et al., 2011).

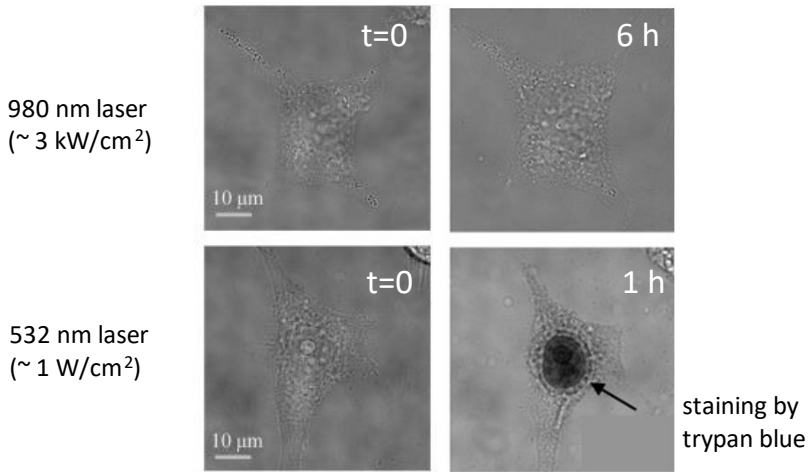

Figure 3. *Comparison of different illumination impact on HeLa cells. Bright-field images of HeLa cells treated with* $NaYF_4$*:* Yb^{3+}*,* Er^{3+} *UCNPs for 1h and 6 hours,* respectively (Nam et al., 2011).

Typically, UCNPs are excited by NIR radiation in the optical biological window (at 750–950 nm) where light absorption and scattering in tissues is the lowest, meaning that UCNPs can be excited in deeper tissue layers, thus ensuring optimal diagnostic and therapeutic processes (Jalani et al., 2018;

Skripka et al., 2019). UCNPs are quite photostable (S. Wu et al., 2009), and NIR light does not cause photodamage, which is extremely important for imaging living cells.

2.1.2. Chemical composition of upconverting nanoparticles

UCNPs are compounds of various transition metals and RE metals with the structure of an inorganic crystal lattice doped with transition metal, lanthanide or actinoid ions. UCNPs usually consists of three components: matrix (core), doped with sensitizer (donor) and activator (acceptor) ions (Yao et al., 2020). Typical structure of an UCNP shown in **Figure 4**.

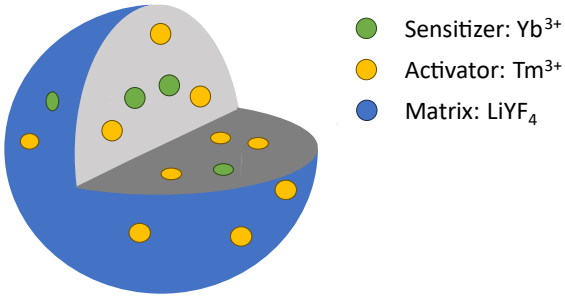

Figure 4. *UCNPs' composed of a $LiYF_4$ matrix, with a schematic diagram depicting sensitizer Yb^{3+} ions and activator Tm^{3+}. Sphere in a picture was chosen only as a model.*

The essential requirements for the matrix are components that have low phonon energy (that is why fluorides are used for UCNPs synthesis), suitability for inserting sensitizer and activator ions, and transparency in the NIR region. According to other authors, sodium or calcium fluorides are the best materials for matrix production (Kang et al., 2020). The final emission of UCNPs is strongly influenced by the choise of matrix. The more efficient emission of UCNPs, the more suitable they are for diagnostics and therapy. For example, studies comparing $NaYF_4$ and $LiYF_4$ UCNPs optical characteristics observed that $LiYF_4$ UCNPs exhibits stronger emission that its sodium counterpart (Jiang et al., 2016).

Sensitizers

UCNPs are typically obtained by replacing the Y^{3+} ions in the matrix with sensitizer Yb^{3+}, which has only two energy levels and a relatively large absorption cross-section at 976 nm. Due to these sensitizer energy levels,

cross-relaxation (CR) is avoided (Dong et al., 2015). Yb^{3+} exhibits intense NIR absorption, which leads to effective resonant nonradiative energy transfer from Yb^{3+} to the activator (**Figure 5**). In the matrix, intense energy migration between $Yb^{3+} \rightarrow Yb^{3+}$ is observed. Here, activator ions act as a "trap" for migrating Yb^{3+} excitation (Haase & Schäfer, 2011). Moreover, energy of the excited states of sensitizer is very similar to activator ions what makes Yb^{3+} an ideal energy donor to other ions.

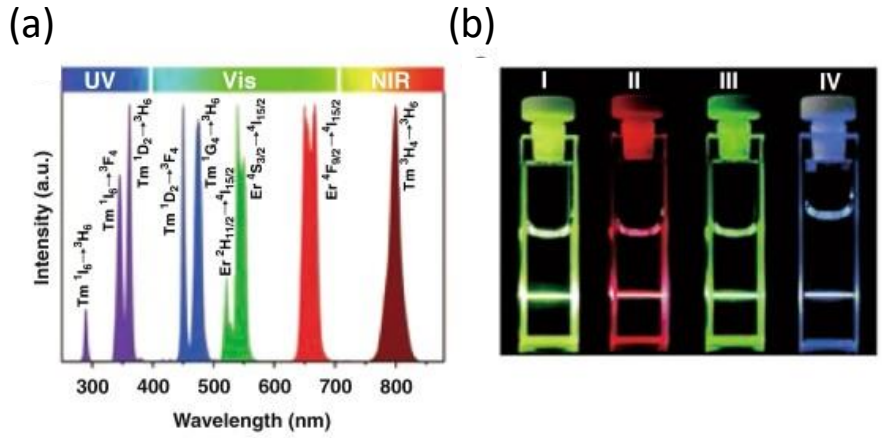

Figure 5. *(a) Shown above are the upconversion emissions of UCNPs containing Yb-Er and Yb-Tm dopants, spanning from the UV to NIR regions when exposed to 980 nm irradiation. (b) Additionally, photographs of emission of UCNPs in a colloidal solution: I - the overall emission of the $NaYF_4$:Yb, Er sample (cuvette under number I); emissions of the NaYF4:Yb,Er sample, observed through red and green filters (II and III, respectively) and the emission of the NaYF4:Yb,Tm sample* (Dong et al., 2015).

For the development of new UCNPs materials it is important to change the concentrations of dopant ions and the matrix composition, as these changes can alter UCNPs' radiative and non-radiative properties, resulting in different emission spectra. Typically, doped ions are inserted into the matrix in small concentrations: ~20% for the sensitizer and <2% for the activator (Haase & Schäfer, 2011).

Activators

While numerous RE ions demonstrate UC emission, it is noteworthy that only a selected few of the commonly used activator ions display effective emission at low levels of excitation intensity. Examples of those ions are –

Er^{3+}, Tm^{3+}, Ho^{3+}. These ions possess ladder-like energy levels and are highly compatible with commercially available high-power diode lasers.

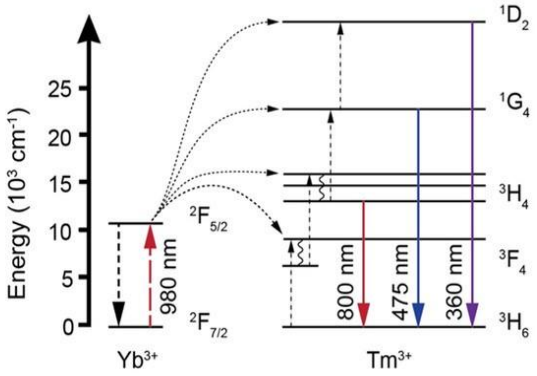

Figure 6. *In system featuring Yb^{3+}/Tm^{3+} dopants, these ions serve as sensitizer and activator ions, respectively. They absorb incoming excitation light at 980 nm wavelength, and this energy is subsequently transferred to the Yb^{3+}/Tm^{3+} activator ions through a sequence of radiative, nonradiative energy transfer, and multiphonon relaxation processes as indicated by arrows* (Mettenbrink et al., 2022).

For example, Tm^{3+} ions (**Figure 6**) typically exhibit three UC emission bands and Tm^{3+} has the most intense emission bands at 360, 475 and 800 nm. However, depending on the concentration of doped ions and the matrix composition, the jumps at these bands change, but the following mostly remain: $^1D_2 \rightarrow {}^3H_6$ (360 nm), $^1G_4 \rightarrow {}^3H_6$ (475 nm), $^3H_4 \rightarrow {}^3H_6$ (800 nm). The main emission band of Tm^{3+} is in the tissue transparency window (650-950 nm range), which makes it possible to apply UCNPs doped with these ions for deep tissue imaging (Jalani et al., 2018).

2.1.3.Morphology of upconverting nanoparticles

When choosing or synthesizing an appropriate UCNP material for study, it's crucial to consider not just the composition but also the crystal structure of the UCNPs. The morphology of UCNPs depend on the chemical composition and method of synthesis. For example, the most widely studied material $NaYF_4$ has two forms – cubic (α-phase) and hexagonal (β-phase). During thermal decomposition, first the α-phase is formed, and only later the β-phase forms. It is known that the hexagonal structure is thermodynamically more stable compared to the cubic form, and the

$NaYF_4$:Yb^{3+},Tm^{3+} crystals with the hexagonal phase have an UC emission that is even 4 times higher than the cubic phase crystals (M. Wang et al., 2011). **Figure 7** shows some of the possible crystal structure examples of the UCNPs.

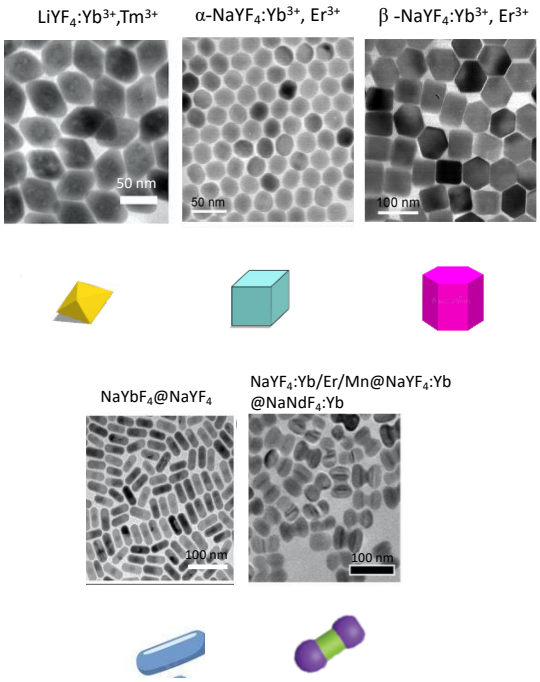

Figure 7. *Transmission electron microscopy images of the diversity of UCNPs forms: tetragonal* (Skripka et al., 2019), *cubic, hexagonal* (Haase & Schäfer, 2011), *elongated, rod-like shaped* (B. Chen et al., 2021)(B. Chen et al., 2021)(B. Chen et al., 2021) *and dumbbell shaped* (Lei et al., 2020).

However, the shape and composition of the nanomaterial alone are only part of the components that influence the entry of NPs into cells. The following NP biological and chemical properties are distinguished: NP‘ size, morphology, surface charge, surface coating (chemical groups covering the NP‘ surface, NP‘ hydrophilicity/hydrophobicity), presence of protein on the NP‘ surface (Behzadi et al., 2017).

2.1.4. Upconversion mechanisms

UC is a nonlinear optical process in which the absorption of two or more photons results in the emission of energy higher than the excitation

wavelength. UCNPs are excited by NIR radiation and emit light in the UV, visible and NIR region (Haase & Schäfer, 2011). The phenomenon of UC was first described about 60 years ago during Auzel's experiments (Auzel, 2004). UCNPs are characterized by high anti-Stokes shift, long luminescence lifetimes (K. Zheng et al., 2019), narrow emission bands (J. Zhou et al., 2015). UCNPs are also characterized by UC mechanisms such as excited state absorption (ESA), energy transfer upconversion (ETU), CR, energy migration-mediated UC, cooperative UC, and photon collapse. Two of these are shown in **Figure 8**.

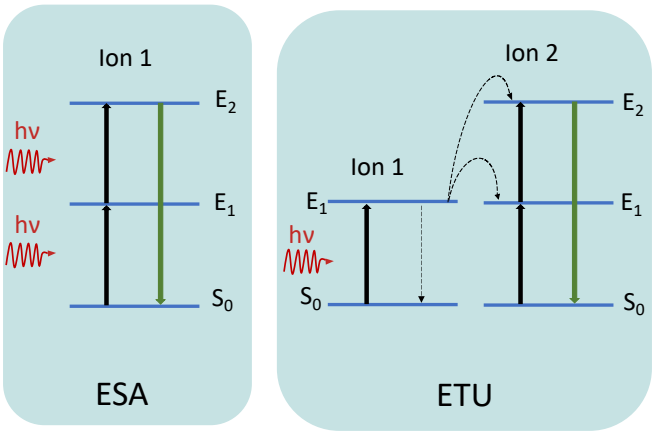

Figure 8. *Schematic representation of excited state absorption (ESA), energy transfer upconversion (ETU) mechanisms.*

Excited-state absorption

During this UC process, one ion successively absorbs one or two photons and moves from the ground unexcited state (S0) to a higher excited state (E1 or E2). If the ion is still excited to the E1 level, it is ready to accept another photon to reach the E2 level. Finally, UC emission from the E2 level to S0 is observed (Rodriguez Burbano et al., 2015; X. Wang et al., 2018). The ESA process uses Er^{3+}, Ho^{3+} and Tm^{3+} ions .

Energy transfer upconversion

ETU is one of the most effective mechanisms of UCNPs, which does not depend on the excitation power. Two adjacent ions are required for this process to occur. During ETU, there is a nonradiative energy transfer between

ion 1 (donor or sensitizer) and ion 2 (acceptor or activator). As can be seen from **Figure 8**, the filling of the E1 level of ion 1 occurs first. Then, a non-radiative energy transfer occurs between the donor and acceptor ions to the E1 excited state. During the second energy transfer, photons are absorbed into the excited E2 level before ion 2 finally relaxes to the ground unexcited state (S0)(G. Chen et al., 2014; K. Zheng et al., 2019). Sensitizer-activator pairs such as Yb^{3+}-Er^{3+}, Yb^{3+}-Ho^{3+}, and Yb^{3+}-Tm^{3+} are used in UCNPs synthesis for the ETU process (G. Chen et al., 2014; Gu & Zhang, 2018).

2.1.5.Surface modification of upconverting nanoparticles

After synthesis, UCNPs usually are capped with hydrophobic ligands (as oleic acid) that render them unstable in aqueous solutions (Gnach & Bednarkiewicz, 2012). To ensure and increase UCNPs dispersibility, hydrophobic capping is being removed. However, these "bare" UCNPs can agglomerate or even dissolve (Andresen et al., 2020). Also, UCNPs' surface interacts with water molecules, especially OH groups with high energy vibrations modes (around 3500 cm^{-1}) that results in UCNPs' emission quenching (Arppe et al., 2015). To counteract emission loss, achieve colloidal stability of UCNPs, and improve their ability to disperse in water, an extra surface modification becomes necessary. Options for potential coatings include: SiO_2, citrate, phospholipids, polymers as polyethylene glycol (PEG), polyethylene amine (Gnach & Bednarkiewicz, 2012; Rojas-Gutierrez et al., 2019), etc. These surface modifications can be divided into ligand replacement, where oleic acid is replaced by a new surface ligand, and encapsulation techniques, when oleic acid remains on the surface and the NP' surface itself is coated with an additional shell.

Ligand substitution method for surface modification of upconverting nanoparticles

In the case of ligand substitution, oleate-coated UCNPs can be coated with hydrophilic or hydrophobic polymers (Wilhelm et al., 2015), for example, with PEG, polyacrylic acid, polyvinylpyrrolidone (PVP), dextran, chitosan or small molecules of citric acid or cucurbit[7]uril (Sun et al., 2018). PEG is known as a non-toxic, neutral polymer that provides stable dispersions in buffer solutions and low binding of non-specific molecules. Several negatively charged groups that efficiently attach PEG to the lanthanide ions on the surface of UCNPs include carboxylates, sulfonates, and phosphonates. Duong et al. (Duong et al., 2018) prepared negatively charged copolymers

(ligands) with PEG to modify the UCNPs' surface and observed that their modified UCNPs were stable for up to a week in different solutions: water, phosphate buffered saline (PBS), and 2-(N-morpholino)ethanesulfonic acid.

Surface modification by encapsulation method

There are already several methods described for UCNPs surface coating via encapsulation method, as:

- surface coating with silica layer (Palo et al., 2018);
- layer by layer deposition of polyelectrolyte on UCNPs' surface (Palo et al., 2018);
- adsorption of the amphiphilic polymer, which interacts with oleic acid in its hydrophobic part (L. Le Li et al., 2012; Märkl et al., 2020),
- photopolymerization of the polymer coating on the UCNPs' surface (Beyazit et al., 2014).

Silica-coated NPs are easily dispersed in water because of partially deprotonated silanol groups (pKa ~ 7) on the NP' surface. Silicon is chemically stable and optically transparent, which is particularly relevant for the use of UCNPs as optical markers (Hlaváček et al., 2014). In addition, it has been observed that the silicon coating is sensitive to non-specific interactions and PC rapidly forms around silica-coated NPs (Pisani et al., 2017). This can be avoided by coating the silica with bovine serum albumin (BSA) (Poláchová et al., 2019).

2.1.6. Upconverting nanoparticles for biological imaging

Application of UCNPs emission to biological imaging is extremely useful for early diagnosis and image-guided therapy. A tissue-specific optical transparency window allows light to penetrate deeper into the tissue while reducing autofluorescence and light scattering (G. Chen et al., 2014). UCNPs are known to be efficient contrast markers to obtain excitation and/or emission in the NIR window (Jalani et al., 2018).

In the literature there are several examples of UCNPs application for imaging. For instance, hydrogen peroxide (H_2O_2) plays an important role in homeostasis, signal transduction in cells, so abnormal H_2O_2 level regulation is reflected in structural changes such as DNA damage, Alzheimer's disease, cancer, heart disease (Wei et al., 2021). Cellular redox levels were shown to

be determined by glutathione (GSH)/H_2O_2 detection using A549 cells implanted into mouse. The Zheng authors' group synthesized a GSH-sensitive marker and a H_2O_2-sensitive marker, which they loaded into UCNPs and monitored the redox status *in vivo* (J. Zheng et al., 2020). Also, a hydroxide radical (•OH)-sensitive marker was developed by other researchers via luminescence resonance energy transfer having UCNPs as a marker (Z. Li et al., 2015). The synthesized UCNPs did not have functional groups on the surface and had a sandwich structure ($NaYF_4$@$NaYF_4$:Yb^{3+}/Tm^{3+}@$NaYF_4$), while mOG, an azo dye, performed the function of an energy acceptor and •OH recognition marker. The results of the study showed the ability of the UCNP-based nanomarker to monitor •OH in living tissues and cells.

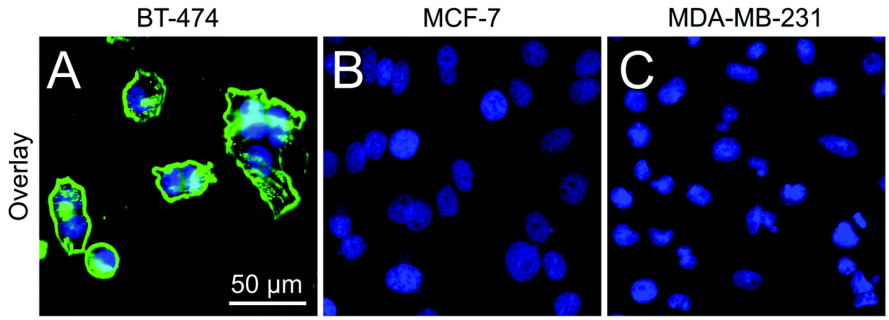

Figure 9. *Labeling of cancer cells with SA-PEG-Ner-UCNPs. The image shows an overlay of DAPI and UCNPs channels for (A) BT-474, (B) MCF-7 and (C) MDA-MB-231 cells* (Farka et al., 2020).

Another example of applicability of UCNPs in diagnostics is the use of UCNPs for single-molecule immunoenzymatic analysis, which in the case of UCNPs is called ULISA (upconversion-linked immunosorbent assay). ULISA is a method for the detection of cancer markers such as prostate-specific antigen (PSA). Farka and others used 48 nm β-phase $NaYF_4$:Yb^{3+}, Tm^{3+} UCNPs coated with a carboxylated silicon layer, to which the detection antigen polyclonal anti-PSA antibody was attached. The researchers proved in their work that the UCNPs they used for the ULISA method increased the detection limit even 10 times compared to the commercial immunoenzymatic analysis method ELISA. Multiplex detection of multiple analytes by observing/detecting different UCNPs emission colors is also possible using ULISA (Farka et al., 2017).

Immunohistochemistry and immunocytochemistry methods are used in tissues and cell culture analysis for the microscopic identification and

diagnosis of cancer cells. For example, Farka et al. scientific group developed several conjugates of streptavidin-UCNPs for the detection of the cancer marker human epidermal growth factor 2 receptor (HER2) in breast cancer cells. For this study, HER2-positive BT-474 cells and two HER2-negative lines as MCF-7 and MDA-MB-231 were used (Error! Reference source not f ound.). This team of scientists demonstrated the potential to achieve a significantly greater, up to 50 times higher, contrast in comparison to existing fluorescent markers, all within identical experimental parameters, utilizing SA-PEG-Ner-UCNPs (streptavidin-polyethylene glycol and neridronate-coated UCNPs). The size of the uncoated UCNPs itself is 44 nm, and the coated one is about 90 nm (Farka et al., 2020).

2.2. Cellular uptake of nanoparticles

2.2.1.Cellular internalization routes

Before the NPs appear near the cell membrane (CM), they encounter not only the proteins in the cell surroundings (and form NP-PC complex) but also the extracellular matrix, pH, etc. These factors, as well as PC, can change the properties of the NPs before their internalization. Normally, the interaction of the NP-PC complex with the cell starts with its adsorption on the cell membrane. The plasma membrane then folds into the cell, enveloping the complex, forming a vesicle, and entrapping the NP-PC complex into the cell interior. This mechanism of NP-PC entry into the cell is called endocytosis. Endocytic mechanism depends on the NPs' surface composition, size and PC formed around the NP (Docter et al., 2015; Sikora et al., 2017). However, there is evidence that cellular uptake mechanisms or kinetics can depend on NP preparation conditions. First proof — when cell growth medium supplemented with heat-inactivated serum reduces the uptake of polystyrene NPs comparing to uptake results with non-inactivated serum (Lesniak et al., 2010). Another evidence is the cell culture media composition differences, that result in PC size variations in time when media is supplemented with the same serum (Maiorano et al., 2010). To eliminate the possibility of variations, future comparative experiments need to employ precise matching of the media.

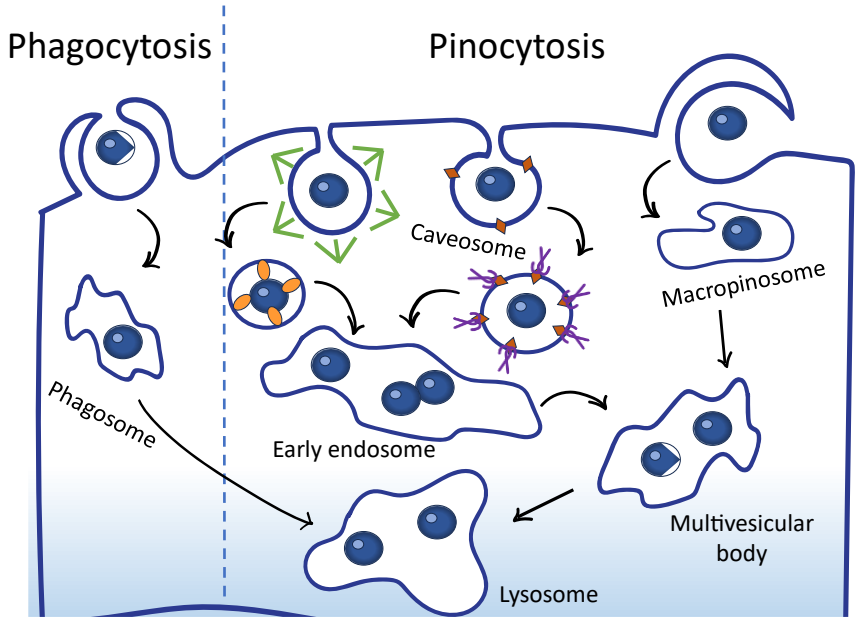

Figure 10. *A representation of endocytotic processes and intracellular transportation involves the internalization of nanoparticles (depicted as dark blue spheres) and various substances, which are enveloped in early endosomes, phagosomes, or macropinosomes. The vesicles containing nanoparticles progress along the degradation pathway, transforming into late endosomes/multivesicular bodies, and ultimately undergo fusion with lysosomes.*

There are two types of endocytosis: pinocytosis (entry of liquids and insoluble substances into cells) and phagocytosis (entry of large particles into cells) (**Figure 10**) (Behzadi et al., 2017; Docter et al., 2015; Sikora et al., 2017). Pinocytosis can occur in all cells and their types depend on which proteins engage in endocytosis. Pinocytosis is divided into clathrin/caveolin-dependent endocytosis, clathrin/caveolin-independent endocytosis, and macropinocytosis (Behzadi et al., 2017). Also, cellular internalization mechanisms are classified into micropinocytosis and macropinocytosis. The difference in the mechanisms lies in the fact that micropinocytosis is an actin-independent mechanism, while macropinocytosis is an actin-dependent mechanism.

Clathrin-mediated endocytosis

CME occurs on the sites where structures called coated pits are assembled. Coated pits mainly consist of clathrin and adaptor protein-2 (AP-2). Clathrin is a three-leg structure (called triskelion) that possess three heavy and three light chains (**Figure 11**). Distal domain controls the clathrin assembly, curvature, and orientation. N-terminal domain contains a binding area that interacts with endocytic proteins. Proximal domain is responsible for enclosed basket framework. The light chain regulates the assembly level of triskelion.

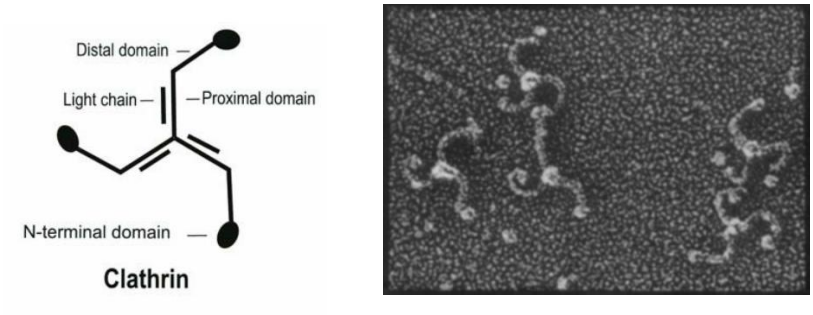

Figure 11. *On the left – clathrin-coated vesicle component clathrin* (Mousavi et al., 2004). *On the right – triskelion view under electron microscope (Heuser & Kirchhausen, 1985).*

AP-2 has domains responsible for targeting the AP-2 to the plasma membrane and interaction with clathrin (Mousavi et al., 2004). Moreover, there are accessory proteins as epsin, amphiphysin, EPS15, dynamin1, endophilin that help to stabilize CM[2] curvature. In the CM there are only 0.5-2 % of coated pits (Mousavi et al., 2004). During CME, vesicles with the size of 100-150 nm are assembled. When nanomaterials interact with receptors on the cell membrane (**Figure 12**), the protein clathrin-1 undergoes polymerization within the cytosol, resulting in the formation of a vesicle containing the NPs. Gradually, a vesicle is formed that encapsulates the NPs. Once the vesicle is fully formed, the small GTPase[3] protein dynamin hydrolyzes GTP, causing the vesicle to detach from the membrane. Dynamin

[2] Cell membrane is made of amphiphilic lipids that have hydrophilic heads and hydrophobic tails and protects the cell from surroundings and is semi-permeable (Behzadi et al., 2017).

[3] GTP is a guanosine triphosphate, a molecule similar to adenosine triphosphate and serves energy for enzyme called GTPase.

assembles into a polymeric helix around the narrow portion of the coated vesicle, facilitating its separation from the membrane and subsequent movement into the cytoplasm (Behzadi et al., 2017; Mousavi et al., 2004).

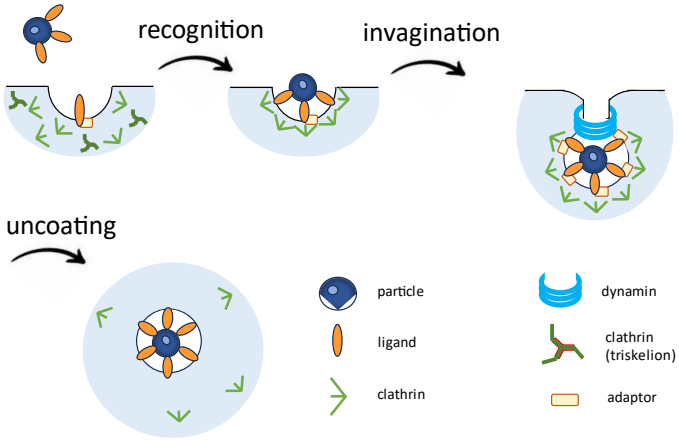

Figure 12. *Schematic representation of clathrin-mediated endocytosis. The sequence of events in clathrin-dependent endocytosis begins with the identification of the ligand, followed by the formation of a vesicle coated with clathrin. The triskelion of clathrin facilitates the creation of a hexagonal lattice, which aids in the inward folding of the plasma membrane. Later, dynamin, a hydrolysis protein, releases the vesicle into the cytoplasm, leading to the disintegration of the clathrin coating.*

Caveolin-mediated endocytosis

In caveolae[4]-dependent endocytosis (or CVME), the protein caveolin plays a crucial role in bending the cytoplasmic membrane, formation, and function of caveolae (**Figure 13**). Caveolin is particularly abundant in endothelial cells, fibroblasts, smooth muscle myocytes, and adipocytes. Similar to clathrin-dependent endocytosis, caveolin vesicles rely on actin to travel towards caveosomes, with which they later fuse. The caveosomes, along with NPs, are then transported to the endoplasmic reticulum. Compared to CME, this process is slower and involves smaller vesicles. Unlike ordinary endocytosis, where specific receptors are involved, CVME incorporates all substances present in the environment. This process sometimes serves not

[4] Caveolae is a subunit of glycolipid raft.

only to transport materials into the cell, but also to restore membrane area following intense secretion and regulate cholesterol levels within the membrane, among other functions (Behzadi et al., 2017).

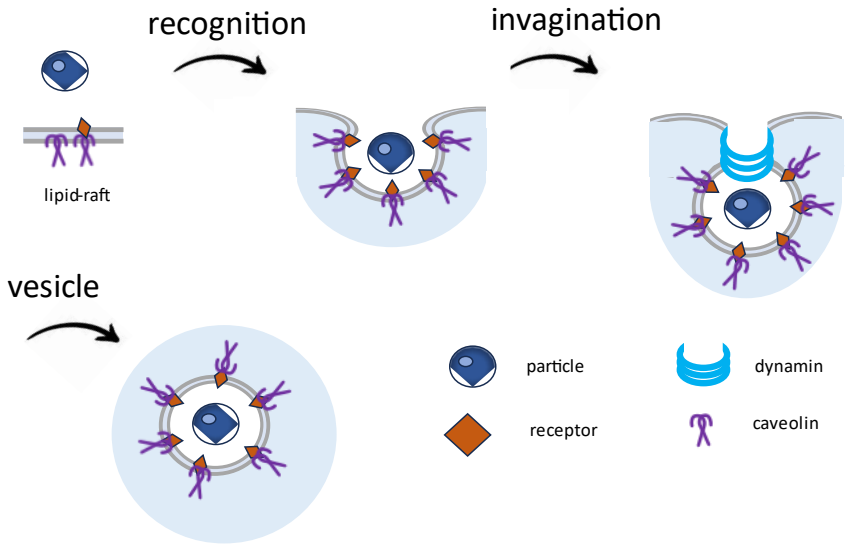

Figure 13. *Schematic representation of caveolae-mediated endocytosis.*

Canadian researchers proposed that caveolae- and raft-dependent endocytosis is defined by the same pathway and should be called caveolae/raft-dependent endocytosis. CVME is dependent on dynamin and cholesterol depletion. For the caveolae uptake actin cytoskeleton needs to be disrupted while internalization requires caveolin-1. However, caveolin expression does not play a role in the independent internalization of other caveolae/raft ligands (Nabi & Le, 2003).

Macropinocytosis

Macropinocytosis (MP), a distinct form of pinocytosis, is actin driven, and differs from other endocytic processes by not relying on lipid rafts or pit-forming proteins comparing to micropinocytic pathways (CME or CVME). Instead, it involves the formation of expansive membrane extensions or ruffles through rearrangement of the cytoskeleton. These extensions subsequently merge back with the plasma membrane, resulting in the creation of large vesicles (ranging from 0.2 to 5 μm) that engulf considerable amounts of extracellular fluid, resembling a substantial "gulp" (**Figure 14**) (Behzadi et

al., 2017). Even though MP has been studied since 1930s, it is unknown which proteins are responsible for exogenous materials uptake in each case (Means et al., 2022). MP is sensitive to growth factors. The initiation of MP has been observed through the influence of various growth factors, such as EGF, platelet-derived growth factor, and macrophage colony-stimulating factor. In numerous instances, these growth factors trigger the formation of membrane ruffles by activating small GTPases as Ras, Rac, and Cdc42[5].

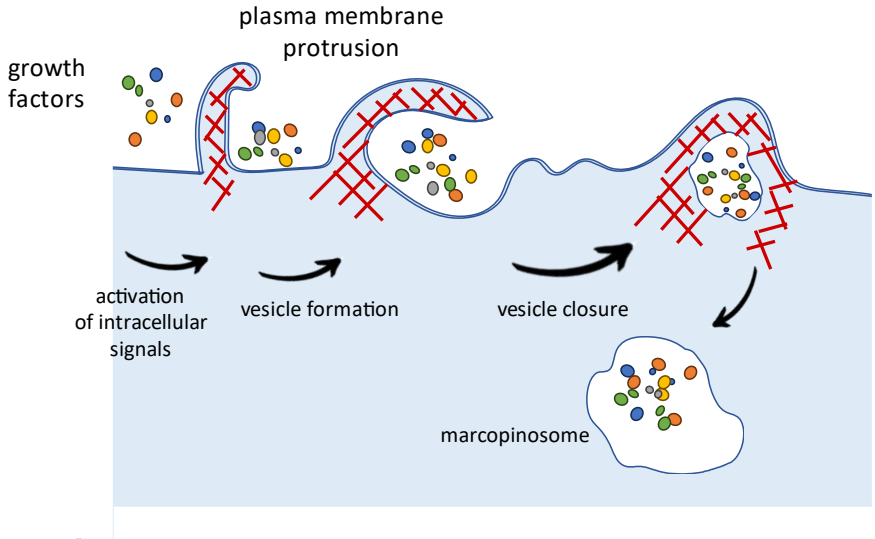

Figure 14. *Schematic representation of macropinocytic route.*

Under suitable conditions, practically any mammalian cell cultured in a laboratory setting displays the capability of MP (King & Kay, 2019). When NPs are introduced into biological system, specific proteins are responsible for facilitating the intracellular transport of NPs through distinct endocytosis mechanisms. These mechanisms may vary based on the current state of the cell. Within first 30 seconds of contact with proteins, NPs are covered up with PC. One unique aspect of MP is its indiscriminate uptake of all particles and dissolved substances present in the extracellular fluid, regardless of specific receptors presence. This feature makes it a nonspecific mechanism for bulk fluid uptake. The process of MP plays crucial roles in various physiological functions, such as antigen presentation, and serves as a portal of entry for microbial pathogens, including bacteria and viruses.

[5] Cdc42 - cell division control protein 42.

The process of MP is closely connected with the formation of actin polymers (**Figure 14**) thus polymerization inhibitors as cytochalasin D, phosphoinositide 3-kinase blockers or Na/H exchange inhibitors as 5-(N-Ethyl-N-isopropyl)amiloride (EIPA) can be used to confirm this actin driven pathway. Actin filaments undergo polymerization adjacent to the plasma membrane, leading to the creation of extensions known as membrane ruffles. In cases of prominent membrane ruffling, a portion of these ruffles could bend inward towards the basal membrane. As they merge, these inwardly folded ruffles generate a substantial vesicle structure known as a macropinosome. Macropinosomes are primarily differentiated from other endosomes that utilize receptor-mediated endocytosis by their notable dimensions, which vary from 0.2 μm to 10 μm in diameter (Means et al., 2022). Since macropinocytosis involves the formation of large vesicles, it serves as an important mechanism for the uptake of larger NPs that would not be efficiently taken up through clathrin- or caveolae-dependent endocytosis (Behzadi et al., 2017).

2.3. Factors affecting nanoparticle endocytosis routes

2.3.1.Factor I. Nanoparticles' size, shape, surface

NPs' size, shape and surface charge have tremendous impact on cellular uptake routes. NPs with the size of 100 nm are internalized via clathrin-(CME) or caveolin-mediated endocytosis (CVME). If the size is around 200 nm and more, macropinocytic pathway is being activated (Means et al., 2022). In general, NPs' size affects cell or tissue distribution, circulation half-life and cellular accumulation (Albanese et al., 2012). The literature describes the appropriate size of NPs for cellular accumulation to range from 10 to 60 nm (Hoshyar et al., 2016). Meanwhile, if NP size > 150 nm, NP will be recognized by macrophages and accumulate in MPS as lymph nodes, liver, spleen, and lungs (Y. Zhou & Dai, 2018). According to recent research results, the size of NPs should be around 50 nm for optimal cellular accumulation (Means et al., 2022; Rojas-Gutierrez et al., 2019).

NPs that have a rod-like structure, particularly those with diamond-like shapes and aspect ratios close to 1.7, have demonstrated the most effective internalization and extended presence within cells (Rojas-Gutierrez et al., 2019; W. Wang et al., 2019). These characteristics, involving both size and morphology, help overcome the swift renal filtration and the body's clearance mechanisms through the MPS (Grodzinski et al., 2019). Other investigations have highlighted that rod-like NPs can be more swiftly infiltrated and amassed

within cancerous tissues compared to spherical counterparts (Toy et al., 2014). In contrast, a recent study by Chen et al. observed a higher accumulation of quasi-spherical UCNPs around 18 nm in size, in comparison to rod-shaped UCNPs (B. Chen et al., 2021).

Surface charge also plays a role in cellular accumulation of NPs. For instance, bare gold NPs are taken up via macropinocytosis due to partial NPs aggregation, while PEGylated counterparts are internalized via clathrin or caveolae mediated uptake. Also, negatively charged NPs possess greater uptake than neutral NPs. For charged NPs, their endocytosis process is significantly influenced by the way their surfaces are modified. Generally, NPs that engage in CVME tend to avoid association with lysosomes, resulting in enhanced cellular uptake. This characteristic holds potential benefits for advanced NP engineering in the field of NM. A study conducted by Dausend et al. revealed that positively charged NPs are predominantly internalized via macropinocytosis, while Foroozandeh showed that negatively charged NPs are taken up through clathrin-/caveolae-dependent endocytosis mechanisms (Foroozandeh & Aziz, 2018).

However, to enhance accumulation of NPs in the body, NPs surface can be additionally modified. This further enhancement of surface properties can help NPs to reach the target more successfully. Some information found in the literature is described in the section 2.3.2.

2.3.2.Factor II. Additional nanoparticles' surface functionalization

Ligand conjugation

Specific targeting of tumor cells is typically accomplished by modifying nanocarriers with different types of targeting molecules such as antibodies, antibody fragments, aptamers, proteins, peptides, carbohydrates, and small molecules. These targeting molecules can specifically attach to antigens or receptors that are either unique to tumors or present in higher quantities on tumor cell surfaces. This binding helps increase the retention of nanocarriers in tumor tissues and improves the internalization of the nanocarriers by tumor cells. For instance, NPs covered with the widely studied targeting protein transferrin (Tf), successfully target Tf receptor in tumor cells and show great results in cancer therapy (K. Wang et al., 2016). Apart from Tf, numerous other proteins like epidermal growth factor (EGF, which binds the EGF receptor), lactoferrin (which is ligand for the low-density lipoprotein receptor), and high-density lipoproteins (which target scavenger receptor type

B-1) have been utilized to direct NPs toward specific receptors that are excessively expressed on the outer membranes of tumor cells (Fan et al., 2023).

Coating with cell membrane

To get a biomimetic targeting of NPs into the cells there are several approaches that were used by researchers as: coating with red blood cell (RBC) membrane, cancer cell membrane, stem cell membrane and others (Fan et al., 2023). One of the examples of blood cell membrane coating is presented in Rao et al. work published in 2017 (Rao et al., 2017). RBCs themselves possess 120 days long lifespan, long blood circulation time, have glycans and sialic acid on the surface, which effectively reduces immune response. In this work, UCNPs were coated with RBCs and additionally RBCs on its surface were complemented with cancer targeting molecule 1,2-distearoyl-sn-glycero-3-phosphoethanolamine-N-[folate (polyethylene glycol)-2000] (DSPE-PEG-FA) and RBCs itself. Later, targeting capability was investigated on MCF-7 cells. **Figure 15** shows that in presence of RBCs on the UCNPs surface maximize UCNPs' targeting capability and PC formation around UCNPs is prevented.

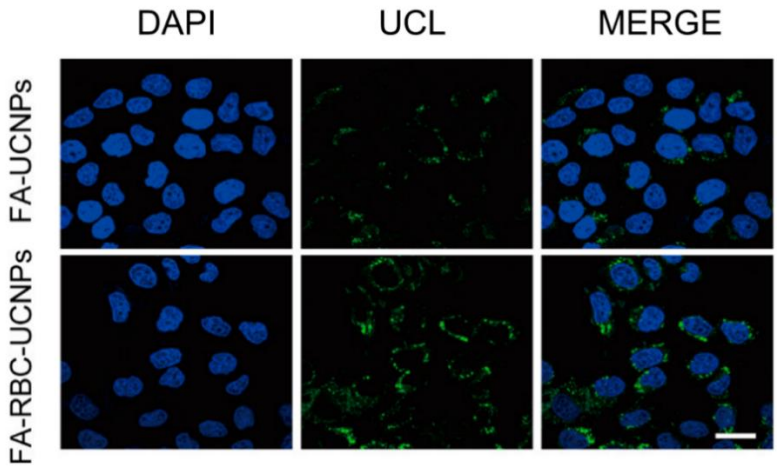

Figure 15. *Confocal laser scanning microscopy images of MCF-7 cells after exposure to red blood cell coated UCNPs with and without folic acid on the surface* (Rao et al., 2017). *Nucleus is stained with DAPI, UCL stands for upconversion luminescence. Green color represents emission of* $NaYF_4$*:* Yb^{3+}*,* Er^{3+} *UCNPs. Scale bar: 20* μm*.*

As it is already known, the size, shape, surface charge, additional functionalization of NPs has tremendous impact on cellular internalization of NPs inside the cell or body. Yet, cellular internalization also relies heavily on another crucial factor that is perceived, comprehended, and exerts a substantial influence: the protein corona.

2.3.3.Factor III. The protein corona

In biological fluids (cell culture medium or blood) UCNPs face proteins or biomolecules that instantly (less than in 0.5 min) cover up the NPs creating additional layer called PC. Some authors PCs' term refers to "biomolecular corona" term, because of the biological fluids' complexity. PC transforms surface of the NPs and changes its functionality. PC composition is of utmost importance in creating NPs for drug delivery (Docter et al., 2015; Moore et al., 2015). It is known that less than 1 % of administered NPs are delivered to tumors (Wilhelm et al., 2016). This knowledge forces researchers to fill the gap between designing promising NPs and real NPs' fate in the living organism that can be unpredictable. Furthermore, studies on UCNPs' PC are notably limited.

Protein corona composition and size

PC composition depends on the morphology of NP (shape, size, surface charge) as well as biological environment NPs are in, such as proteins present in the bloodstream or components of the biological medium (Docter et al., 2015; Fleischer & Payne, 2014; Francia et al., 2019). The PC consists of hard and soft layers (**Figure 16**). The hard corona is a high-affinity protein layer consisting of proteins irreversibly bound to the NP surface (as opsonins, fibrinogen, apolipoproteins, coagulation factors, plasma proteins). In contrast, the soft layer above the hard corona that is dynamic and changes over time, is composed of less related proteins (as serum albumin, immunoglobulins, complement proteins, transport proteins) that interact weakly with the NP. The PC structure is complex and unique to each NP surface coating (Docter et al., 2015).

The relative number of proteins adsorbed on the NP surface usually differs from the relative concentrations of the media components (Nguyen & Lee, 2017). PC alters NPs' hydrodynamic size, surface charge, and NP colloidal stability. The interaction of NP with cells and the mechanisms of entry into cells depend on the PC composition, cell line and surface charge of NP (Behzadi et al., 2017; Docter et al., 2015; Ritz et al., 2015). In the literature

it is stated that for endocytosis the size of NPs plays a crucial role and usually is up to 50 nm. That means, NP together with PC cannot exceed the NP-PC complex "size limit" that the cell is willing to uptake. When modifying the size of PC, the NP's surface will be significant. In some cases, PC interferes with the precise transport of NPs and drug, resulting in less NPs' uptake into cells. In addition, opsonized NPs do not escape MPS (Zhang et al., 2019), which means that the circulation time of NPs in the blood shortens. To avoid these negative results, the amount of protein adsorbed on the NPs' surface should be reduced. Protein adsorption can be partially reduced by appropriate coating of the NP surface with PEG, dextran, PVP (Mosquera et al., 2020; Nguyen & Lee, 2017; Schöttler et al., 2016). It is also important to keep in mind that the surface coating of NPs changes not only the composition and size of PCs, but also the biocompatibility of NPs.

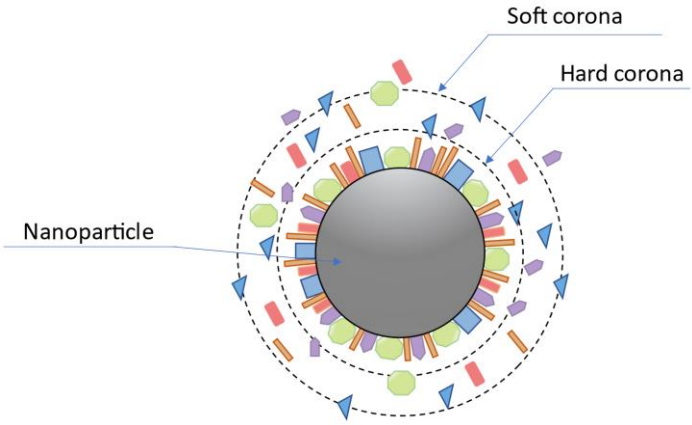

Figure 16. *Schematic representation of the protein corona forming around a nanoparticle. Adapted from* Wolfram et al., 2014.

Depending on the UCNPs surface chemistry the total amount and composition of proteins adsorbed on NPs differ. For instance, if UCNPs are put in the environment full of FBS proteins, various PCs around UCNPs surfaces will form (Voronovic et al., 2021) (refer to **Table 1**). The amount of each PC is highly dynamic and changing within 24 hours incubation, what proves that some proteins are in hard or in soft corona composition.

Table 1. *The most abundant proteins found in PCs of differently modified UCNPs and their fuction.*

Protein name (Gene name)	Function
Thrombospondin-1 (THBS1)	THBS1 is a extracellular matrix glycoprotein involved in various cellular processes, including cell adhesion, migration, proliferation, and differentiation. For example, THBS1 can bind to various cell surface receptors, such as integrins and CD36, which are involved in endocytosis and signal transduction. Moreover, it has been suggested that THBS1 may modulate lipid rafts or lipid microdomains on the cell membrane, which are involved in the formation of clathrin-coated pits and caveolae, two major pathways of endocytosis (Murphy-Ullrich, 2022).
Adenylyl cyclase-associated protein 1 (CAP1)	CAP1 is multifunctional molecule involed in actin cytoskeleton regulation and dynamics (Hubberstey & Mottillo, 2002). There are several instances in the literature about CAP1 found in NPs' PC: CAP1 was detected in PC formed around cationic surface bearing NPs (Capriotti et al., 2011) as well as 4-30 nm sized negatively charged gold NPs (AuNPs) (Correard et al., 2014).
Apolipoprotein E (ApoE)	ApoE is a protein involved in lipid metabolism, particularly in the transportation and redistribution of lipids (Yamazaki et al., 2019). If ApoE interacts with low density lipoproteins, there is a possibility that ApoE can be implicated in modulating lipid raft composition and dynamics.
Kininogen-1 (KNG1)	KNG1 is a multifunctional plasma protein involved in blood coagulation, inflammation. H-kininogen also known as KNG1, involved in kallikrein-kinin system, can function as ligand promoting caveolae-mediated endocytosis (Motta & Tersariol, 2017).

Antithrombin-III (Serpinc1)	This protein role is regulation of blood coagulation. Serpinc1 interacts mainly with low-density lipoprotein receptor-related protein 1 (LRP-1),and is important in receptor mediated endocytosis (as clathrin, caveolae -mediated endocytosis) (Bres & Faissner, 2019).
Alpha-2-macroglobulin (A2M)	A2M protein is responsible for immune response and he regulation of protease activity and activates receptor-mediated endocytosis (Borth, 1992) or appears in uptake of apoptotic cells and is suggested to be driven by macropinocytosis (Ogden et al., 2001).
Coagulation factor V and IX (F5, F9)	F9 is a key protein involved in the blood coagulation cascade. In the literature it can be found that F9 mediates macropinocytosis (Gangadharan et al., 2017).
Serum albumin (ALB)	ALB functions as transport protein of hormones, fatty acids and various other compounds in the blood stream. ALB can be internalized by receptor mediated endocytosis (Lambot et al., 2006) and macropinocytosis (Francia et al., 2019)

Protein corona composition impact on cellular uptake

Blood plasma proteins as albumin and apolipoproteins decrease monocytic cells and macrophages uptake of exomaterial. In some cases, BSA or human serum albumin (HSA) may reduce the uptake of certain molecules or particles by dendritic cells. This reduction in uptake can be due to several factors: BSA and HSA can compete with other molecules for binding sites; BSA and HSA can stabilize moleucles in the cell culture media that might prevent the degradation of certain ligands and result in uptake reduction; BSA or HSA could influence signaling pathways resulting in affected ability of dendritic cells to recognize and internalize specific molecules or particles (Thiele et al., 2003; Yan et al., 2013).

Moreover, macrophages do not uptake nanocarriers that are covered with clusterin (Aoyama et al., 2016). However, if opsonins as immunoglobulins and complement proteins are in PC, macrophages uptake these carriers and later remove them with the help of MPS (Saha et al., 2016).

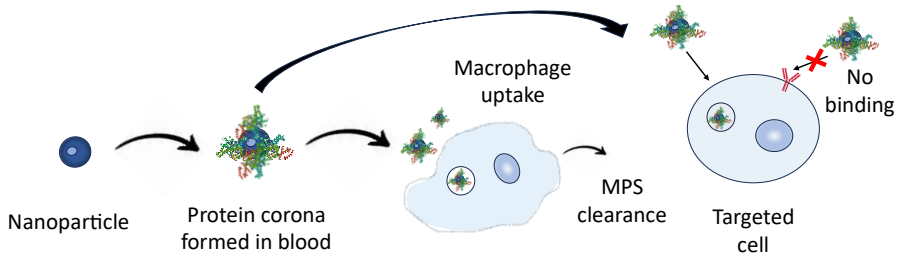

Figure 17. *The impact of the protein corona on the pharmacokinetics of nanomedicine.*

In a nutshell, after nanomedicine (NM) administration (**Figure 17**), the presence of certain proteins like albumin and apolipoproteins in the PC extends the time the NPs remain in the bloodstream, while the presence of proteins like complement proteins and immunoglobulins shortens this circulation time (Cai & Chen, 2019). During the biodistribution phase, when NPs encounter the MPS, albumin and apoliproteins as ApoE reduce the amount of NPs held in the liver and apolipoprotein A (ApoA) enhance its retention in the brain (Schäffler et al., 2014). When NPs that have not been cleared from the system but were transported to their intended destination due to biological circulation process, the PC diminishes their ability to target effectively, decreases the initial release of the drug, and initiates the biodegradation of the NPs (Cai & Chen, 2019). It is known that antibodies can assist during the NPs' travel to the target tissue. Yet, there are instances that sometimes PC totally changes cellular uptake capacity and shields the targeting ligands. For instance, accumulation of NPs can be lost *in vivo*, even though *in vitro* these results were promising. Also, *in vivo* opsonins rather than albumin adhere to the NP surface compared to *in vitro* results (Caracciolo et al., 2018). Here, the major role is played by ligands: whether they possess affinity and whether they are conjugated with the nanocarrier surface. Targeting capacity is lost when ligands are covalently bound to the surface compared to noncovalently bound ligands that retain directing capability (Tonigold et al., 2018).

The composition of the PC significantly influences the internalization of NPs by cancer cells. When complements are removed from the PC through serum heat inactivation, the uptake of carboxylate-modified polystyrene NPs by A549 cells decreases due to reduced opsonization by complements (Lesniak et al., 2010). It's important to note that the PC composition is not static; external factors like a magnetic field can enhance the cellular uptake of superparamagnetic iron oxide NPs by HepG2 cells by increasing the

adsorption of apolipoprotein (Z. Liu et al., 2016). Moreover, the number of proteins bound to NPs correlates with their cellular uptake behavior (Qiu et al., 2010). The PC can also impact the endocytic pathway of liposomes, shifting the cell entry mechanism from micropinocytosis to clathrin-dependent endocytosis (Digiacomo et al., 2017).

Overall, the PC plays a significant role in facilitating specific interactions between NPs and cells, offering opportunities for the rational design of effective nanomedicines. It is extremely important to study the influence of NPs' exposure to cells as early as possible during the development process, which is vital for the development of new NP diagnostics (Docter et al., 2015; Gnach et al., 2015; Qin et al., 2020). There are instances in the literature, stating that if NPs are without PC, NPs experience stronger affinity to the cell membrane that results in cell damage and, as a result, NPs can be found free in the cytosol (Lesniak et al., 2012). Hence, thorough examinations of the PC are crucial for identifying the optimal surface modification of NPs for biomedical applications, because up to date there is no consensus on the PC impact on biodistribution of NPs since.

2.4. Toxicity of upconverting nanonoparticles

2.4.1. Current knowledge on the UCNPs' toxicity

Despite the many potential applications of UCNPs in biomedicine, studies on ecosystem and human health effects of UCNPs are necessary. With the rapid development of UCNPs and the increasing demand for nano-sized products, the need for effective toxicity testing systems also arises. Studies show that nanomaterials accumulate differently than larger (micro or macro) materials. Micro/macro materials can cause different toxicity compared to nano sized materials due to small crystal size, high surface area and high particle mobility (Chávez-García et al., 2018; Guller et al., 2015). The interactions of NPs with biological molecules also differ. Once NPs enter the body, they interact with immune cells, somatic cells, and tissues. This interaction is beneficial for certain NP applications but also can lead to undesirable responses (Guller et al., 2015). In addition, high, specific surface/volume ratio of nanomaterials can promote the agglomeration and adsorption of bioactive molecules on the surface. The large specific surface area of nanomaterials facilitates the accumulation in cells and the transfer of NP to the target site such as the brain, bone marrow, lymph nodes, heart, but may cause harmful effects at the level of cells or proteins, may affect genotoxicity. Since UCNPs are a completely new type of NPs, their toxic

effects on human health or the environment are not yet fully known, and the entry of NP into cells, cytotoxicity, and intracellular distribution are still not fully understood (Chávez-García et al., 2018; Guller et al., 2015; Wysokińska et al., 2016). For example, UCNPs‘ surface coating not only improves UCNPs colloidal stability, biocompatibility, but also helps to avoid toxicity. The same UCNPs without coating (bare UCNPs) can cause cell death (Tian et al., 2015). Additional studies are needed to elucidate the mechanisms of NP-cell interactions, the fate of NPs in the cell, and interactions between them. One of the most important tasks of materials and biological sciences is to study the connection of UCNPs with biological processes, especially the effect on living cells (Guller et al., 2015). In the literature, there are studies with UCNPs in various cells: healthy, cancerous, stem cells (Idris et al., 2012; Khabir et al., 2019; Q. Liu et al., 2013; Yang et al., 2022; L. Zhou et al., 2015). NP size, morphology, solubility, surface charge, method of synthesis, surface functionalization affects the toxicity of UCNPs. Moreover, it is not possible to fully predict the physicochemical properties of UCNPs even with identically synthesized NPs. For example, when UCNPs are synthesized by thermal decomposition or solvothermal method, hydrophobic substances with limited solubility in media are obtained. In addition, NPs are smaller than organelles within the cell, which increases the likelihood that NPs will enter biological structures, disrupting the normal functioning of the organelles/structures.

The surface of NP has an effect when they enter through the skin, cell membranes, crossing the BBB, accumulating in the lymphatic system, entering the bone marrow, heart, lungs, central nervous system. In addition, several *in vivo* studies have shown that UCNPs can induce inflammatory responses, oxidative stress, myocardial infarction, and thrombosis (Guller et al., 2015; Wysokińska et al., 2016). UCNPs can also alter the permeability of the BBB and "translocate" through the bloodstream or lymphatic system to other parts of the body, regardless of where the UCNPs first appeared. Phagocytosis, MP, receptor endocytosis and passive diffusion are the essential processes by which many UCNPs enter cells/tissues. Therefore, it is important to consider the significance of the toxicological effects of UCNPs and to identify indicators that allow early detection of adverse health effects resulting from NP exposure.

In the literature, there are studies that mention biological damage in cells if an excess of free radicals occurs in the body, as, for instance, ROS excess, usually due to the weakening of the cell's antioxidant system (Guller et al., 2015; Wysokińska et al., 2016). Physiologically, ROS is necessary but potentially damaging. During pathophysiological states, ROS are responsible

for tissue damage and participate in many cellular processes: signal transduction, proliferation, apoptosis, DNA destruction, gene expression, protein redox control. A high level of ROS itself suggests that there is oxidative stress and that cell signal transduction mechanisms such as pro-inflammatory signaling pathways and the expression of various genes will be affected. The most widely discussed example of a redox-controlling gene in mammals is Ho-1 (Chávez-García et al., 2018; Wysokińska et al., 2016). During heme degradation, ROS can induce Ho-1, the rate-limiting enzyme, as well as obtain electrons from lipids in the cell membrane after cell damage and cell death. The process of apoptosis in cells caused by the excessive production of ROS in the cell is well known. Thus, ROS generation plays an important role in UCNPs-induced apoptosis. In addition, the p53 protein is often known as the main "defender" of the cell, as it can activate cell cycle control points, DNA repair and apoptotic responses to maintain the constancy of the genotoxin response. The p53 protein activates cell cycle arrest during DNA damage or cellular stress to allow time for repair or self-healing apoptosis. Therefore, p53 has been used as a sensitive biomarker in response to genetic toxicity (Guller et al., 2015).

2.4.2.Requirements for proper UCNPs' selection for the bioresearch

From both regulatory and industrial perspectives, ensuring the effectiveness, reliability, and safety of new biomedical applications involving UCNPs is critical for end-users. There is a global need for a standardized evaluation of nanomaterials. Lately, the European Upconversion Network (COST Action CM1403) was formed with the aim of creating and advancing innovative methods and strategies for characterizing UCNPs. According to this network, the decision tree for development and applicapibility of UCNPs was made (Oliveira et al., 2019).

Despite many scientific papers available, there is a translational gap between the laboratories and clinics. The decision tree is a great tool and risk assessment to save a lot of time, effort, money and experimental animals. The proposal outlines specific measures for acquiring particular pieces of crucial information, acknowledging that obtaining or generating such data may pose challenges.

Without access to high-quality data and the means to evaluate its reliability, the information gathered or generated may prove insufficient for conducting risk assessments (Dekkers et al., 2016; Oliveira et al., 2019).

Ultimately, it is essential to guide (**Figure 18**) the progression of emerging biomedical applications employing UCNP technology through

efficient approaches that account for both time and cost considerations. Additionally, evaluating the environmental quality standards of UCNPs in real biological contexts is imperative. These collective efforts will bridge the gap between research institutions and clinical or biomedical settings, facilitating a smoother and safer integration of UCNP-based theranostics (Oliveira et al., 2019).

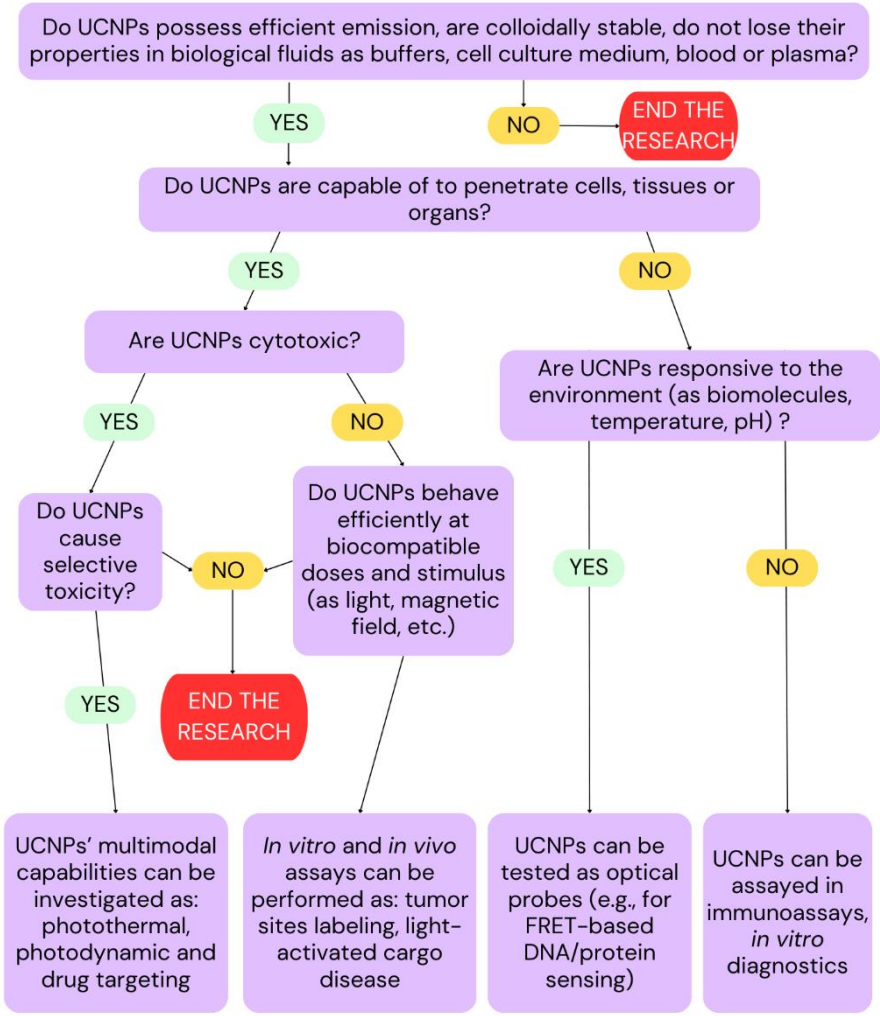

Figure 18. *The decision tree according to European Upconversion Network for proper UCNPs' selection for biomedical applications* (Oliveira et al., 2019).

2.5. Cancer cell lines as model systems for cancer research

Cancer remains one of the biggest obstacles in modern society for prolonging the lifespan of humanity. According to the World Health Organization, the second leading cause of death globally is due to oncological diseases. Breast cancer has the highest incidence rate, affecting over 2200 thousand women annually with the mortality rate over 650 thousand (Sung et al., 2021). In 2022, one in eight women worldwide was diagnosed with breast cancer, compared to only one in eleven women in 1975. Scientific progress has helped to reduce the mortality of women, but with the increasing number of cases, early cancer diagnosis is more important than ever for human life (Giaquinto et al., 2022). However, cancer treatment remains one of the biggest challenges in biomedicine, as finding effective and safe treatments for cancer is still a major obstacle (W. Wu et al., 2022).

In laboratory settings, breast cancer is frequently replicated or simulated with well-established cell lines. Using cell lines as a primary model system for cancer research is a common and valuable approach. Cancer cell lines offer several advantages that make them useful for studying various aspects of cancer biology (Gillet et al., 2013; Holliday & Speirs, 2011):

- accessibility: cancer cell lines are readily available from cell repositories;
- proliferation: cancer cell lines can be grown indefinitely in culture;
- genetic manipulation: cancer cell lines can be genetically modified using techniques such as gene editing;
- homogeneity: cancer cell lines are a homogeneous population of cells derived from a single source;
- cost-effectiveness: using cell lines for experiments is generally more cost-effective than using animal models or patient-derived samples.

By utilizing not just one but several different types of cell lines, researchers can gather the data necessary to create a partial breast carcinoma model. The classification of breast cancer relies on several criteria, including histological type, tumor grade, lymph node status, and the presence of predictive markers like estrogen receptor (ER), progesterone receptor (PR), and, more recently, HER2. Thus, breast cancer can be classified into five different subtypes: luminal A or B, HER2, basal or normal cancer type. Luminal A and B are chemotherapy responsive. If the cells lack the expression of markers, those tumors are difficult to cure, they are aggressive and have unpromising prognosis. Such phenotypes when ER, PR and HER2 are negative is called triple-negative breast cancer (TNBC) phenotype and can be classified into basal or claudin-low phenotypes. Claudin-low phenotype was

distinguished due to this subtype tumors show low expression of proliferation marker Ki67, have epithelial-mesenchymal markers and express cancer stem cells markers as $CD44^{+}CD24^{-/low}$ (Holliday & Speirs, 2011). CD44 and CD24 are responsible for cellular adhesion, cell-cell interactions, mobility, and metastases. When cells express $CD44^{+}CD24^{-/low}$, such cells actively multiply, and form tumors. Otherwise, $CD44^{+}CD24^{+}$ cells do not form tumors (Al-Hajj et al., 2003).

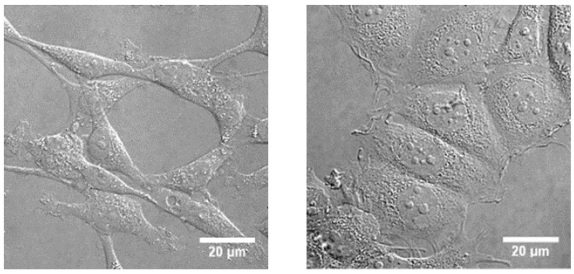

Figure 19. *Differential interference contrast microscopy images were captured 24 hours after seeding untreated cells, with a magnification of 600×* (Steponkiene, 2015).

Two types of breast cancer cell lines (**Figure 19**) often used as a model system for various anticancer drug trials are MDA-MB-231 and MCF-7. These cell lines are conveniently employed together to establish tumor model systems with varying properties for comparative purposes.

MDA-MB-231 cell line

MDA-MB-231 cell line (**Figure 19**) originates from the pleural effusion of a 51-year-old Caucasian female diagnosed with metastatic mammary adenocarcinoma from patient treated in Monroe Dunnaway Anderson hospital (currently MD Anderson cancer center) in USA. It is an epithelial human breast cancer cell line which holds a prominent place in medical research labs as one of the frequently employed cell lines (Cailleau et al., 1978).

The MDA-MB-231 cell line is classified as a highly aggressive, invasive, and poorly differentiated type of TNBC because it lacks the expression of ER and PR, as well as the amplification of HER2. Like other invasive cancer cell lines, MDA-MB-231 cells rely on proteolytic degradation of the extracellular matrix for their invasiveness. Originally categorized as a 'basal' breast cancer cell line due to the absence of ER, PR, and HER2, it is now recognized as belonging to the claudin-low molecular subtype. This reclassification is based

on characteristics such as down-regulation of claudin-3 and claudin-4, low expression of the Ki-67 proliferation marker, the presence of markers associated with epithelial-mesenchymal transition, and the expression of features linked to mammary cancer stem cells, such as the $CD44^{+}CD24^{-/low}$ phenotype. In 3D culture, this cell line exhibits a spindle-shape appearance and is known for its invasive nature, featuring stellate projections that often connect multiple cell colonies (Holliday & Speirs, 2011).

MCF-7 cell line

MCF-7 cells (**Figure 19**) were obtained from the pleural effusion of a 69-year-old female with breast adenocarcinoma (Soule et al., 1973). They were given the name which stands for Michigan Cancer Foundation, and have since become the most extensively researched human breast cancer cell line globally.

MCF-7 cells are a subject of significant interest because they exhibit several characteristics akin to mammary epithelium. These cells display an epithelial-like appearance, and when grown as monolayers, they form dome structures due to fluid accumulation beneath the cell layer. Notably, MCF-7 is one of the rare breast cancer cell lines that express estrogen receptor alpha (ER-α). When subjected to estrogen treatment, MCF-7 cells have been observed to exhibit an antiapoptotic effect, whereas anti-estrogen chemotherapy drugs like tamoxifen can inhibit proliferation and induce apoptosis, leading to reduced culture growth (Holliday & Speirs, 2011). Moreover, MCF-7 cell line has PR receptor.

2.6. Summary of literature part

Nanomaterials are extensively studied as promising tools for theranostics (G. Chen et al., 2014). The increasing demand for multifunctional biomedical applications has spurred the development of PhNPs capable of providing imaging capabilities alongside targeted and on-demand therapeutics. These NPs need to be biocompatible, able to accumulate rapidly, and effectively deliver drugs to the diseased site. Additionally, they should exhibit multispectral photoluminescence, covering wavelengths from UV-VIS to NIR, to meet the requirements for theranostic NPs (Jalani et al., 2018). However, many PhNPs have limited functionality as their excitation and emission wavelengths are confined within a narrow UV-VIS spectral range. For effective imaging, NP emissions must fall within the tissue optical transparency window, while therapeutic applications require drug release or activation by high-energy photons in the UV-VIS range (Skripka et al., 2019).

One of the promising examples of the new class of multifunctional NPs that demonstrate significant promise for biomedical applications are UCNPs. They absorb and convert NIR radiation within the optical tissue transparency window into VIS and even UV light (Jalani et al., 2018). The use of NIR excitation reduces scattering and autofluorescence in biological samples, while emitted UV-VIS and NIR photons can be utilized for cancer treatment and imaging, respectively. Despite these advantages, UCNPs are typically synthesized in organic solvents, making them unsuitable for biomedical use due to their hydrophobic surface. Rendering UCNPs hydrophilic, specific coatings as citrate, phospholipids, SiO_2, PEG, etc., are needed (Gnach & Bednarkiewicz, 2012; Rojas-Gutierrez et al., 2019).

In order to use UCNPs for diagnostics and therapy, chemical composition of UCNPs plays a major role. The final emission of the UCNPs to use NPs for theranostics should comprise of UV (for drug delivery) and NIR (for diagnostics). Great example is $LiYF_4$: Yb^{3+}, Tm^{3+}. Studies show that these UCNPs possess stronger emission bands than widely used $NaYF_4$, especially in the NIR region. Tm^{3+} in the UCNPs composition gives three main bands at 360 nm, 475 nm and 800 nm. Band at 800 nm is quite strong in emission that makes it great tool for diagnostics (Jiang et al., 2016).

Other characteristics of UCNPs, apart from surface modification to make them suitable for biomedical research, include size, shape and PC formed around them. The optimal size of the NPs for cellular accumulation, according to the literature, is around 50 nm, with a diamond-like shape and the PC – as small as possible, preferably with PEG in the PC. PEG is used to extend NP blood circulation time due to lower affinity of proteins binding to the NPs surface, rendering higher accumulation in cells.

Before NPs approach the cell membrane (CM), they encounter various factors such as surrounding proteins and extracellular matrix, which can alter their properties along with the pH, etc. These factors, along with the surrounding proteins, can modify the characteristics of the NPs prior to their internalization. Typically, the interaction of the NP-protein complex with the cell begins with its adherence to the cell membrane. Later, endocytosis, the process of NP-protein complex entry into the cell, occurs. There exist two forms of endocytosis: pinocytosis, which involves the intake of liquids and insoluble substances into cells, and phagocytosis, which entails the ingestion of large particles into cells (Behzadi et al., 2017; Docter et al., 2015; Sikora et al., 2017).

Cells uptake not bare NPs, but NPs covered with protein layer – PC. PC composition depends on the relative concentration of components of the environment in which NPs are dispersed. Usually, the PC consists of proteins

as serum albumin, complement proteins, immunoglobulins, etc. The composition of the PC is intricate and distinct for every NPs' surface coating. To enhance blood circulation time, NPs should avoid MPS, meaning that the size and composition of the PC should be controlled. Protein adsorption on the NPs' surface can be minimized by modifying the NPs' surface with PEG, PVP and dextran (Mosquera et al., 2020; Nguyen & Lee, 2017; Schöttler et al., 2016). Moreover, the amount of proteins adsorbed on NPs' surface correlates with their cellular accumulation (Qiu et al., 2010). PC affects the endocytosis mechanisms cells use to uptake NPs (Francia et al., 2019).

As UCNPs represent a novel category of NPs, their potential adverse impacts on human health and the environment remain largely unexplored. Understanding their mechanisms of cell entry, cytotoxicity, and distribution within cells is still incomplete, as highlighted by previous studies (Chávez-García et al., 2018; Guller et al., 2015; Wysokińska et al., 2016). Both from regulatory and industrial standpoints, it is imperative to guarantee the efficiency, dependability, and safety of emerging biomedical uses incorporating UCNPs for end-users. There exists a worldwide demand for a uniform assessment framework for NPs. Recently, the establishment of the European Upconversion Network (COST Action CM1403) has been initiated with the objective of devising and enhancing innovative approaches and tactics for assessing UCNPs. In accordance with this network, a decision-making framework for the advancement and suitability of UCNPs has been formulated (Oliveira et al., 2019). According to Upconversion Network members, if these instructions are followed, translational gap between laboratories and clinics will vanish faster.

For the study of multifunctional NPs (as UCNPs), it is imperative to apply right model system. Nowadays, breast cancer is one of the most leading maladies worldwide. In laboratory environments, breast cancer is often mimicked or reproduced using established cell lines. Employing cell lines as a principal model system for cancer investigation is a widely adopted and valuable method. There are two types of breast cancer cell lines that are applied as model system for various studies – human adenocarcinoma cell lines MCF-7 and MDA-MB-231. MCF-7 cells have ER and PR, making them particularly valuable for studying hormone-responsive breast cancers. The MDA-MB-231 cells have a mesenchymal-like morphology and display high migratory and invasive capabilities, resembling features of TNBC, a subtype associated with poor prognosis (Holliday & Speirs, 2011).

In conclusion, the interaction between UCNPs and cancer cells is influenced by various factors, including the coatings on the UCNPs and the formation of a PC upon exposure to biological environments. The choice of

coating can significantly impact the behavior of UCNPs within biological systems, affecting their uptake, cytotoxicity, and intracellular distribution in cancer cells. Additionally, the formation of a PC around UCNPs can alter their surface properties and biological interactions, further influencing their behavior in cancer cell environments. Understanding these complex interactions is crucial for the development of effective and safe nanoparticle-based therapies for cancer treatment.

3. METHODS

The UCNPs used in this research were synthesized, coated with citrate, phospholipids, and SiO_2 and structurally characterized at the National Institute for Scientific Research (INRS[6]), Quebec, Canada by Dr. Artiom Skripka. For further research, the surface of synthesized UCNPs was modified with brush-type polymers by Dr. Vaidas Klimkevičius at Institute of Chemistry, Vilnius University.

3.1. Synthesis and coating of upconverting nanoparticles

$LiYF_4:Yb^{3+}$ (25 mol %), Tm^{3+} (0.5 mol %) UCNPs were synthesized via thermal decomposition method by Dr. A. Skripka. The result of such synthesis is oleate-capped UCNPs. Further, these hydrophobic UCNPs were additionally coated with citrate, phospholipids, silica, brush-type polyelectrolytes or ligand-free to make them hydrophilic.

Citrate coating

Citrate coating was carried via ligand exchange procedure. Primarily obtained oleate-capped UCNPs were mixed with trisodium citrate buffer, aqueous phase of UCNPs was isolated through separatory funnel and precipitated with acetone. The pellet was redispersed with trisodium citrate buffer and stirred for 2 hours. Then, precipitation with acetone was carried. Finally citrate capped UCNPs (cUCNPs) were redispersed in distilled water (DW) and put for storage at 4 °C.

Phospholipid coating

Phospholipid coating was carried via phospholipids encapsulation method. Oleate-capped UCNPs were dispersed in chloroform, together with 1,2-dioleoyl-sn-glycero-3-phosphoethanolamine-N-[methoxy (polyethylene glycol) - 2000] (PEG-DOPE) and 1,2-dipalmitoleoyl-sn-glycero-3-phosphocholine (DOPC) phospholipids. Final phospholipid concentration is 1:4, respectively. Chloroform was evaporated with the help of argon gas and as a result dry phospholipid-UCNPs (pUCNPs) film was obtained. This film was later hydrated, filtered, and stored at 4 °C for later experiments.

[6] Institut national de la recherche scientifique.

Silica coating

Silica coating was carried via silica encapsulation method. Oleate-capped UCNPs were dispersed under stirring in cyclohexane, Igepal (nonionic, non-denaturing detergent) and ammonium hydroxide. Further, tetraethylorthosilicate was added and the mixture was left for 24 h at ambient temperature. Finally, silica coated UCNPs (sUCNPs) were precipitated with acetone and washed with pure ethanol, redispersed in DW, and stored at 4 °C for later experiments.

Ligand removal

Oleate-capped UCNPs were mixed with DW (adjusted with HCl, pH 4) and left for 3 h stirring. The aqueous phase was isolated with separatory funnel. Then UCNPs were precipitated with acetone, centrifuged. UCNPs pellet was redispersed with DW (pH 4) and was stirred for 2 h. Later, UCNPs were centrifuged with acetone, redispersed in DW, and washed with water/acetone mixture. As a result, oleate-free UCNPs were obtained and were dispersed in DW and stored at 4 °C for later experiments.

Brush-type polyelectrolyte coating

Dry ligand-free UCNPs were redispersed in aqueous polymer solution (with the pH of 5.0), then with polymer solution with the same pH and finally the solution was stirred for 1 hour at ambient temperature. The possible excess of polymer was removed via centrifugation and washing cycles. After this procedure, UCNPs were redispersed in deionized water (DI) and stored at 4 °C for later experiments. Here, two different types of polymer coating UCNPs were obtained: containing 25% of PEG ([MAA]:[PEO_9MEMA], molar ratio 3:1) and 75% of PEG ([MAA]:[PEO_9MEMA], molar ratio 1:3).

Throughout whole dissertation cUCNPs, pUCNPs, sUCNPs are abbreviated as I-UCNPs. Polymer coated and ligand-free UCNPs as II-UCNPs.

3.2. Spectral characteristics

During the dissertation, research was conducted on I- and II-UCNPs. The UC spectra of I-UCNPs were measured using an Edinburgh Instruments FLS920 fluorometer (Edinburgh Instruments, UK). This fluorometer was

modified with an additional continuous laser (λ = 980 nm, MDL–III–980–2W, Changchun New Industries Optoelectronics Technology Co., China) for UCNPs' excitation. The spectra of the I-UCNPs' colloidal solutions prepared in various media were obtained in polystyrene cuvettes with an optical path length of 1 cm. The width of the emission slit was kept constant at 5 nm.

II-UCNPs were investigated in quartz spectrofluorometric cuvettes and measured with Edinburgh Instruments FLS980 (Edinburgh Instruments, UK) fluorimeter. The emission slit was kept at 0.5 nm.

3.3. Colloidal stability

The colloidal stability of UCNPs were tested in various solutions, including DW, PBS, cell culture medium (Dulbecco's modified eagle medium, DMEM) either alone or supplemented with 10 % (v/v) fetal bovine serum (FBS, Gibco, Waltham, MA, USA, standard, origin: Brazil, REF 10270-106, LOT 24440035) for 7-8 days, with a concentration of 0.1 mg/mL (for II-UCNPs) or 1 mg/mL (for I-UCNPs). The stability was evaluated as emission intensity change at λ = 793 nm (where is Tm^{3+} emission $^3H_4 \rightarrow {}^3H_6$) in time. Cuvettes were positioned within a temperature-controlled holder set at 25°C to reduce any heat generated within the solution during extended laser exposure. All measurements were conducted in total of n=3 replicates.

3.4. Hydrodynamic size and charge evaluation

The hydrodynamic size of I-UCNPs was measured using dynamic light scattering (DLS) method. NP size was measured with a ZetaPALS particle hydrodynamic size and zeta potential meter using 633 nm laser (Brookhaven Inc., USA) after setting 10 measurement cycles without pause.

The hydrodynamic size of II-UCNPs was measured as I-UCNPs, but using ZetaSizer nano ZS (Malvern, UK). Measurements were performed at 25 °C.

3.5. Cell cultivation

For the cell experiment, two human adenocarcinoma cell lines, MDA-MB-231 and MCF-7, were used. The MDA-MB-231 cell line was purchased from the American Type Culture Collection, while the MCF-7 cell line was obtained from the European Collection of Cell Cultures. For the assays, cells were cultured in a complete cell culture medium comprising DMEM, 10% FBS, and a mixture of the antibiotic penicillin (100 U/mL) and streptomycin

(0.1 g/mL) (Pen-Strep 10000 U/mL and 0.01 g/mL, P/S, Gibco, Germany). The cells were grown in an incubator at 37°C and 5 % CO_2.

3.6. Incubation of cells with nanoparticles

Cellular imaging, uptake dynamics and intracellular localization experiments with UCNPs were performed using confocal microscopy technique. Since experiments involve UCNPs, it was necessary to make modifications to the confocal microscope to accommodate the 980 nm laser. To enable the alternate stimulation of UCNPs, optical fibers were integrated into the scanning system. The NIR laser's radiation is directed through mirrors and a lens system to the fiber optic. Subsequently, lens systems are employed to shape the laser light beam, ensuring its maximum concentration within the fiber optic cable. Achieving this required the use of a 5-axis transmitter to which a fiber optic holder-adapter was attached. This method involved the use of a 200 μm diameter multimode fiber, and images were captured using a Nikon Plan Apochromat 60.0x/1.40/0.13 immersion lens.

3.6.1. Confocal scanning microscope for UCNPs imaging

A confocal scanning laser microscope (LSCM) possesses a unique capability known as optical layering, which allows it to capture clear and well-focused images from different depths within the same specimen. In this type of microscope, a focused laser beam is used to excite the specimen, causing it to emit coherent radiation. This laser beam precisely targets a single point on the object. The result of this excitation is the emission of fluorescence. It's important to differentiate between the light emitted by molecules situated in the focal plane of the objective lens and the light emitted by molecules located outside of this focal plane.

In both cases, the emitted light from these molecules passes through the lens and the scanning system. However, a confocal microscope eliminates out-of-focus fluorescence by incorporating a confocal diaphragm in front of the detector. This diaphragm blocks out-of-focus light coming from planes above or below the focal plane, as well as any stray light entering the detector. As a result, only the fluorescence emitted by molecules in the focal plane of the objective lens is recorded. This unique feature allows the confocal scanning laser microscope to simultaneously illuminate a specific spot on the sample and detect the light emitted from a distinct volume segment.

The excitation laser radiation is directed by a dichroic mirror to the lens, which focuses it onto the sample. This mirror reflects the excitation light and

transmits the emitted fluorescence. By employing mirrors, the excitation laser radiation can be sequentially directed to different points within the focal plane through scanning in the x and y axes. This approach allows for the excitation of a larger portion of the object, rather than just a single specific point. While the focal length remains fixed in the z-axis during scanning, the volume element of interest moves across the desired area of the sample within one focal plane. By adjusting the focal length, individual optical layers of the sample can be captured, and subsequently, a 3D image and the structure of the specimen can be reconstructed.

3.6.2.Experiments with I-UCNPs: accumulation dynamics and in vitro imaging

To conduct the accumulation experiments, a dosage of 0.04 g/mL for I-UCNPs was selected. Cells were initially seeded in 12-well plates (TPP tissue culture plates from Switzerland), at the density of $1 \cdot 10^5$ cells/well, at 37 °C in a humidified environment with 5 % CO_2 for 24 hours. Following this, the cells were exposed to I-UCNPs for varying durations of 0.5, 1, 3, 6, 9, and 24 hours under the same cell incubation conditions. After the incubation period, the culture medium containing I-UCNPs was gently aspirated, and the cells were washed three times with PBS. Subsequently, the cells were trypsinized with 0.25% (v/v) trypsin (Gibco, USA) and centrifuged in fresh medium at 200 *g* for 7 minutes.

To evaluate the dynamics of I-UCNPs accumulation within the cells, the emission intensity of the I-UCNPs that had accumulated in the cells was measured using an Edinburgh spectrometer FLS920 with a 980 nm laser. The emission intensity of cell suspensions was recorded with continuous stirring. The accumulation dynamics were determined by calculating the emission intensity at specific time points divided by the number of cells in the suspension at those times, and data was plotted as emission intensity per cell.

To conduct intracellular imaging experiments, cells were initially placed in specialized 8-well chamber slides with removable wells (Lab-Tek chambers from Nunc, Thermo Fisher in Denmark). These cells were seeded in each chamber at a density of $3 \cdot 10^4$ cells and then incubated at 37 °C in a controlled, humidified atmosphere with 5% CO_2 for a 24-hour period.

To investigate the dynamics of uptake and intracellular distribution of I-UCNPs with different coatings, the cells were exposed to I-UCNPs at a concentration of 0.1 g/mL for varying durations, of 1, 3, 6, and 24 hours. Prior to capturing images, the cells were fixed by an ample amount of 4% paraformaldehyde (Sigma-Aldrich, Germany) for a duration of 15 minutes to

ensure comprehensive cell coverage. After the fixation process, the cells were stained with a nuclear dye, specifically Hoechst 33258 from Sigma-Aldrich in Germany, at a concentration of 0.01 g/mL. Furthermore, the cells were stained with Phalloidin-Alexa 488 at 165 mM, a staining agent that specifically targets the filamentous actin within the cells. This staining agent is sourced from Invitrogen, Thermo Fisher in the US.

The accumulation of I-UCNPs within cancer cells was observed utilizing a confocal Nikon Eclipse Te2000-S C1 Plus Laser scanning microscope. This microscope was equipped with continuous wave lasers emitting at wavelengths of 405 nm and 488 nm from Melles Griot in the USA, as well as a 980 nm laser from Changchun New Industries Optoelectronics Tech. Co., Ltd. in China.

To visualize specific components, the nucleus stain Hoechst 33258 was excited at 404 nm, Phalloidin-Alexa 488 at 488 nm, and the UCNPs were excited at 980 nm. The imaging process involved the use of a 60x/1.4 NA oil immersion objective from Nikon made in Japan. A three-channel RGB detector was employed: the emission of I-UCNPs was recorded in the blue channel using a 450/17 bandpass filter, although a red pseudo color was applied to the images for enhanced visualization. The fluorescence emitted by Hoechst 33258 and Phalloidin-Alexa 488 was detected in the blue (450/17) and green (545/45) channels, respectively. For image processing, Nikon EZ-C1 Bronze version 3.80 and ImageJ 1.46 software were utilized.

All cell experiments were conducted in triplicates (n=3), with a total subject count of N=3.

3.6.3.Experiments with II-UCNPs: in vitro imaging

In vitro imaging for II-UCNPs experiments were performed in the same manner as for I-UCNPs. Cells were seeded in 8-well chamber slide with removable wells, cultivated for 24 hours to achieve full cell attachment. Later, cells were treated with 0.1 mg/mL of II-UCNPs for 24 hours. Before capturing images, the cells were covered and fixed with 4% paraformaldehyde, the cell nuclei were stained using Hoechst 33258 and actin filaments were stained with Alexa Fluor 488 phalloidin. The accumulation of II-UCNPs within the cells was observed using a confocal Nikon Eclipse Te2000-S C1 Plus Laser scanning microscope equipped with continuous wave lasers: 405 nm, 488 nm and 980 nm. Both cellular dyes were excited by 404 nm (Hoechst) and 488 nm (Alexa Fluor 488 phalloidin) excitation wavelengths, while II-UCNPs were excited at 980 nm. All images were captured with consistent imaging parameters. 3D cellular imaging was obtained with a 1 μm step size, and the

images were processed using Nikon EZ-C1 Bronze version 3.80 and ImageJ 1.46 software.

3.7. Cell viability assays

Cell viability for MDA-MB-231 and MCF-7 cells was evaluated using three different methods: lactate dehydrogenase (LDH), ADAM-MC Automatic Cell Counter, and sodium 3′-[1- (phenylaminocarbonyl)- 3,4-tetrazolium]-bis (4-methoxy6-nitro) benzene sulfonic acid hydrate (XTT) methods.

LDH assay is a sensitive method to detect LDH release from damaged cells. LDH can be found in many cells as cytosolic enzyme. When plasma membrane is damaged, LDH is released into environment. The amount of LDH present in the extracellular media can be measured through an enzymatic process where LDH converts lactate into pyruvate by reducing NAD^+ to NADH. Subsequently, diaphorase utilizes NADH to reduce a tetrazolium salt called INT into a red formazan product that can be quantified at 490 nm. The extent of formazan formation is directly related to the quantity of LDH released into the medium, serving as an indicator of cytotoxicity.

In the LDH assay cells were initially seeded in a 96-well plate (BD Falcon, USA) at a density of 20,000 cells per well. After 24 hours, the old medium was replaced with fresh medium containing I-UCNPs at concentrations of 0.004 g/mL, 0.04 g/mL, or 0.4 g/mL. Medium without I-UCNPs served as the control. The cells were then incubated in the dark for 24 hours. I-UCNPs have the potential to induce cell cytotoxicity and increase membrane permeability, leading to the release of LDH into the cell medium. The LDH released into the medium was subsequently transferred to a new plate and detected using the LDH cytotoxicity assay (Thermo Scientific, USA) by measuring absorbance at both 490 nm and 680 nm with a plate-reading absorption spectrophotometer (BioTek, USA). The detection procedure was performed following the manufacturer's instructions. The obtained absorbance values were then converted into percentage values of cell viability.

ADAM-MC automated fluorescence cell counter performs cell counting and cell viability assays. Principle of viability measurements is based on fluorescent DNA intercalating dye – propidium iodide (PI) and non-viable cells interaction. The counter counts two types of cells: total cell count and non-viable cells. For total cell number, PI with lysis buffer is added into cell suspension. In this case, all cells have permeable membrane resulting in

stained DNA. For non-viable cell number, only cells with permeable membrane are stained with PI.

In the study, cells were resuspended in 100 μL of PBS, and both cell viability and the total cell count were determined using the ADAM-MC automatic cell counter (Digital Bio, Seoul, Korea). The assessment of cell viability and the total cell count was performed automatically by the ADAM-MC software.

The XTT method is utilized to examine the metabolic activity of cells based on their redox potential. Viable cells possess the mitochondrial succinate dehydrogenase system, which cleaves XTT salt into a water-soluble, orange-colored formazan. This formazan can be directly quantified using a spectrophotometer. The XTT assay was conducted following the manufacturer's instructions. Six wells were used for each type of II-UCNPs, and an additional six wells served as a control, without any II-UCNPs, to provide baseline absorbance readings. The optical density at 490 nm was determined using a BioTek 800 TS microplate reader after the incubation with the tetrazolium dye was completed.

All measurements were carried out with a sample size (n) of six. To assess the significance of differences between groups, a two-tailed independent Student's t-test was performed at a 95% confidence level, with significance denoted as a p-value less than 0.05.

3.8. Localisation analysis

Cells were cultured in complete DMEM medium and were exposed to 0.1 mg/mL of II-UCNPs for a duration of 24 hours. Additionally, they were treated with 75 nM of a lysosome dye, LysoTracker Deep Red from Invitrogen, USA, for 2 hours. Confocal fluorescence images were captured separately in each fluorescence channel and then combined into a single composite image. The Pearson's correlation coefficient (PCC) was subsequently computed from a set of five images for each sample.

3.9. Cell endocytic pathway inhibition

Cells were cultured in 12-well plates for two days at a density of $1 \cdot 10^5$ cells per well. Subsequently, they were exposed to various endocytosis inhibitors: nystatin (Nys), chlorpromazine (Chlor), nocodazole (Noc), or 5-(N-Ethyl-N-isopropyl) amiloride (EIPA), for 1 hour at concentrations as detailed in **Table 1**. These inhibitors were prepared in DMEM complete medium. After the incubation period, the medium containing the inhibitors

was removed, and the cells were washed three times with fresh medium. The cells were then exposed to DMEM complete medium containing 40 μg/mL of I-UCNPs and incubated for 3 hours in a 37 °C humidified CO_2 incubator.

Table 2. *Endocytic pathway inhibitors and their concentrations*

Name of inhibitor and its abbreviation in brackets	Concentration, μg/mL	Inhibition mechanism
4 °C	-	Metabolism of the cell
Nystatin (Nys)	25	Depletes lipid raft formation
Chlorpromazine (Chlor)	10	Inhibition of clathrin-mediated endocytosis
Nocodazole (Noc)	5	Microtubule formation; clathrin mediated endocytosis
5-(N-ethyl-N-isopropyl)amiloride (EIPA)	3	Macropinocytosis

Following incubation with the I-UCNPs, the cells were again washed three times with PBS, trypsinized, and centrifuged at 200 *g* for 7 minutes. The cells were resuspended in 500 μL of PBS, counted, and the inhibition of endocytosis was assessed by measuring the emission of I-UCNPs that had accumulated within the cells using an FLS920 spectrometer under 980 nm laser excitation.

Additionally, the accumulation of I-UCNPs in cells after treatment with the inhibitors was visualized using a confocal microscope. Both MDA-MB-231 and MCF-7 cells were seeded in 8-well chamber slides with removable wells at a density of $3 \cdot 10^4$ cells per chamber. They were then incubated with 40 μg/mL of I-UCNPs at 37 °C in a humidified atmosphere with 5% CO_2 for 24 hours. Following incubation, the cells were treated with endocytosis inhibitors (Nys, Chlor, Noc, or EIPA) for 1 hour at the concentrations specified in Table 1. The cell medium containing the inhibitors was then replaced with DMEM complete medium containing 100 μg/mL of I-UCNPs. The cells were incubated with the I-UCNPs for 3 hours in a 37 °C humidified CO_2 incubator. After the incubation, the cells were fixed and stained as previously described in 3.6.2.

3.10. Proteomic analysis

Electrophoresis

To identify dynamics and changes in PC forming around I-UCNPs in 24 hours, 3 independent replicates were prepared and assayed with UCNPs. Firstly, 0.04 mg/mL of UCNPs were incubated in 1.2 mL of cell growth medium DMEM supplemented with 10% FBS at 37 °C and rotated for 3 hours in tube rotator following centrifuging for 15 min at 15,000 *g*. Then the samples were washed four times with PBS and suspended by vortexing for max 20 sec. Subsequently, samples were dilluted with sample buffer, then heated for 3 min at 100 °C. SDS PAGE was conducted. Electrophoresis gel was stained with Page Blue for 6 hours. Later, samples were prepared for proteomics and analysed.

Preparing samples for proteomics

I-UCNPs at concentrations of 0.04 mg/mL were subjected to incubation in 1.3 mL of DMEM containing 10% FBS at 37 ºC for varying durations of 1, 3, 12, or 24 hours. Following the incubation, I-UCNPs were cleansed through four rounds of washing with PBS via centrifugation. To extract proteins from the I-UCNPs, an elution buffer was employed, which contained 4% sodium dodecyl sulfate, 100 mM Tris/HCl at pH 7.6, and 100 mM dithiothreitol. The extracted proteins were stored at -86 ºC for subsequent analysis.

For trypsin digestion, proteins were diluted in 8 M urea and loaded onto protein concentrators featuring a polyethersulfone membrane with a molecular weight cutoff of 30 kDa. After two washes with urea, proteins were subjected to alkylation using 50 mM iodoacetamide. The protein concentrators were rinsed twice with urea and twice with 50 mM NH_4HCO_3. Proteins were digested overnight using L-1-tosylamido-2-phenylethyl chloromethyl ketone-treated trypsin.

Following the overnight digestion, peptides were collected from the concentrators via centrifugation at 14000 *g* for 1 minute and further eluted through two washes using 20% CH_3CN. The eluates were combined, acidified with 0.1% CF_3COOH, and then subjected to lyophilization in a vacuum centrifuge. The lyophilized peptides were subsequently reconstituted in 0.1% formic acid.

3.11. Cell surface proteome analysis

Comparative proteomic analysis of MDA-MB-231 cell surface proteome was performed firstly labeling proteins on the cell surface with biotin, later identifying them by liquid chromatography mass-spectrometry (LC-MS).

Surface proteins from MCF-7 or MDA-MB-231 cells were concentrated through a biotin labeling method. For each sample, cells were cultured in 6 dishes with a 10 cm diameter until they reached a subconfluent density, using DMEM medium supplemented with 10% (v/v) FBS. The cells were then washed three times with ice-cold PBS (pH 7.4), containing 2 mM $MgCl_2$ and 1 mM $CaCl_2$ (PBS/Ca/Mg), and incubated in the dark on ice for 20 minutes with a solution of 1 mM NaIO4 in 0.1 M sodium acetate and 0.15 M NaCl at pH 5.5. This step was carried out to oxidize polysaccharide groups. The reaction was halted by adding glycerol to achieve a final concentration of 1 mM, and the cell monolayer was washed three times with ice-cold PBS/Ca/Mg.

To biotinylate proteins, the cells were treated for 1 hour with a solution of 100 mM EZ-Link Alkoxyamine-PEG4-Biotin from Thermo Fisher Scientific in ice-cold PBS supplemented with 5% (v/v) FBS and 10 mM aniline. The cell monolayer was washed three times with ice-cold PBS and then solubilized in a lysis buffer, consisting of 150 mM NaCl, 1% (v/v) IGEPAL CA-630, 10 mM Tris HCl at pH 7.5, and Pierce Protease Inhibitor Tablet (EDTA-free) from Thermo Fisher Scientific. Lysates were cleared by centrifugation at 4 °C, 22000 *g* for 15 minutes and subsequently incubated for 1 hour on an end-over-end shaker with 70 µL bed volume of High-Capacity Streptavidin Agarose at 4 °C. The agarose resin was washed three times with the lysis solution, and bound proteins were eluted using 200 µL elution buffer. This elution buffer contained 4% (w/v) 3-((3-cholamidopropyl) dimethylammonio)-1-propanesulfonate, 7 M urea, 2 M thiourea, 10 mM Tris-HCl at pH 8.3, and 3 mM biotin. Unbiotinylated cells were employed as a negative control. The eluted proteins were digested following a modified FASP protocol, as previously described.

3.12. Statistical analysis

All data were reported as the mean value with the corresponding standard deviation. The sample size (n) was 3-6, except for the results regarding the dynamics of I-UCNPs accumulation, which had a sample size of 9. Statistical significance was determined by conducting a two-tailed independent Student's t-test with a confidence level of 95%. Any findings with a p-value less than 0.05 were considered statistically significant.

4. RESULTS AND DISCUSSION

In this study, two types (different by size) of $LiYF_4$:Yb^{3+}, Tm^{3+} UCNPs coated with various coatings were studied. The concentration of dopant ions for both types of UCNPs were: 25 % for Yb^{3+} and 0,5 % for Tm^{3+}. All obtained results are described in each of the subchapter.

4.1. Structure of upconverting nanoparticles

UCNPs are required to be hydrophilic and biocompatible. To render them well-suited to use for biological purposes, in this research $LiYF_4$: Yb^{3+}, Tm^{3+} UCNPs were coated with five coatings:

- citrate, SiO_2, phospholipids (PEG-DOPE:DOPC with the molar ratio 1:4). Throughout the thesis these three modifications are abbreviated to first modification UCNPs, or I-UCNPs;
- two types of brush-type polymer coatings and abbreviated as P_9MAA-25 and P_9MAA-75 (the general formula for both coatings are p(MAA-*co*-PEG$_9$MEMA)), called as second modification UCNPs, or II-UCNPs. Here, numbers 25 or 75 indicate low and high charge densities, where differences lie in PEGylation density. P_9MAA-25 is highly PEGylated, whereas P_9MAA-75 has three times lower PEGylation density than P_9MAA-25.

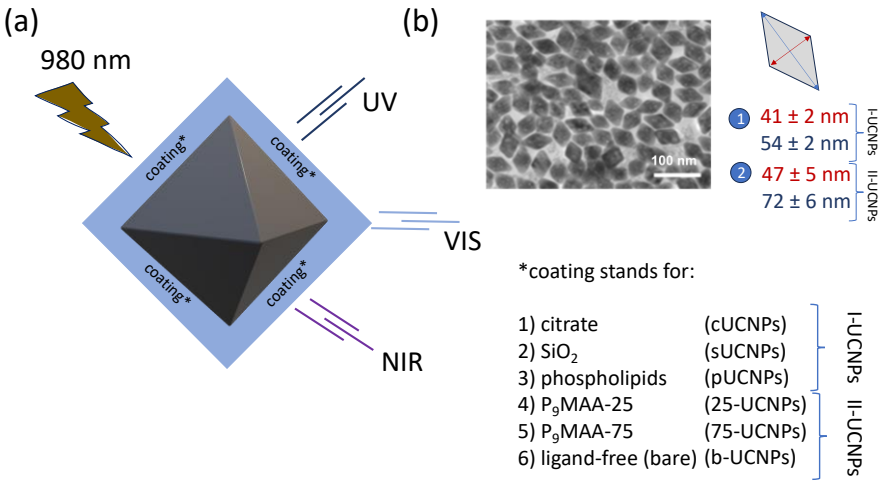

Figure 20. *(a) – structural characterization of $LiYF_4$:Yb^{3+},Tm^{3+} UCNPs. As it seen from the scheme, UCNPs are excited by 980 nm wavelength and emitting emission from UV to NIR. (b) – transmission electron microscopy (TEM) image of ligand-free UCNPs. Also, UCNPs are*

coated with six coatings as stated in a figure. 1, 2, 3 coating bearing UCNPs in a thesis are called first modification UCNPs (I-UCNPs) with size around 41 nm and 54 nm along minor and major axes (1). 4, 5, 6 coating bearing UCNPs in a thesis are called second modification UCNPs (II-UCNPs) with size around 47 nm and 72 nm along minor and major axes (2).

Representative scheme of UCNPs is shown in **Figure 20**. UCNPs were excited by 980 nm continuous wave laser and upon the UC NIR irradiation was converted to the light spanning from UV to NIR emission (**Figure 20 a**). Transmission electron microscopy (TEM) image taken for b-UCNPs (**Figure 20 b**) shows UCNPs to be of "diamond" morphology, well dispersed, homogenous. NPs of this unusual shape accumulate in cells better and have greater optical properties than $NaYF_4$:Yb^{3+}, Tm^{3+} UCNPs (Rojas-Gutierrez et al., 2019). A similar bipyramidal morphology was observed in the I-UCNPs (results are not shown). The size of the I-UCNPs was approximately. 41 nm in the minor axis and 54 nm in major axis. For the second type of UCNPs (II-UCNPs) – size was 47 nm and 72 nm, minor and major axes respectively.

4.2. Optical properties of upconverting nanoparticles

To use UCNPs for biomedical purposes, it is important to synthesize NPs that possess great emission intensity. Usually, emission intensity of UCNPs differs depending on the surface coating (Liras et al., 2014). However, there are reports claiming there are no changes in emission intensity of UCNPs coated by cationic, anionic, or neutral coatings (Palo et al., 2018). In this work, $LiYF_4$: Yb^{3+}, Tm^{3+} coated UCNPs emission spectra in DW are shown in **Figure 21**.

These UCNPs samples were excited by 980 nm wavelength laser. Under this excitation Yb^{3+} ions are being excited and energy transfer from Yb^{3+} to Tm^{3+} ion occurs. As a result, emission from Tm^{3+} excited states give spectra that are recorded by fluorimeter. As seen from the **Figure 21**, UCNPs emit the light from UV to NIR region. In the spectra six main peaks at 345, 360, 450, 481, 646, and 793 nm can be distinguished, which correspond to electronic transitions of thulium ions. Two of these peaks, 345 and 360 nm, are in the UV region, while one at 793 nm is in the NIR region. Therefore, these UCNPs are suitable for both the diagnosis and therapy. UCNPs emission in the NIR region (at 800 nm) is suitable for deep tumor diagnosis, due to the emission at 793 nm lays in biological optical transparency window (750 – 950 nm) (Skripka et al., 2019). Moreover, emission at UV region can be used for

photodynamic therapy if UV absorbing sensitizer is linked to the UCNPs. Sensitizer itself does not do any damage to the cell unless it is excited by the UV wavelength. Such approach can be used for selective therapy: if UCNPs are inside the cell, UCNPs are excited by NIR, and UCNPs emission excites the photosensitizer and no damage of the UV is done to the cell or organism due to non-harmful NIR excitation of the UCNPs (Z. Zhang et al., 2020).

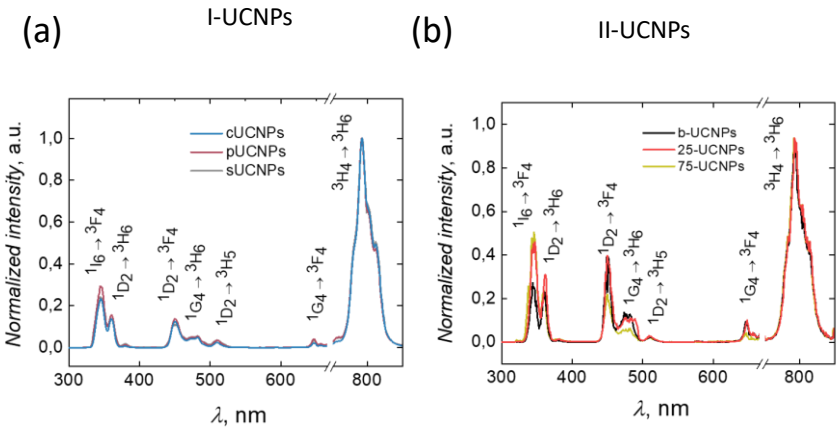

Figure 21. *(a) Emission spectra of cUCNPs, pUCNPs, sUCNPs, 25-UCNPs, 75-UCNPs and (b)-UCNPs in distilled water (DW) under 980 nm excitation. The concentration of UCNPs in all samples were 0.1 mg/mL. Radiative transitions of* Tm^{3+} *are shown above the peaks of emission bands.*

Almost no change in emission is detected for I-UCNPs, independent of the coating. If results are normalized to the highest emission peak (at 793 nm) no changes in emission bands spanning from UV to NIR are observed. In case of II-UCNPs, emission in the NIR region is lower for the ligand-free UCNPs. It can be due to water molecules interaction with UCNPs, and the phenomena called as water quenching (K. Zheng et al., 2019). Usually, water quenching on UCNPs emission is minimized by amphiphilic or hydrophobic polymer coatings (Steponaviciute et al., 2020). Comparing coated and uncoated UCNPs higher emission intensity is detected because of coatings' protection from water molecules (Steponaviciute et al., 2021). Normalized spectra show only slight difference in UV b-UCNPS emission bands that also can be explained via water quenching phenomena.

4.3. Evaluation of the size and zeta potential of the upconverting nanoparticles

NPs parameters as proper size and zeta potential (ζ) determine whether those NPs are usable for cellular studies. Small NPs can accumulate at higher rates than bigger counterparts in cells. Optimal size of NPs to be engulfed by the cells is around 50 nm (Rojas-Gutierrez et al., 2019). On the other hand, the size of NPs should not exceed the "red line" of 200 nm to escape uptake by the MPS.

Table 3. *Differently coated $LiYF_4$:Yb^{3+}, Tm^{3+} nanoparticles' mean size and zeta potential in distilled water.*

	Approx. hydrodynamic size (nm)	PdI	ζ (mV)
cUCNPs	46.0	0.2	- 25.1
pUCNPs	56.0	0.2	- 10.7
sUCNPs	85.0	0.1	- 44.0
b-UCNPs	45.0	0.2	27.9
25-UCNPs	90.0	0.2	- 1.6
75-UCNPs	85.0	0.2	- 14.3

For NPs size and charge evaluation hydrodynamic size measurements as well as ζ were performed in DW. Results are shown in **Table 3**. As seen from the results, all differently coated UCNPs are negatively charged (except bare counterparts) and the size of UCNPs varies from 45 nm to 90 nm. A small PdI of the tested suspension refers to the uniformity of particle size in the suspension.

Based on ISO standard ISO 22412:2017[7], the PdI value < 0.07 is common for monodisperse samples, whereas values > 0.7 show broad size (i.e., polydisperse) distribution of NPs. In line with Fleischer *et al.*, it is very important what kind of charge the NPs have. If they possess a negative surface charge, after the formation of a PC around the NP, NP-PC complexes are more easily recognized by albumin receptors on the surface of the cells. Whereas if the NP charge is positive, and positive charged particles form complexes with serum, these complexes are directed to scavenger receptors in the cell (Fleischer & Payne, 2014).

[7] ISO, Particle Size Analysis-Dynamic Light Scattering (DLS) (ISO 22412:2017E), 2017, pp. 1–34.

According to the results, coated UCNPs had negative surface charge. Besides, the size of the UCNPs is suitable for biological studies as UCNPs do not exceed the “red line”.

4.4. Colloidal stability of upconverting nanoparticles in different media

UCNPs‘ colloidal stability studies were performed in different aqueous solutions at room temperature: DI or DW, cell growth medium DMEM, DMEM supplemented with 10 % of fetal bovine serum (FBS), and PBS. I-UCNPs, at the concentration of 1 mg/mL and II-UCNPs, at the concentration of 0.1 mg/mL, were incubated for 9 days in aqueous media.

The colloidal stability of UCNPs was measured as emission intensity changes over time for 9 days (**Figure 22**). In the case of I-UCNPs stability measurements, proteins in FBS prevent UCNPs from aggregation and stabilize the UCNPs comparing to exposure results only in DMEM. Alterations in I-UCNPs stability can be an early indication of PC formation around the particles. II-UCNPs behave slightly differently. Stability results in full cell growth medium show polymer coated UCNPs to be colloidally stable over time. On the other hand, stability results in non-supplemented DMEM are favorable only for 75-UCNPs, while other coating sedimented over time.

DMEM consists of many various ions, amino acids, inorganic salts, glucose. Such solvent composition can influence agglomeration and stability of I-UCNPs and II-UCNPs. Ions from DMEM can form diffuse layer around the UCNPs that can lead to rapid NPs agglomeration. However, 75-UCNPs have many anionic anchoring groups, that are strongly attached to the surface of UCNPs. Hence, these polymers need time to be replaced by amino acids. In the case of II-UCNPs‘ stability in protein-supplemented DMEM, tendency is like I-UCNPs‘ stability. These results assure the PC formation and stabilization of UCNPs in dispersion (Moore et al., 2015). However, polymer coated II-UCNPs reflect long-term precisely perfect colloidal stability that can be explained as reduction of fouling proteins on the surface of UCNPs due to PEGylation. PEG reduces adsorption of proteins bound on the surface excess preventing the sedimentation of NPs (Sahoo et al., 2007).

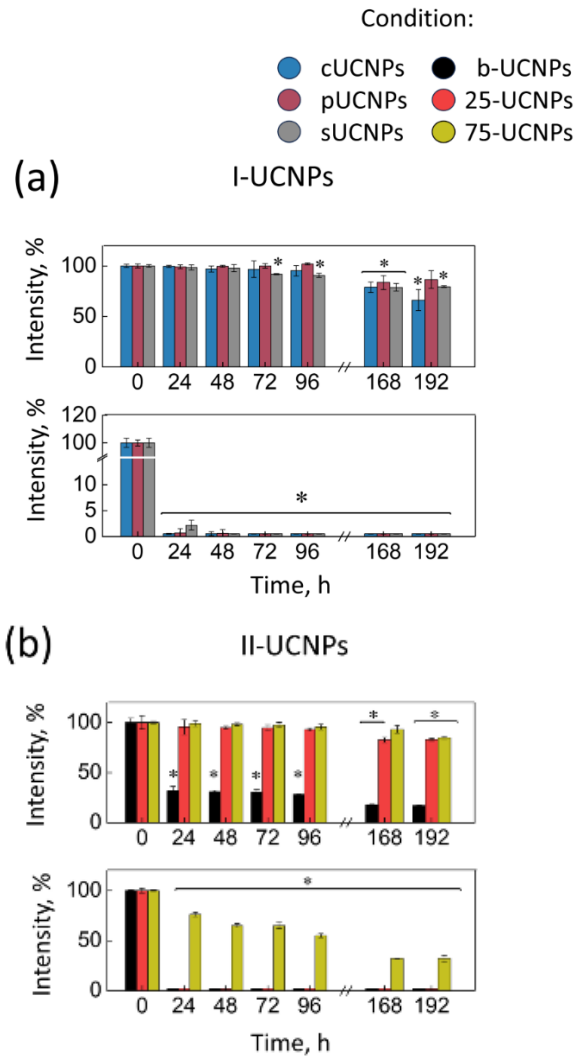

Figure 22. *Colloidal stability of I-UCNPs (a) and II-UCNPs (b) in different media: results of the upper panel show colloidal stability of UCNPs in DMEM supplemented with FBS, results of the bottom panel are for data obtained in DMEM without FBS. Stability measured for 9 days (192 hours). Error bars represent the standard deviation. * indicates significant differences compared to control data ($p < 0.05$).*

As seen from the results, UCNPs are colloidally stable and can be used further for cellular experiments. Nevertheless, their behavior in cells as biocompatibility, accumulation should be examined.

4.5. Studies on the biocompatibility and accumulation of upconverting nanoparticles in cancer cells

Before each cellular experiment it is very important to find whether UCNPs are biocompatible. Two model human adenocarcinoma cell lines, MDA-MB-231 and MCF-7, were selected for this study. MDA-MB-231 cells represent the claudin-low subtype, belonging to the group of TNBC. On the other hand, MCF-7 cells are indicative of luminal A breast carcinoma type (Holliday & Speirs, 2011). Considering this, biocompatibility of cells after exposure to I-UCNPs at set concentration of 0.04 mg/mL was determined by direct automated enumeration of viable cells using ADAM-MC cell counter and LDH assay. For II-UCNPs cell viability was verified by XTT colorimetric assay. Concentrations of II-UCNPs were 0.01 and 0.1 mg/mL (**Figure 23**).

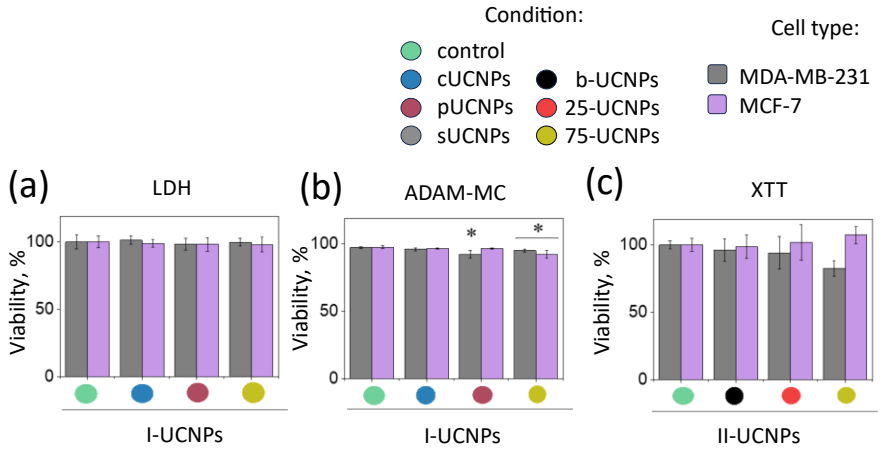

Figure 23. *Viability of two human adenocarcinoma cell lines, MDA-MB-231 and MCF-7, after 24-hour exposure to I-UCNPs and II-UCNPs. (a) LDH assay results, (b) – direct counting assay of viable cells with automatic cell counter ADAM-MC. (c) results of XTT assay. Error bars represent the standard deviation. * indicates significant differences compared to control data ($p < 0.05$).*

As it is presented in the **Figure 23**, UCNPs do not elicit cellular toxicity. The research findings demonstrated that varying shell types of I-UCNPs at set concentration of 0.04 mg/mL did not exhibit a statistically significant impact on the viability of MDA-MB-231 and MCF-7 cells. Another LDH cytotoxicity study was performed on cells ranging I-UCNPs' concentrations from 0.04-0.4 mg/mL (results are not shown). No effect on cellular viability was observed. Yet, observations with II-UCNPs revealed that MDA-MB-231

cells exhibited mild toxicity (with a decrease in viability to 70-80%) following 24-hour incubation with II-UCNPs at a concentration of 0.1 mg/mL. However, no significant effect on MCF-7 cell viability was observed under the same conditions. According to the ISO standard No. 10993-5, if NPs viability drops below 70 % such NPs should be considered toxic to cells. Viability values in **Figure 23** are above 70 % after UCNPs' exposure, so II-UCNPs are considered as non-toxic. Both biocompatibility studies demonstrated the suitability of UCNPs for subsequent investigations. However, slight decrease in MDA-MB-231 viability was shown in our research teamwork (Skripka et al., 2019). Here, accumulation of UCNPs ($LiYF_4$:Tm^{3+},Yb^{3+}@ $LiYF_4$@$LiYF_4$:Nd^{3+}) in MDA-MB-231 and MCF-7 lines showed only a slight, but not significant decrease in MDA-MB-231 cell viability comparing to MCF-7 results after exposure to UCNPs.

Even though *in vitro* cytotoxicity of UCNPs is negligible according to the literature, considering *in vivo* studies with UCNPs, a substantial number of them are limited due to safety considerations. UCNPs behave differently *in vivo* due to many factors, as:

- biological barriers. For instance, NPs change their PC when passing through the BBB. Cox *et al*. showed that PC of gold NPs coated with11-mercapto-1-undecanesulfonate changes after NPs crossed the BBB (Cox et al., 2018).
- longer circulation time of UCNPs in blood can affect cell viability differently than results obtained *in vitro*. There are papers showing that longer exposure of polymer coated NaYF4:Yb^{3+}, Er^{3+} UCNPs to human hepatocellular carcinoma cells (HepG2) can significantly reduce cell viability after 48 hours, even though no changes were detected after 24 hours incubation (C. Wang et al., 2020). A study with oleate-free, oleate-capped and lipid bilayer coated $LiYF_4$:Yb, Tm UCNPs revealed small, yet statistically significant viability decreases of human lung cancer cells A549 after longer exposure (for 72 hours) than after 24 hours incubation with UCNPs (Rojas-Gutierrez et al., 2019).
- UCNPs' coatings. Cytotoxicity depends on the UCNPs' surface coating. For instance, in a work of Sun *et al*. citrate coated NaLuF4:Yb,Tm UCNPs showed slight reduction (up to 90 %) in cell viability on human nasopharyngeal epidermal carcinoma cell line KB at the 1 mg/mL concentration (Sun et al., 2013). Another paper of Liu *et al*. studied silica coated NaYF4:Tm/Yb/Gd UCNPs influence on MCF-7. UCNPs concentration starting from 62.5 μg/mL to 250 μg/mL

reduced cell viability by 20 % comparing to control group (J. Liu et al., 2012).

- stability of UCNPs *in vivo.* Exposure of UCNPs should be evaluated not only on the cells of interest, but many cells that are present in an organism, for instance, liver cells, brain cells, cells of immunity system, etc. If UCNPs are not stable in biological environment at the cellular level, they cannot be used for *in vivo* experiments. However, sometimes UCNPs can be biocompatible with cancer and normal cells, but intolerable to macrophages. This effect was shown in Wysokińska's study (Wysokińska et al., 2019). Here, $NaGdF_4$: Yb^{3+}, Er^{3+} showed detrimental effect on macrophages viability. Exposure to UCNPs for 48 hours at the concentration range 5-25 μg/mL reduced viability by almost 80 % compared to the control.

And up till now, there is a translational gap between research laboratory and clinical trials. Therefore, a global standardization of UCNPs assessment is required (Gnach et al., 2015; Oliveira et al., 2019).

4.6. Assessment of cellular accumulation

UCNPs face several obstacles that must be overcome for successful application *in vivo*, including achieving a long blood circulation time, evading elimination by phagocytic cells, and successfully reaching the target area. When it comes to *in vitro* research, there are challenges such as the cytotoxicity of UCNPs to cells, the presence of proteins in cell growth medium that adsorb to the surface of UCNPs, and the hurdle of interacting of protein-UCNPs complex with the cellular membrane and being engulfed by the cell. These three aspects can be referred to as barriers that need to be overcome before cellular accumulation. In the previous subchapter, viability results demonstrated that UCNPs are non-toxic to cells, meaning one barrier is overcome. Another two barriers, as two additional challenges will be examined in this subchapter. Specifically, the focus will be on the cellular accumulation of UCNPs, depending on the surface coating, in different cancer cells such as MDA-MB-231 and MCF-7.

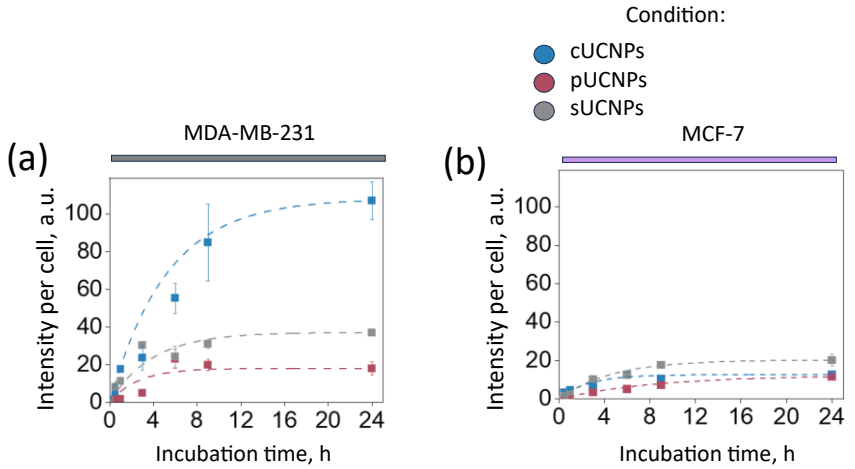

Figure 24. *In time comparison of coated I-UCNPs uptake in breast cancer cells MDA-MB-231 and MCF-7. (a) – uptake dynamics in MDA-MB-231 cells, (b) – uptake in MCF-7 cells. Dashes are guide to the eye.*

The accumulation dynamics of 0.04 mg/mL of I-UCNPs in cancer cells were recorded at 0.5, 1, 3, 6, 9, and 24 hours. Two evaluation methods were used: emission of UCNPs was measured in cells with the help of fluorimeter (**Figure 24**), and cells at these points were visualized by LSCM (**Figure 28**). The emission intensity of I-UCNPs accumulated in the cells is depicted in a **Figure 24** graph at each time point as emission intensity per cell. The kinetics of UCNPs accumulation in cells can be divided into several phases (Damalakiene et al., 2013): lag, exponential (up to 9 hours), and saturation phase at 24 hours. Comparing the accumulation of I-UCNPs in both cancer cell lines, it is observed that the uptake depends on the cell line and the coating. cUCNPs have the highest accumulation rate in MDA-MB-231 compared to UCNPs coated with phospholipids and SiO_2, while lowest was for pUCNPs. In MCF-7 cells accumulation is five times lower than accumulation in MDA-MB-231 cells. The accumulation rates are almost similar regardless of UCNPs' coatings. Several studies have been carried out and it was determined that the entry and accumulation of NPs in cells and velocity depends on the NPs surface charge, size, concentration, incubation time and cell line (Albanese et al., 2012; Damalakiene et al., 2013). The best shape and size for the uptake of $LiYF_4$:Yb^{3+}, Tm^{3+} is diamond-like (or rod-like), and around 50 nm (Rojas-Gutierrez et al., 2019). However, there are studies claiming opposite, that quasi-sphere $NaYbF_4$ UCNPs are internalized faster than rod-like shaped counterparts (B. Chen et al., 2021).

4.7. Endocytic pathways evaluation with endocytosis inhibitors

To obtain a deeper understanding of the internalization pathways of UCNPs within cancer cells, a comprehensive investigation into the accumulation of UCNPs inside these cells was conducted. This investigation involved treating the cells with different inhibitors targeting specific endocytic mechanisms. For this study several endocytosis inhibitors were used. They are presented in **Table 2**:

- nystatin (Nys) – lipid raft/CVME inhibitor;
- chlorpromazine (Chlor) – CME inhibitor;
- nocodazole (Noc) – microtubule assembly/disassembly disrupter;
- 5-(N-Ethyl-N-isopropyl)-amiloride (EIPA) – MP inhibitor.

Before inhibitory experiments different concentrations of inhibitors were tried on cells. Results (**Figure 25**) reveal suitable concentrations to cells and that is why both cancer cells were treated with the same concentrations listed in Methodology part **Table 2**.

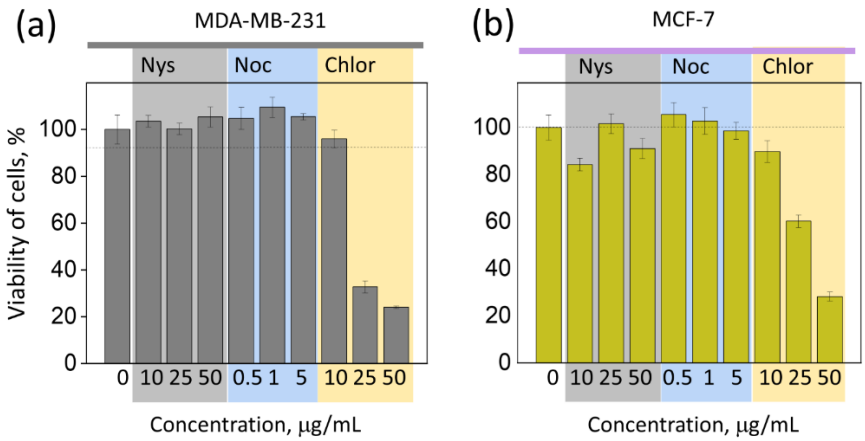

***Figure 25**. Cell viability of breast cancer cell lines (a) MDA-MB-231 and (b) MCF-7 was assessed after a 1-hour treatment with different concentrations of endocytosis inhibitors: 10, 25, and 50 µg/mL of nystatin (Nys) and chlorpromazine (Chlor), as well as 0.5, 1, and 5 µg/mL of nocodazole (Noc).*

Both cell lines (MDA-MB-231 and MCF-7) were incubated with inhibitors for 1 hour, later exposed to I-UCNPs for 3 hours. To tell whether endocytosis for I-UCNPs is energy dependent, cultivation of cells at very low temperature 4 °C was carried out.

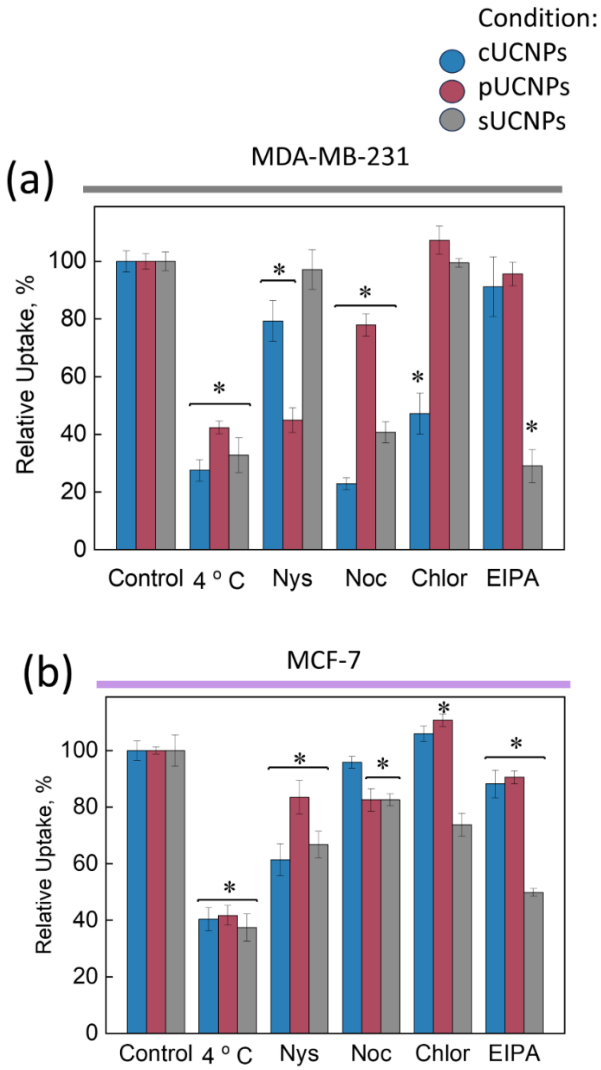

Figure 26. *The impact of inhibiting internalization pathways on the uptake of differently coated UCNPs by MDA-MB-231 (a) and MCF-7 (b) breast cancer cells was assessed. As a control, cells without inhibitor treatment were incubated with UCNPs at 37 °C. The uptake values were calculated as the mean ± standard deviation. Significant differences compared to the control ($p \leq 0.05$) are denoted by an asterisk (*).*

Results in **Figure 26** illustrate that the inhibition of endocytosis is evidently influenced by both the surface coating of the UCNPs and the

specific cell line. In MDA-MB-231 cells, the uptake of pUCNPs was significantly inhibited by Nys, resulting in a 45% reduction in relative uptake compared to the control. However, Nys showed minimal inhibition for cUCNPs (79%) and sUCNPs (97%). Noc treatment inhibited the uptake of cUCNPs (23%), sUCNPs (41%), and exhibited the least inhibition for pUCNPs (78%). Similar to Noc, Chlor also reduced the internalization rate of cUCNPs to 47%, while it had no effect on sUCNPs and pUCNPs compared to the control samples. EIPA demonstrated inhibitory effects solely on the uptake of sUCNPs, reducing it to 29%. In the case of the MCF-7 cell line, Nys treatment led to a reduction in the internalization efficiency of cUCNPs and sUCNPs by 61% and 67%, respectively. Noc inhibition resulted in a decrease in the uptake of pUCNPs and sUCNPs to 83%, while it had no effect on the internalization of cUCNPs in MCF-7 cells. Chlor treatment enhanced the internalization of cUCNPs and pUCNPs but slightly reduced the uptake of sUCNPs (74%). EIPA exhibited a slight reduction in the uptake of cUCNPs (88%) and pUCNPs (91%), while the internalization of sUCNPs was reduced to 50%.

The cellular internalization pathway of UCNPs typically relies on the interaction between specific proteins and corresponding receptors on the cell membrane (Behzadi et al., 2017). It is evident that there are significant differences in the cellular uptake of various UCNPs between MDA-MB-231 and MCF-7 cells following treatment with inhibitors (**Figure 26**). Observations indicate that cUCNPs enter MDA-MB-231 cells primarily through CME, as shown in **Figure 26**. In various cell lines, carboxylated NPs within the size range of 40 to 200 nm are commonly internalized via CME, including MDA-MB-231 and MCF-7 cells (Chaves et al., 2017). On the other hand, pUCNPs were found to enter MDA-MB-231 cells through CVME, which aligns with Rojas-Gutierrez *et al.* research (Rojas-Gutierrez et al., 2019) indicating that lipid-coated UCNPs, with dimensions of 92 nm along the major axis and 53 nm along the minor axis, utilize CVME for cellular entry. However, it should be noted that the same authors also suggested the possibility of lipid coated UCNPs entering cells through CME, indicating the potential existence of multiple internalization pathways for the same UCNPs. No evidence was observed of CME-based uptake of pUCNPs. Findings regarding sUCNPs in MDA-MB-231 and MCF-7 cells align with previous data reported by Francia et al., where SiO_2 NPs with a hydrodynamic size of 50 nm were confirmed to be internalized via macropinocytosis in HeLa cells (Francia et al., 2019). All the inhibitors used in study (**Figure 26**) exhibited weaker effects on UCNPs‘ endocytosis in the MCF-7 cell line compared to MDA-MB-231 cells. This discrepancy may be attributed to the tendency of

MCF-7 cells to form colonies, where only the outer layer of the colony is influenced by the inhibitors and exposed to UCNPs. In the case of MCF-7 cells, CME and macropinocytosis serve as internalization routes for cUCNPs and sUCNPs, respectively.

4.8. Proteomics of PC around UCNPs

Electrophoresis was performed as qualitative analysis of protein amount in each UCNPs' PC (**Figure 27 a**). To measure the differences between the differently coated UCNPs' PCs, proteomic analysis via LC-MS was performed. Results revealed that SiO_2 coated UCNPs' PC possess 5 times higher amount of proteins than other UCNPs coutnerparts (**Figure 27 b**).

The variation in the PC composition plays a critical role in the internalization and transportation pathways of NPs (Docter et al., 2015; Fleischer & Payne, 2014; Qin et al., 2020). Proteomic analysis of the composition of PC formed around I-UCNPs was carried out by Dr. Marija Ger at Institute of Biochemistry, Vilnius University. Firstly, total amount of protein adsorbed on I-UCNPs surface at various time sets up to 24 hours incubation in DMEM with FBS was assessed by gel electrophoresis.

Dr. Algirdas Kaupinis performed liquid chromatography mass-spectrometry analysis to identify the proteins eluted from UCNPs. In total, 67 proteins were detected on the surface of cUCNPs, 63 proteins on pUCNPs, and 86 proteins on sUCNPs. The protein analysis revealed that the most abundant proteins found around cUCNPs were serum albumin, α-2-HS-glycoprotein, and α-1-antiproteinase. Similarly, pUCNPs exhibited high levels of serum albumin and α-2-HS-glycoprotein, along with apolipoprotein A-I. On the other hand, sUCNPs showed a different protein profile with the presence of serum albumin, α-2-macroglobulin (A2M), and coagulation factor V (F5).

(a)

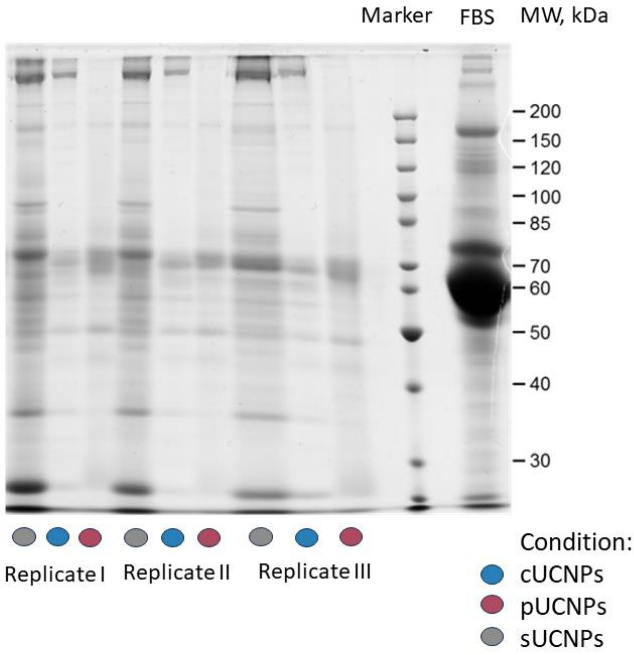

(b)

UCNPs	Amount of protein, ng
cUCNPs	65 ± 12
pUCNPs	100 ± 20
sUCNPs	450 ± 150

Figure 27. *(a) The proteins eluted from I-UCNPs after being incubated with FBS-containing DMEM (incubation time of 24 hours, N = 3) were subjected to gel electrophoresis and compared to proteins eluted from I-UCNPs incubated with FBS. (b) Proteomic data of total amount of protein in UCNPs samples.*

These results highlight the contrasting protein compositions of the differently coated I-UCNPs.

The proteomic analysis was performed at different time points, specifically 1 and 3 hours (**Figure S1**), before the uptake dynamics reached a plateau. Among the findings, two proteins, thrombospondin-I (THBS1) and adenylyl cyclase-associated protein 1 (CAP1), were found to be overexpressed in the PC of cUCNPs. In the case of pUCNPs, six proteins were identified as potentially contributing to the differences in their cellular uptake: apolipoprotein E (ApoE), kininogen-1 (KNG1), antithrombin-III (Serpinc1),

alpha-2-macroglobulin (A2M), coagulation factor II (F2) and coagulation factor IX (F9). sUCNPS exhibited distinct proteins as serum albumin, A2M, F5, complement factor H.

As previously mentioned, sUCNPs exhibited a significantly higher binding capacity for total proteins, which could be attributed to their larger surface area and negative surface charge compared to the other coatings. In total, 51 proteins displayed varying quantities between sUCNPs and pUCNPs at 1 hour, while 44 proteins showed differences at both 1 and 3 hours. Among these proteins, 46 were overrepresented in the PC of sUCNPs after 1 hour of incubation, and 39 proteins were consistently overrepresented at both time points. Furthermore, pathway enrichment analysis using the Enrichr tool revealed a dominance of proteins involved in blood clotting and the complement system in the PC of sUCNPs. The proteins unique to each PC as CAP1 and THBS1 for cUCNPs, F5 and ApoA1 for pUCNPs, and A2M and F5 for sUCNPs, are considered as the likely candidates responsible for the observed differences in cellular uptake between the different types of coated UCNPs.

4.9. Cellular proteome

To understand the factors contributing to the differential uptake of UCNPs in MDA-MB-231 and MCF-7 cell lines, a study on differences between these cells' cellular proteome was conducted. In total, 399 proteins were identified, with 99 proteins found exclusively or significantly increased in MCF-7 cells, and 157 proteins unique to or significantly increased in MDA-MB-231 cells. The cell membrane fraction of MCF-7 cells is predominantly characterized by a high abundance of cytoskeletal proteins and intermediate filaments.

After the number and names of cell surface proteins were known, a comparative proteomic analysis, called gene ontology (GO), of these proteins was conducted. GO is classification system, used to categorize genes and their products (proteins) based on their known or predicted biological roles. After cellular component analysis, data set of 10 the highest enrichment bearing proteins was assigned to each cell line. GO enrichment component comparison between cell line surface proteome is shown in **Table 4**.

As is seen from the results, only 2 of top 10 proteins can be assigned to both cell lines. MDA-MB-231 cells show an enrichment of proteins associated with cellular transport and endocytosis, particularly components of clathrin-coated vesicle membranes. The observed variations in the plasma membrane and associated proteins between the two cell lines correlate with

the experimental differences in the uptake of UCNPs. The use of Chlor and Noc, which target CME and disrupt microtubule assembly, resulted in a more significant decrease in UCNPs' uptake in MDA-MB-231 cells compared to MCF-7 cells.

Table 4. *GO cellular component comparison between MDA-MB-231 and MCF-7 cell surface proteins.*

GO cellular component	MDA-MB-231	MCF-7
Integral component of plasma membrane	+	+
Intermediate filament		+
Polymeric cytoskeletal fiber		+
Keratin filament		+
Focal adhesion	+	+
Catenin complex		+
Endocytic vesicle		+
Axon		+
Cytoskeleton		+
Specific granule		+
Clathrin coated vesicle membrane	+	
ER to Golgi transport vesicle membrane	+	
Integral component of luminal side of endoplasmic reticulum membrane	+	
MHC protein complex	+	
Lysosomal membrane	+	
COPII-coated ER to Golgi transport vesicle	+	
Integral component of endoplasmic reticulum membrane	+	
Specific granule membrane	+	

Comparing cUCNPs and pUCNPs PCs, amount of two proteins was significantly increased: THBS1 and CAP1. THBS1, the aforementioned protein, is a secreted adhesive lipoprotein that plays multiple biological roles. One of its functions involves binding to cell surface glycoproteins and facilitating the internalization of complexes that interact with THBS1 (Sid et

al., 2004). It has been demonstrated that interaction with the low-density lipoprotein receptor-related protein (LRP) promotes the internalization of THBS1 through endocytosis (Mikhailenko et al., 1997). Additionally, it has been observed that MDA-MB-231 cells upregulate the expression of LRP receptors when treated with NPs up to 200 nm in size. This altered expression leads to a more efficient receptor-mediated uptake of UCNPs in MDA-MB-231 cells compared to MCF-7 cells (Roy et al., 2016). These findings are consistent with the increased uptake of cUCNPs observed in MDA-MB-231 cells and its effective inhibition by Chlor (**Figure 24** and **Figure 26**). Moreover, THBS1 expression is upregulated in certain proliferating and tumor stromal cells (Sid et al., 2004). This suggests that the interaction between THBS1 and the citrate coating on UCNPs may enhance specificity when targeting tumors with these NPs (Sid et al., 2004). CAP1, another protein found to associate differentially with the PC, is a member of the cyclase-associated protein class. These proteins play a role in linking receptor signaling to actin polymerization (Hubberstey & Mottillo, 2002). CAP1 is often identified in the PC of various NPs, as liposomes (Capriotti et al., 2011), gold NP prepared in pure DI with no additional coating (Correard et al., 2014). However, no information about the role of CAP1 on the internalization of UCNPs is available to the best of our knowledge.

In the case of the PC of pUCNPs, an increase in the abundance of two proteins, ApoA1 and F5 is observed. However, when comparing the total PC proteomes of pUCNPs and cUCNPs, another protein called ApoA4 is also found to be overrepresented in the PC of pUCNPs (data not shown). It is known that ApoA4 can decrease the cellular uptake of NPs (Ritz et al., 2015), which aligns with observation of decreased uptake of pUCNPs by both MDA-MB-231 and MCF-7 cells compared to cUCNPs (**Figure 24**). Based on these findings, the hypothesis is that both ApoA4 and ApoA1 proteins play a role in guiding the UCNPs towards internalization via CVME rather than CME. Up to now, limited information is available regarding the role of the most abundant proteins, A2M and F5, found in the PC of sUCNPs and their involvement in UCNP internalization. However, based on their high abundance, it can be inferred that these proteins might play a crucial role in the macropinocytosis pathway of sUCNPs in both cancer cell lines. Consequently, the identification of distinct PC components, specific to UCNPs with different surface coatings, offers valuable insights into their cellular uptake mechanisms.

The variations in the uptake of I-UCNPs are influenced not only by the composition of the PC but also by the inherent differences between the MDA-MB-231 and MCF-7 cell lines. Active endocytosis is a crucial prerequisite for

MDA-MB-231 cells, which are characterized by their high invasiveness and motility (Polo & Di Fiore, 2006; Ziegler et al., 2014).

In addition, the MDA-MB-231 cells exhibit several characteristics of the epithelial-mesenchymal transition (Ziegler et al., 2014), which is known to be associated with increased internalization dynamics of various receptors, including the EGF receptor (Y. L. Liu et al., 2019).

Protein-protein interaction analysis performed with STRING database to predict interactions between specific proteins in the PC with the cellular surface proteins. It was found that in the case of MCF-7 cell line THBS1 and syndecan1 can bind with two members of the integrin family as ITGB5 and ITGAV. Integrins are responsible for cell adhesion, cell migration, signaling, angiogenesis, tissue development and homeostasis, disease processes (Paul et al., 2015). In the case of MDA-MB-231 THBS1 can interact also with integrins as ITGA1, ITGA2, ITGA3, ITGB4, ITGA5, ITGA6.

4.10. Polyethylene glycol impact on cellular internalization

I-UCNPs accumulation dynamics with pUCNPs did not show high uptake level. pUCNPs on the surface possess PEG. One of the thesis aims was to investigate uptake dynamics depending on the PEG amount on the UCNPs surface. That is why 25-UCNPs and 75-UCNPs were synthesized, with a 3 fold difference of PEG between these surface modifications. According to the literature, PEG on the surface helps to decrease PC around the NPs resulting in prolonged blood circulation time, enhanced or not affected cellular uptake and great biocompatibility (Sahoo et al., 2007; Soenen et al., 2014). However, results in **Figure 24** show the lowest uptake for MDA-MB-231 and MCF-7 cell lines. Cellular uptake experiments were performed with II-UCNPs to observe the impact of various PEG amounts on cellular internalization.

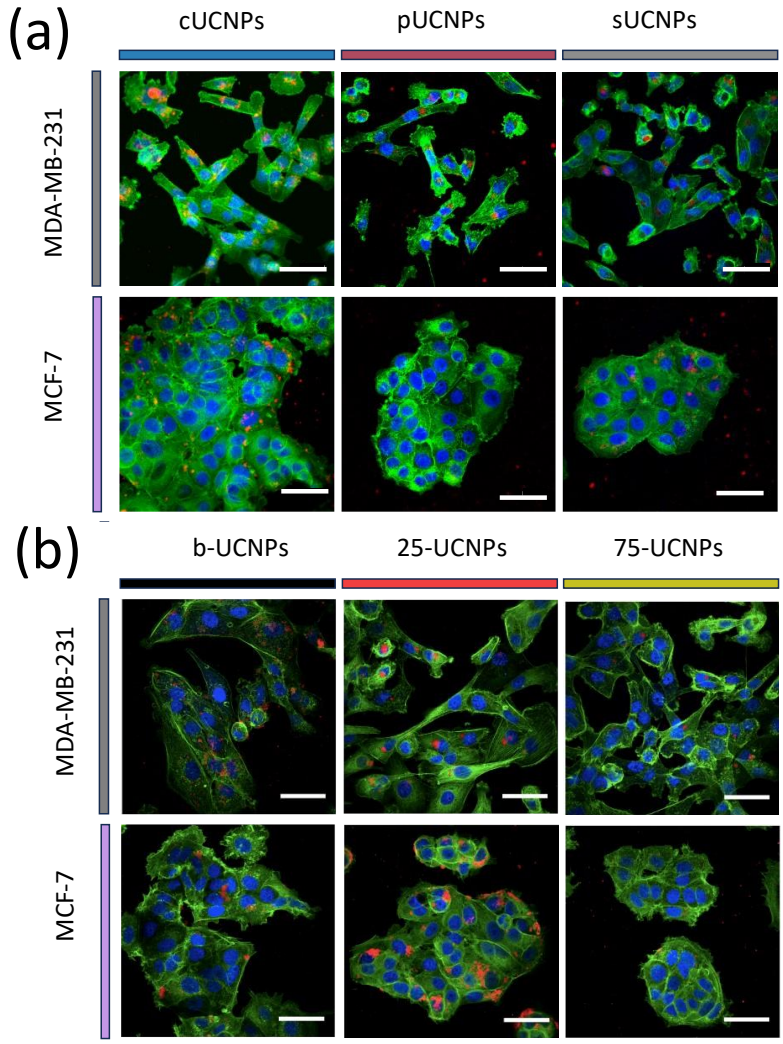

Figure 28. *A Comparison of the accumulation of I-UCNPs (A) and II-UCNPs (B) in MDA-MB-231 and MCF-7 breast cancer cell lines after 24 hours of incubation. UCNPs (λ_{ex} = 980 nm) in all confocal microscopy images are represented by the red color. Cell nuclei were stained with Hoechst 33258 (blue, λ_{ex} = 404 nm), cytoskeleton with Phalloidin-Alexa 488 (green, λ_{ex} = 488 nm). Scale bars in all images are 50 μm.*

Uptake dynamics curves in **Figure 24** showed after 24 hours the highest accumulation rate of I-UCNPs. For this reason, uptake dynamics of II-UCNPs were performed after 24 hour incubation with II-UCNPs with the help of LSCM method. If compare I-UCNPs and II-UCNPs uptake after 24 hours

visually (**Figure 28**), it is obvious how UCNPs accumulation depends on cell line and coatings. MCF-7 cells show lower UCNPs accumulation compared to MDA-MB-231 cells. MDA-MB-231 cells are enriched in stemness properties and more aggressive. Also, LSCM images stand as qualitative analysis, to support quantitative **(Figure 24**) data visually.

Figure 28 (a) represent visualized cancer cells after 24 hours exposure to I-UCNPs. As it seen from the pictures, the tendency is similar to as depicted in (a) I-UCNPs uptake velocity graphs. Cellular uptake for II-UCNPs uptake in cells shows the best accumulation for b-UCNPs and 25-UCNPs in both cell lines. Compared to investigation data of pUCNPs uptake, MDA-MB-231 cells tend do uptake more UCNPs than MCF-7. In case of b-UCNPs and 25-UCNPs – tendency is the same for both cell lines. However, 75-UCNPs are internalized by the cells at the lowest.

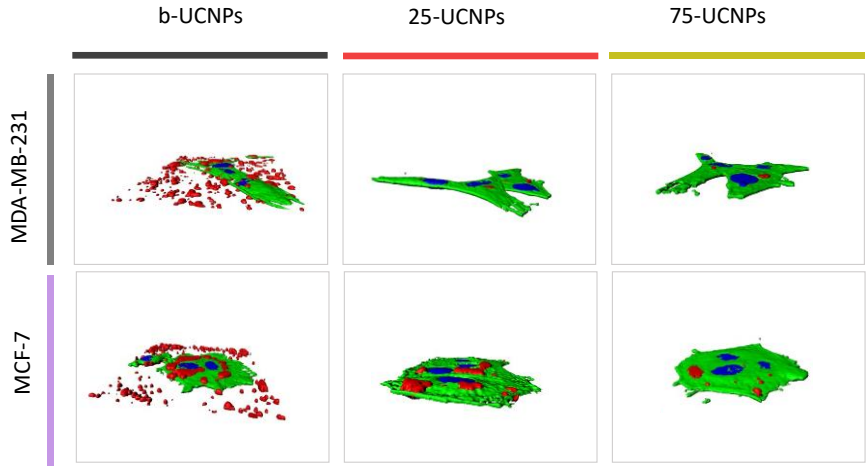

Figure 29. *A series of images were captured at 0.3 μm intervals using a confocal laser scanning microscope to create a Z-stack. The cells were cultured with II-UCNPs in DMEM supplemented with FBS. The red color in the images corresponds to the UC emission signal, which was generated by exciting the UCNPs at 980 nm. The cell nuclei were dyed blue using Hoechst, and F-actin was labeled in green with Phalloidin-Alexa 488. All images depict the three-dimensional reconstruction of cells from MDA-MB-231 and MCF-7.*

It is very difficult to tell where the UCNPs are in the cell: above, below or inside the cells. To answer this question confocal sectioning and 3D reconstruction was made. **Figure 29** results show how II-UCNPs differently accumulate when cells with II-UCNPs are incubated in cell culture medium supplemented with FBS. It is obvious, that only b-UCNPs accumulate in

aggregates above the cells, whereas other coatings bearing II-UCNPs are taken up more packed and found mainly inside the cells.

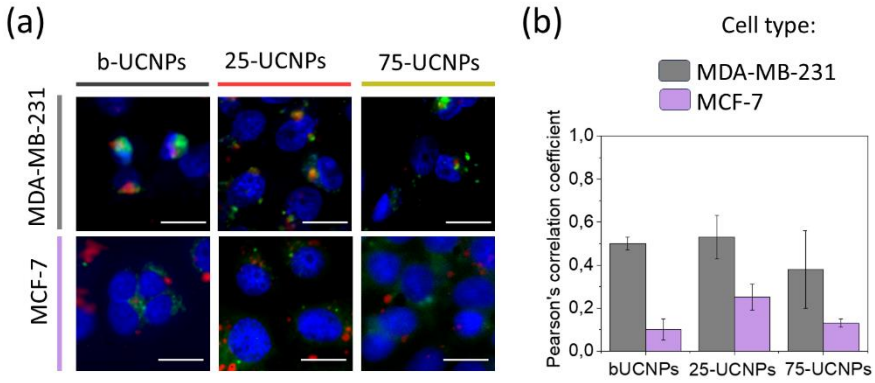

Figure 30. *(a) LSCM images depict the localization of II-UCNPs within MDA-MB-231 and MCF-7 cells following a 24-hour incubation in DMEM supplemented with FBS. The Lysotracker fluorescence, represented in green, highlights the presence of lysosomes in the images. The red color corresponds to the emission of II-UCNPs within the cells, while the blue color represents the cell nuclei. The cell images are displayed as 4x zoom views, with a scale bar of 20 μm provided in all images. (b) Graphs depict calculated Pearson's correlation coefficient to evaluate colocalization between b-UCNPs, 25- and 75-UCNPs and lysosomes.*

Some studies have demonstrated that after a 24-hour incubation period, NPs tend to localize within lysosomes (Sousa De Almeida et al., 2021). Following internalization, NPs are anticipated to localize within endocytic vesicles, which subsequently merge with early endosomes/phagosomes and eventually with lysosomes (Bourquin et al., 2018). Thus, it is important to note that accumulation of NPs is not exclusively limited to lysosomes, they can also be taken up by late endosomes or multivesicular bodies (Damalakiene et al., 2013). To experimentally determine the fate of II-UCNPs within breast cancer cells, colocalization analysis was conducted using a LysoTracker fluorescent probe. This probe allows for labeling and tracking of acidic organelles within the cells, providing valuable insights into whether II-UCNPs enter the cells through endocytosis and reach lysosomes. The colocalization of II-UCNPs with lysosomes varied depending on the specific cancer cell type employed. The analysis of PCC, indicating the degree of colocalization between II-UCNPs and lysosomes, was calculated for both cell lines. If the value lies between 0.5 and 1.0 there is strong correlation, if below

0.5 there is partial colocalization. PCC values for b-UCNPs, 25-UCNPs, or 75-UCNPs were (**Figure 30 b**):

1) in MDA-MB-231 cell line 0.46 ± 0.03, 0.51 ± 0.10 and 0.36 ± 0.05, respectively, showing partial colocalization;
2) values for MCF-7 cells were 0.04 ± 0.02, 0.23 ± 0.02, and 0.05 ± 0.01, respectively, showing minimal to negligible colocalization.

Upon comparing the two cell lines, it is evident that MDA-MB-231 cells exhibit greater individual proliferation compared to MCF-7 cells. In the acquired images of MCF-7 cells, the presence of cell colonies is observed, potentially impeding the effective delivery of UCNPs to these cells. Moreover, differences in uptake can be due to different PC formed around the NPs. According to the literature, PEGylated NPs stays longer in blood circulation system, because PEG repels most of the proteins in blood, thus favors formation of smaller PC (Pelaz et al., 2015). In case of this study, 25-UCNPs are highly PEGylated, thus, PC could form smaller than on 75-UCNPs surface resulting in higher uptake rate. b-UCNPs were used only as control, and they cannot be used for further studies due to insufficient colloidal stability and aggregation in cell biological media.

5. RECAPITULATION OF THE THESIS

The significance of this study lies in the crucial need to optimize the infiltration of NPs into cells, with a focus on their precise localization for therapeutic purposes. The central theme of this dissertation revolves around the role of surface functionalization of UCNPs in the creation of a suitable PC. This, in consequence, improves the colloidal stability of NPs and promotes their delivery to cells through diverse endocytosis mechanisms, ensuring efficient distribution within the intracellular environment.

In this dissertation six surface modifications of $LiYF_4$: Yb^{3+}, Tm^{3+} UCNPs' were used: citrate, phospholipids (PEG-DOPE:DOPC, ratio 1:4), SiO_2, bare (with no coating), brush-type polymer[8] coatings as P_9MAA-25 (highly PEGylated) and P_9MAA-75 (three times lower PEGylation compared to P_9MAA-25). Afterwards, UCNPs were characterized by size, surface charge, colloidal stability, and biocompatibility. Additionally, experiments were conducted on MDA-MB-231 and MCF-7 cancer cell uptake dynamics, endocytosis inhibitory assays, PC formation around UCNPs (including PC size and composition analysis), cancer cells proteome analysis, and cellular localization studies.

When NPs encounter with proteins, they promptly surround the NP, resulting in the formation of what is known as a PC (Docter et al., 2015). Here, surface chemistry of NPs plays a crucial role in terms of PC size, thickness, and composition. PC and surface chemistry of NPs are important while creating stable, biocompatible NPs (M. Wang et al., 2011). In this thesis, stability analysis of UCNPs revealed that serum proteins stabilized all coated UCNPs, formed PC around UCNPs and ensured colloidal stability, and steric hidrance. Moreover, in absence of serum proteins surface chemistry can play a role. If many anchoring groups are present on the surface of UCNPs (case of 75-UCNPs), the polymer is not easily replaced by amino acids, and UCNPs are stabilized.

Nowadays many concerns revolve around NPs toxicity (Gnach et al., 2015). Some materials can be biocompatible *in vitro*, but not *in vivo*, compatible with one cell line but not the other. That is why two different cancer cell line, as model cell lines, were chosen for the research – MDA-MB-231 and MCF-7. MDA-MB-231 are more aggressive, stem-cell like cells, MCF-7 are luminal cancer type, grow in colonies. However, there is one similarity between the cells - doubling time, which is around 24-25 hours.

[8] The abbreviation of which comes from general formula as p(MAA-*co*-PEG_9MEMA).

After exposure to UCNPs for 24 hours these cells remained viable, meaning that UCNPs do no harm to cancer cells, their viability, growth, and division.

The cell itself sees only the PC not the NP (Trojan horse effect) (Oliveira et al., 2019), the PC sees the surface of UCNPs, and UCNPs depends on surface chemistry. PC size and composition induce the corresponding pinocytic uptake mechanism as clathrin / caveolin mediated endocytosis or macropinocytosis as well as uptake dynamics. Cellular UCNPs‘ uptake kinetic curves were gathered after various time points for 24 hours. Results showed uptake curves to have log and stationary phases. Moreover, there were differences spotted between the cell lines and between the surface chemistry of UCNPs. These results partially reveal that coating of UCNPs can be connected to PC size and composition.

In the subsequent steps, an analysis was performed on the size and composition of the PC, along with an examination of the cell surface proteome. The number of receptors present on the cell membrane plays a role in determining uptake mechanisms. MDA-MB-231 cells predominantly express integrin family proteins on their surface, whereas MCF-7 cells also exhibit integrins but in lesser quantities. The PC of cUCNPs includes the THBS1 protein, which interacts with integrins, elucidating the reason behind the heightened uptake dynamics of cUCNPs in the MDA-MB-231 cell line.

UCNPs’ coatings activate the corresponding endocytic pathways. Clathrin-dependent endocytosis was observed for cUCNPs only in MDA-MB-231 cells. Caveolin-dependent endocytosis was observed for cUCNPs in MCF-7 cells, and pUCNPs entered through this mechanism in both cell lines. Macropinocytosis was observed in both cell lines for sUCNPs.

All examined coatings exhibit a negative charge, resulting in higher cellular accumulation when compared to their positively charged counterparts (**Figure 31**). sUCNPs have a fivefold higher protein count in their PC compared to pUCNPs or cUCNPs, leading to macropinocytosis. The PC of cUCNPs plays a crucial role in clathrin-mediated endocytosis. Additionally, cUCNPs, being the smallest in size with a smaller PC, are taken up by aggressive MDA-MB-231 cells at higher rates than by MCF-7 cells. The distinctive proteins in cUCNPs' PC, such as CAP1 and THBS1, interact with the cell membrane, influencing this entry mechanism. In the case of MCF-7, cUCNPs enter through caveolin-dependent endocytosis. pUCNPs' PC includes ApoA1 and F5, and they also enter cells through caveolin-dependent endocytosis. Lastly, sUCNPs, containing A2M and F5, enter cells through macropinocytosis.

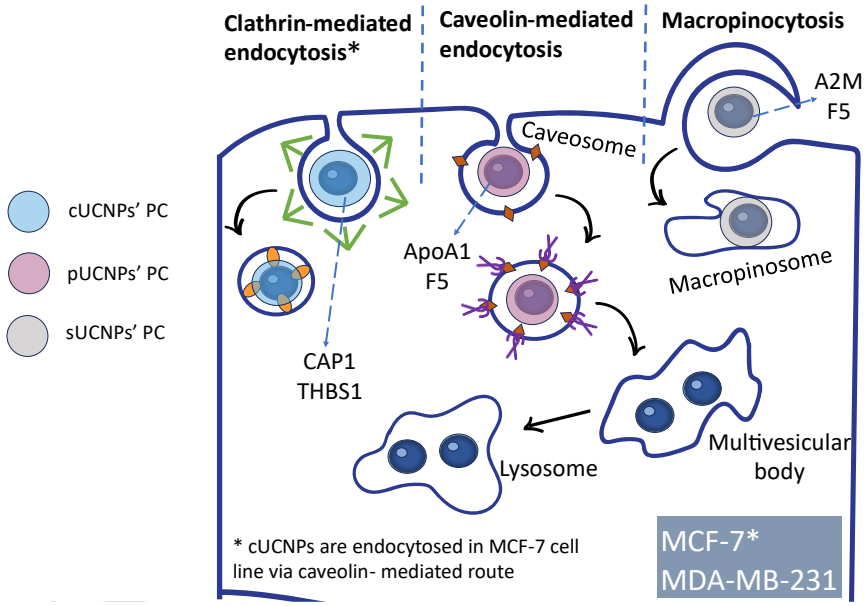

Figure 31. *A Schematic representation of endocytic uptake routes in two breast cancer cell lines MDA-MB-231 and MCF-7 depending on I-UCNPs surface chemistry and protein corona. cUCNPs in its PC possess CAP1 and THBS1 that are responsible for clahrin-mediated uptake in MDA-MB-231 cells, and caveolin-mediated endocytosis in MCF-7 cell line. Other coated UCNPs are taken up by both cell lines via the same routes. pUCNPs have ApoA1 and F5 proteins, that favor caveolin-mediated endocytosis, furthermore, sUCNPs are coated with A2M and F5 proteins that target macropinocytosis. According to the localization results, PEGylated UCNPs (II-UCNPs) partially reach lysosomes.*

Interestingly, results with pUCNPs, particularly regarding uptake dynamics, demonstrated the lowest accumulation in both cell lines compared to their other coated counterparts (cUCNPs and sUCNPs). The coating of pUCNPs included PEG. According to the literature, PEG repels proteins from the NP surface, resulting in a smaller PC and prolonging blood circulation time. To verify whether the PEG density was insufficient for faster uptake dynamics and a smaller PC, polymer-coated UCNPs (II-UCNPs), such as 25-UCNPs and 75-UCNPs, were synthesized with a 3:1 ratio in PEGylation density, respectively. Cellular uptake results revealed that highly PEGylated UCNPs are taken up in higher quantities by both cell lines compared to low PEGylated UCNPs. Typically, after 24 hours of NP exposure, cells localize

NPs into vesicles called lysosomes. Additional studies on NP localization in cells indicated that UCNPs localize in lysosomes after entering cells.

Ultimately, the results in this work can be applied to forecast future experiments or for desirable applications in nanomedicine with similar surface modifications, shape, and size-bearing UCNPs. For example, if significant uptake is needed in MDA-MB-231 cells, cUCNPs can be employed. If a thick or dense PC is required for further additional surface ligand coating, the surface chemistry of UCNPs can be tailored accordingly. Moreover, cellular investigations in a protein-free environment can be conducted with the assistance of 75-UCNPs.

6. CONCLUSIONS

I) Spectroscopic investigations of $LiYF_4:Yb^{3+},Tm^{3+}$ UCNPs coated with citrate, DOPC:PEG-DOPE phospholipids, SiO_2 (I-UCNPs), and polymer coatings such as P_9MAA-25 and P_9MAA-75 (II-UCNPs) showed that serum proteins added to the cell growth medium stabilize UCNPs. This stability is attributed to the protein corona (PC) formed around each UCNP in presence of proteins in the cell growth medium.

II) Accumulation dynamics of UCNPs depends on UCNPs' surface modifications. cUCNPs showed the highest accumulation in MDA-MB-231 cells. This uptake dynamics pattern is related to the size and PC of cUCNPs.

III) No negative effects of UCNPs on either cancer cell line were found using two independent methods to evaluate cytotoxicity (via the LDH assay) and viability (via an automatic cell counting method).

IV) Cell surface proteome investigations revealed that specific protein expression on the plasma membrane of each cancer cell has an impact on accumulation rates of UCNPs. MDA-MB-231 predominantly exhibits integrin family proteins on the surface, which are responsible for clathrin mediated uptake. The PC of cUCNPs contains the THBS1 protein, which interacts with integrins, explaining why the uptake dynamics of cUCNPs are the highest in the MDA-MB-231 cell line.

V) The analysis of PC revealed that PC size and composition have an impact on the endocytosis of UCNPs. sUCNPs, possessing five time more proteins in their PC compared to pUCNPs or cUCNPs, exhibit distinctive proteins such as A2M and F5, leading to macropinocytosis in both cancer cell lines. cUCNPs, being the smallest in size, have proteins in their PC, such as CAP1 and THBS1, responsible for clathrin-mediated endocytosis in the MDA-MB-231 cell line. In the case of MCF-7 cells, cUCNPs enter through caveolin-dependent endocytosis. pUCNPs' PC includes ApoA1 and F5, and they enter cells through caveolin-dependent endocytosis in either cell line.

VI) Studies on the impact of PEGylation density on colloidal stability and cellular accumulation showed that PEGylation density has an effect on both the colloidal stability and accumulation of II-UCNPs in cancer cells. These coated UCNPs demonstrate colloidal stablility in serum-rich media. Highly PEGylated UCNPs, such as 25-UCNPs, accumulate at high rates in both cancer cell lines compared to their lower PEGylation-bearing counterparts (75-UCNPs).

7. SANTRAUKA

SANTRUMPOS

APND – apkonvertuojančios nanodalelės

BV – baltyminis vainikas

CAP1 – su adenililciklaze susijęs baltymas 1

Chlor – chlorpromazinas

CME – nuo klatrino priklausoma endocitozė

CVME – nuo kaveolino priklausoma endocitozė

DMEM – Dulbecco modifikuota Eagle ląstelių mitybinė terpė (angl. Dulbecco's Modified Eagle Medium)

DLS – dinaminė šviesos sklaida

DV – distiliuotas vanduo

EIPA – 5-(N-etil-N-izopropil) amiloridas

F5 – koaguliacijos faktorius V

FBS – veršiuko embriono serumas (angl. fetal bovine serum)

FND – fotoliuminescuojančios nanodalelės

LDH – laktato dehidrogenazė

LSKM – lazerinė skenuojanti konfokalinė mikroskopija

ND – nanodalelės

NIR – artimoji infraraudonoji spinduliuotė

Nys – nistatinas

Noc – nokodazolas

P/S – antibiotikų penicilino ir streptomicino mišinys

PBS – fosfatinio buferio druskų tirpalas (angl. phosphate buffered saline)

PJ – propidžio jodidas

PKK – pirsono koreliacijos koeficientas

RE – retųjų žemių metalų jonai

THBS1 – trombospondinas-I

UV – ultravioletionė spinduliuotė

XTT – 3'-[1-(fenilaminokarbonil)-3,4-tetrazolio]-bis(4-metoksi6-nitro) benzensulfonrūgšties hidratas

1. ĮVADAS

Veiksmingas nanodalelių (ND) panaudojimas biomedicinoje priklauso tiek nuo efektyvaus ND patekimo į ląsteles, tiek ir nuo pačių ND terapinių „agentų“. Efektyvus ND patekimas į ląsteles dar kitaip apibūdinamas kaip efektyvus ir kontroliuojamu vaistų pristatymas / nugabenimas. Nugabenimas dar gali būti suprantamas kaip tikslus vaistų išleidimas tam tikroje vietoje, organe, audinyje ar ląstelėje, kur reikalingas specifinis farmakologinis poveikis. Nanonešėjai atlieka lemiamą vaidmenį siekiant nukreipti į ląsteles. Čia vaistai yra transportuojami į tikslinį organą / ląstelę, remiantis išplėstine farmacinio nešiklio cirkuliacija kraujyje, todėl norimoje vietoje kaupiasi vaistų pakrauta nano tiekimo sistema. Veiksmingas vaisto tiekimas šiuo metodu paprastai priklauso nuo išorinio vaisto / nanonešiklio sluoksnio. Išorinis sluoksnis arba ND padengimas yra svarbus nanonešėjų tarpląstelinėje lokalizacijoje. Tačiau vis dar trūksta žinių apie tai, kas nutinka ND, kai jos patenka į ląstelę: kur ir kaip ND yra lokalizuojamos ląstelėje (Gnach ir kt., 2015). Paprastai įvairių tipų biomolekulės, daugiausia kraujyje esantys baltymai, adsorbuojasi ND paviršiuje ir sudaro papildomą plazmos baltymų sluoksnį, vadinamą „baltyminiu vaniku“ (BV) (Docter ir kt., 2015). BV veikia ND biologinį pasiskirstymą, taikymą, ląstelių kaupimąsi ir lokalizaciją. Kartais BV gali užkirsti kelią ląstelių įsisavinimui ir suaktyvinti mononuklearinę fagocitų sistemą (MFS) (Francia ir kt., 2019; W. Zhang ir kt., 2019). Taip pat žinoma, kad BV daugiausia priklauso nuo ND dydžio, formos ir paviršiaus sudėties (Docter ir kt., 2015; Fleischer & Payne, 2014; Francia ir kt., 2019). Kad terapija būtų sėkminga, nanonešiklio paviršiaus sudėtis yra tik vienas aspektas, į kurį reikia atkreipti dėmesį. Kitas labai svarbus aspektas yra pačios ND. Sėkmingas terapinis nanonešiklis turėtų būti biologiškai suderinamas ir turėti dvigubą modalumą. Augantis daugiafunkciškumo poreikis biomedicinos srityse paskatino fotoliuminescuojančių ND (FND) kūrimą, kurios gali integruoti vaizdo gavimo galimybes su tiksline ir pritaikomąja terapija. FND paprastai yra biologiškai suderinamos, greitai įsisavinamos ląstelėse ir gali nugabenti vaistus į tikslinę vietą. Tačiau daugelis FND turi ribotą funkcionalumą, nes jų sužadinimo ir emisijos bangų ilgiai yra ribojami siaurame ultravioletinio / regimojo (UV / VIS) spektro diapazone (Damalakienė ir kt., 2013; Dreaden ir kt., 2012). Be to, UV spinduliai prasiskverbia į audinių mažesnį gylį, t. y. ~ 400 nm bangos ilgis prasiskverbia tik apie 60 μm. Taigi *in vivo* vaizdavimui būtina sukurti ND, kurias būtų galima žadinti nenaudojant UV / VIS spinduliuotės. Vaizdinimui būtina, kad ND emisija būtų audinių optinio skaidrumo lange (~ 650 – 1100 nm), ypač artimojoje infraraudonųjų spindulių (NIR) spektrinėje srityje. Optinis langas

reiškia tam tikrą elektromagnetinio spektro bangų ilgių diapazoną, kuriame biologiniai audiniai pasižymi minimalia šviesos sugertimi ir sklaida, leidžiančia giliau prasiskverbti ir aiškiau vizualizuoti vidines struktūras ir procesus. NIR šviesos panaudojimas sužadinimui suteikia keletą privalumų, įskaitant didesnį įsiskverbimo gylį, sumažintą fototoksiškumą, minimalų autofluorescencinį foną ir sumažintą šviesos sklaidą. Vienas tokių novatoriškų nanomedžiagų pavyzdžių yra apkonvertuojančios nanodalelės (APND), kurių sudėtyje yra retųjų žemių metalų (RE) jonų, kurių sugertis yra NIR spinduliuotės srityje (Jalani ir kt., 2018; Kobayashi ir kt., 2010; Yao ir kt., 2020).

APND yra tokios ND, kurios geba konvertuoti du ar daugiau mažesnės energijos fotonų (arba NIR spinduliuotę) į vieną didelės energijos fotoną (arba didesnės energijos spinduliuotę) santykinai plačiame spektro diapazone nuo UV iki NIR. Ši APND energijos „metamorfozė“ vadinama apkonversijos reiškiniu, leidžiančiu APND būti naujos kartos biologiškai suderinamomis nanomedžiagoms, turinčioms didelį kvantinį našumą (Auzel, 2004; Jalani ir kt., 2018). Be to, APND sužadinimas NIR patenka į biologinio optinio skaidrumo langą, o tai lemia APND sužadinimą giliau audinyje ir sustiprintus terapinius procesus (Skripka ir kt., 2019). Tačiau APND iškart po sintezės pasižymi hidrofobiškumu ir jų paviršius reikalauja papildomos modifiacijos biologiškai suderinamomis dangomis (Gnach ir Bednarkiewicz, 2012). Literatūroje yra begalė paviršiaus modifikavimo metodų, tačiau vis dar ieškoma optimalių dangų, užtikrinančių koloidinį stabilumą, biologinį suderinamumą ir selektyvų APND kaupimąsi ląstelėse. Terapinis ND efektyvumas daugiausia priklauso nuo ląstelių įsisavinimo efektyvumo ir tarpląstelinės lokalizacijos. Taigi, svarbu ištirti, kokį įsisavinimo mechanizmą naudoja ląstelė, priklausomai nuo ND paviršiaus modifikacijos (Oliveira ir kt., 2019).

1.1. Naujumas ir aktualumas

Literatūroje ND ir jų sąveikos su ląstelėmis tyrimai paprastai atliekami atskirai. Svarbu pažymėti, kad yra mažai tyrimų, skirtų APND ir BV tyrimams. Remiantis *Web of Science* duomenų baze, nuo 2000 iki 2022 m. galima rasti tik 14 įrašų, naudojant raktinius žodžius „apkonvertuojančios nanodalelės“ ir „baltyminis vainikas“.

Šios disertacijos metu buvo tiriama, kaip maksimaliai padidinti ND patekima į vėžines ląsteles norint pagerinti terapinį efektyvumą. Lokalizacija ląstelėse yra labai svarbi terapiniu požiūriu. Šios disertacijos tikslas – ištirti kaip APND paviršiaus funkcionalizavimas turi įtakos formuojant atiitnkamaą

BV. BV padidina ND koloidinį stabilumą ir palengvina jų patekimą į ląsteles aktyvuojantis atitinkamiems endocitozės mechanizmams, užtikrinant veiksmingą tarpląstelinį pasiskirstymą. Tad būtina sukurti ND, su atitinkamomis paviršiaus dangomis, kad susidarytų reikiamas BV, kurio dėka ND geriau ir didesniais keikiais patektų į vėžines ląsteles.

Šioje disertacijoje pirmą kartą buvo atlikti:

1. tyrimai, skirti ištirti, kaip formavimuisi aplink skirtingą paviršiaus dangą turinčias APND BV, taip pat ląstelių APND patekimo į ląsteles mechanizmus, bei APND internalizacijos dinamiką, priklausomai nuo paviršiaus padengimo;

2. tyrimai, skirti ištirti, kaip skirtingas PEG kiekis, APND paviršiaus modifikacijose, turi įtakos APND koloidiniam stabilumui ir šių ND patekimui į ląsteles.

1.2. Disertacijos tikslas ir uždaviniai

Tikslas:

Ištirti skirtingą paviršiaus padengimą turinčių apkonvertuojančių nanodalelių (APND) sąveiką su biologine aplinka, bei jų kaupimąsi ir kaupimosi mechanizmus vėžinėse ląstelėse.

Uždaviniai:

- įvertinti biologinės aplinkos poveikį $LiYF_4$: Yb^{3+}, Tm^{3+} APND, turinčios skirtingas paviršiaus modifikacijas (citratą, fosfolipidus (PEG-DOPE:DOPC), SiO_2, kopolimerus (P_9MAA-25 ir P_9MAA-75));
- ištirti šių, skirtingais dangalais modifikuotų, APND kaupimosi ir pasiskirstymo ląstelėse modelius;
- įvertinti galimą skirtingą paviršiaus modifikaciją turiničių APND toksiškumą ląstelėms, atliekant įvairius gyvybingumo tyrimus;
- išsiaiškinti, ar APND patekimui į ląsteles įtakos turi ląstelės paviršiaus proteoma ir aplink APND susidarantis baltyminis vainikas (BV);
- ištirti skirtingus endocitozės kelius, kuriais į ląsteles patenka skirtingą paviršių turinčios APND;
- nustatyti, ar PEGilinimo kiekis APND paviršiaus modifikacijose turi įtakos APND kaupimuisi ląstelėse.

1.3. Ginamieji teiginiai

I) Baltyminis vainikas padidina APND koloidinį stabilumą, nepriklausomai nuo jų paviršiaus padengimo.

II) APND patekimo į ląsteles greitis priklauso nuo APND paviršiaus dangalų. Paviršiaus modifikacijos turi įtakos APND patekimui į ląsteles. cAPND geriausiai ir greičiausiai patenka į MDA-MB-231 ląstelių liniją.

III) APND yra biologiškai suderinamos, nėra toksiškos ląstelėms ir neturi neigiamo poveikio nei MDA-MB-231, nei MCF-7 ląstelių gyvybingumui.

IV) Ląstelių paviršiaus proteoma ir BV turi įtakos APND kaupimuis ląstelėse. MDA-MB-231 pasižymi padidėjusia integrino ekspresija ir todėl geriau ir greičiau kaupia I-APND tipo ND dėl THBS1 baltymo randamo BV.

V) Mažas cAPND dydis ir BV, susidaręs aplink cAPND bei kuriame gausu CAP1 ir THBS1 baltymų, aktyvuoja nuo klatrino priklausomą endocitozę MDA-MB-231 ląstelėse ir nuo kaveolino priklausomą endocitozę MCF-7 ląstelėse. Didžiausią BV turinčios sAPND pasižymi dideliu kiekiu A2M ir F5 baltymų savo BV. Dėl šių batymų aktyvuojamas makropinocitozės kelias abiejose ląstelių linijose.

VI) PEG kiekis II-APND paviršiaus modifikacijose turi įtakos ląstelių kaupimuisi. Didelį kiekį PEG savo paviršiuje turinčios APND, tokios kaip 25-APND, MDA-MB-231 vėžinėse ląstelėse kaupiasi didesniu greičiu, lyginant su mažesnį PEG kiekį turinčios APND (75-APND).

2. METODINĖ DALIS

APND naudotos šiame darbe buvo susintetintos ir modifikuotos citratu, fosfolipidais ir SiO_2 bei charakterizuotos Nacionaliniame tyrimų institute Kanadoje (INRS[9]) dr. Artiomo Skripkos. Tolimesniems tyrimams APND paviršiaus modifikacijas atliko dr. Vaidas Klimkevičius, kuris sėkmingai padengė APND šepetiniais polimerais Chemijos institute, Vilniuje.

[9] Institut national de la recherche scientifique.

2.1. APND sintezė ir paviršiaus padengimas

$LiYF_4:Yb^{3+}$ (25 mol %), Tm^{3+} (0,5 mol %) APND buvo susintetintos terminio skilimo metodu. Šios sintezės rezultatas oleino rūgštimi dengtos APND. Vėliau, šios hidrofobinės APND buvo papildomai padengtos citratu, fosfolipidais, siliciu, šepetiniais polimerais. Taip pat tyrimuose tirtos ir APND be dangalo, kad šios APND taptų hidrofilinės.

Citratu dengtos APND, šiame darbe žinomos kaip cAPND, buvo gautos ligandų mainų reakcijos metu. Oleino rūgštimi dengtos APND atlikus mainų reakciją pasidengė citrato molekulėmis.

Fosfolipidais dengtos APND (pAPND) buvo gautos taikant fosfolipidų įkapsuliavimo metodą. Reakcijai naudojami 1,2-dioleoil-sn-glicero-3-fosfoetanolamin-N-[metoksi (polietilenglikolis) - 2000] (PEG-DOPE) ir 1,2-dipalmitoleoil-sn-glicero-3-fosphocholino (DOPC) fosfolipidai. Galutinė fosfolipidų koncentracija yra 1:4, atitinkamai.

Siliciu dengtos APND (sAPND) gautos silicio įkapsuliavimo metodu. sAPND disperguotos distiliuotame vandenyje (DV) ir laikomos 4 °C tolimesniems tyrimams. Detalų šių APND sintezės ir paviršiaus padengimo metodinę dalį galima rasti Voronovic ir kt. 2021 publikacijoje.

APND be paviršiaus padengimo gautos oleino rūgšties nuėmimo metodu. Gautos „beligandės“ APND (b-APND) disperguotos DV, kurios buvo laikomos 4 °C tolimesniems tyrimams.

Šepetiniais polimerais dengtos APND gautos b-APND dengiant 25% PEG kiekį turinčiu polimeru ([MAA]:[PEO_9MEMA], molinis santykis 3:1) ir 75% PEG kiekį turinčiu polimeru ([MAA]:[PEO_9MEMA], molinis santykis 1:3). Gautos 25-APND ir 75-APND, kurios disperguotos DV ir laikomos 4 °C tolimesniems tyrimams. Detalesnis šių APND padengimo protokolas yra aprašytas Klimkevicius ir kt. 2022 publikacijoje.

Visos disertacijos metu buvo dirbama su cAPND, pAPND, sAPND, kurios trumpinamos iki santrumpos I-APND. Polimerais dengtos ir „beligandės“ APND žinomos kaip II-APND santrumpa.

2.2. Spektriniai matavimai

I-APND emisijos spektrai buvo tiriami Edinburgh Instruments FLS920 fluorimetru (Edinburgh Instruments, JK). Šis fluorimetras modifikuotas papildomu nuolatinės veikos lazeriu (λ = 980 nm, MDL-III-980-2W, Changchun New Industries Optoelectronics Technology Co., Kinija) APND sužadinimui. II-APND buvo tiriamos kvarcinėse kiuvetėse, emisijos spektrai

registruojami Edinburgh Instruments FLS980 (Edinburgh Instruments, JK) fluorimetru.

2.3. Koloidinio stabilumo matavimai

APND koloidinis stabilumas buvo tiriamas įvairiuose tirpaluose: DV, PBS, ląstelių auginimo terpėje (*Dulbecco's modified eagle medium*, DMEM), papildytoje 10 % (v/v) veršiuko embriono serumo (angl. *fetal bovine serum*, FBS, Gibco, Waltham, MA, JAV) ir beseruminėje terpėje 9 dienas. I-APND koncentracija matavimams buvo 1 mg/mL, II-APND atveju 0,1 mg/mL. Koloidinis stabilumas buvo įvertintas kaip emisijos intensyvumo pokytis laike ties λ = 793 nm (ties intensyviausia Tm^{3+} emisijos juosta).

2.4. Hidrodinaminio dydžio matavimai

I-APND hidrodinaminis dydis buvo matuojamas naudojant dinaminės šviesos sklaidos (DLS) metodą. ND dydis buvo matuojamas ZetaPALS dalelių hidrodinaminio dydžio ir zeta potencialo matuokliu, naudojant 633 nm lazerį (Brookhaven Inc., JAV), nustačius 10 matavimo ciklų be pauzės. II-APND hidrodinaminis dydis buvo matuojamas kaip I-APND atveju, bet pasitelkus ZetaSizer nano ZS (Malvern, JK).

2.5. Ląstelių kultivavimas

Ląsteliniams eksperimentams pasirinktos dvi žmogaus adenokarcinomos ląstelių linijos – MDA-MB-231 ir MCF-7. MDA-MB-231 ląstelių linija buvo įsigyta iš Amerikos ląstelių kultūrų kolekcijos, o MCF-7 ląstelių linija buvo gauta iš Europos ląstelių kultūrų kolekcijos. Tyrimams ląstelės buvo kultivuojamos pilnoje ląstelių auginimo terpėje (DMEM su 10 % FBS) su antibiotiko penicilino (100 V/mL) ir streptomicino (100 mg/mL) mišiniu (Pen-Strep 10000 V/mL ir 10 mg/mL, P/S, Gibco, Vokietija). Ląstelės kultivuojamos inkubatoriuje 37 °C temperatūroje ir 5% CO_2.

2.6. Ląstelių gyvybingumo nustatymas

MDA-MB-231 ir MCF-7 ląstelių gyvybingumas buvo įvertintas naudojant tris skirtingus metodus: laktato dehidrogenazės (LDH) testą, ADAM-MC automatinį gyvybingų ląstelių skaičiuoklį ir natrio 3'-[1-(fenilaminokarbonil)-3,4 – tetrazolio]-bis(4-metoksi6-nitro) benzen sulfonrūgšties hidrato (XTT) metodus.

Atliekant LDH tyrimą, ląstelės pirmiausia buvo sėjamos į 96 šulinėlių plokštelę (BD Falcon, JAV), ląstelių tankis – 20 000 ląstelių į šulinėlį. Po 24 valandų senoji terpė buvo pakeista nauja terpe, kurioje yra 0,004 mg/mL, 0,04 mg/mL arba 0,4 mg/mL I-APND. Kontrolinė terpė – augimo terpė be I-APND. Tuomet ląstelės buvo inkubuojamos tamsoje su ND 24 valandas. Jeigu I-APND turi neigiamą poveikį ląstelių gyvybingumui, ląstelių membrana tampa pralaidi ir į ląstelių auginimo terpę yra išskiriamas LDH. Dėl to, terpė po poveikio ND perkeliama į naują plokštelę sugerties matavimams. Sugertis matuojama ties dviem bangos ilgiais: 490 nm ir 680 nm spektrofotometru (BioTek, JAV). Vėliau gautos sugerties vertės buvo apskaičiuotos kaip ląstelių gyvybingumo procentinės vertės pasitelkus gamintojo protokole esančią formulę.

ADAM-MC automatizuotas ląstelių skaičiuoklis įvertina ląstelių skaičių ir ląstelių gyvybingumą. Gyvybingumo matavimo principas pagrįstas fluorescencinių DNR interkaluojančių dažų – propidžio jodido (PJ) ir negyvybingų ląstelių sąveika. Skačiuoklis įvertina dviejų tipų ląstelių skaičių: bendrą ląstelių skaičių ir negyvybingų ląstelių skaičių. Visų ląstelių skaičiui įvertinti į ląstelių suspensiją pridedama PJ kartu su lizės buferiu. Šiuo atveju, visos skaičiuojamos ląstelės turi pralaidžią membraną, rezultate PJ „išdažo“ DNR ir taip įvertinamas visų ląstelių skaičius. Negyvybingų ląstelių skaičiavimo atveju PJ nudažo ląsteles tik su pralaidžia membrana (negyvybingas).

Disertaciniame darbe vėžinės ląstelės buvo resuspenduotos PBS, o tiek ląstelių gyvybingumas, tiek bendras ląstelių skaičius buvo nustatytas naudojant ADAM-MC automatinį ląstelių skaičiuoklį (Digital Bio, Seulas, Korėja). Ląstelių gyvybingumo ir bendro ląstelių skaičiaus įvertinimas buvo atliktas automatiškai ADAM-MC programine įranga.

XTT metodas naudojamas ląstelių metaboliniam aktyvumui tirti pagal jų redokso potencialą. Gyvybingos ląstelės paverčia XTT į vandenyje tirpų, oranžinės spalvos formazaną, kurio kiekį galima tiesiogiai nustatyti naudojant spektrofotometrą. XTT tyrimas buvo atliktas pagal gamintojo instrukcijas. Kiekvienam II-APND tipui buvo naudojami šeši šulinėliai, o papildomi šeši šulinėliai buvo kontroliniai, be II-APND, tam, kad gauti pradinius sugerties duomenis. Optinis tankis esant 490 nm buvo nustatytas BioTek 800 TS mikroplokštelių skaitytuvu po ląstelių inkubacijos tetrazolio druska.

2.7. Eksperimentai su I-APND: kaupimosi dinamika ir *in vitro* ląstelių vaizdinimas

Kaupimosi dinamikos eksperimentams buvo pasirinkta 0.04 mg/mL I-APND koncentracija. Ląstelės buvo sėjamos į 12 šulinėlių plokšteles 24 val. Vėliau ląstelės buvo veikiamos I-APND 0, 5, 1, 3, 6, 9 ir 24 valandų laikotarpiui. Pasibaigus inkubaciniam laikotarpiui, ląstelių auginimo terpė, kurioje yra I-APND, buvo švelniai išsiurbta, o ląstelės tris kartus plaunamos PBS. Vėliau ląstelės buvo veikiamos 0,25% (v/v) tripsinu (Gibco, JAV) ir centrifuguojamos šviežioje terpėje esant 200 *g* 7 minutes.

Praėjus inkubaciniam laikotarpiui, ląstelių suspensijų emisijos intensyvumas buvo registruojamas naudojant Edinburgo spektrometrą FLS920 nuolat maišant suspensiją magentinę maišykle. Kaupimosi dinamikos kreivės dedamosios buvo nustatytos apskaičiuojant ląstelėse esančių APND emisijos intensyvumą tam tikru laiko momentu, padalijus iš ląstelių skaičiaus suspensijoje tuo laikotarpiu kuriame buvo vykdoma inkubacija. Duomenys vaizduojami kaip APND emisijos intensyvumas ląstelėje.

In vitro ląstelių vaizdinimui ląstelės buvo sėjamos į 8 šulinėlių plokšteles su išimamais šulinėliais (Lab-Tek šulinėliai, Nunc, Thermo Fisher, Danija). Šios ląstelės buvo sėjamos $3x10^4$ ląstelių/šulinėlį tankiu, 24 valandų inkubacijai. Vėliau ląstelės buvo veikiamos I-APND, koncentracija 0.1 mg/mL, įvairiomis trukmėmis: 1, 3, 6 ir 24 valandas. Prieš ląstelių vaizdinimą, ląstelės buvo fiksuojamos 4% paraformaldehido tirpalu (Sigma-Aldrich, Vokietija) 15 minučių. Po fiksacijos ląstelės buvo dažomos branduolių (Hoechst 33258, Sigma-Aldrich, Vokietija) ir aktinų gijų fluoresceniniais dažais (Phalloidin-Alexa 488, Invitrogen, JAV).

I-APND kaupimasis vėžinėse ląstelėse buvo vertinamas naudojant konfokalinį Nikon Eclipse Te2000-S C1 Plus skenuojantį mikroskopą bei naudojant 405 nm, 488 nm bangos ilgių lazerius (Melles Griot, (JAV) bei 980 nm lazerį (Changchun New Industries Optoelectronics Tech. Co., Ltd. Kinija).

2.8. Eksperimentai su II-APND

Šie *in vitro* vaizdinimo eksperimentai buvo atlikti taip pat, kaip ir I-APND atveju. Ląstelės sėjamos į 8 šulinėlių plokštelę, kultivuojamos 24 valandas. Vėliau ląstelės buvo inkubuojamos 0.1 mg/mL II-APND 24 valandas. Prieš vaizdinimą, ląstelės buvo fiksuojamos 4% paraformaldehidu, ląstelių branduoliai dažomi Hoechst 33258, o aktino gijos

- Alexa Fluor 488 faloidinu. II-APND kaupimasis ląstelėse buvo stebimas naudojant konfokalinį Nikon Eclipse Te2000-S C1 Plus lazerinį skenavimo mikroskopą su 405 nm, 488 nm ir 980 nm lazeriais. Visi vaizdai buvo gauti naudojant vienodus parametrus.

2.9. Ląstelių endocitozės kelių inhibicija

Ląstelės dvi dienas buvo kultivuojamos 12 šulinėlių plokštelėse, ląstelių tankis $1x10^5$ ląstelių/šulinėlį. Vėliau ląstelės 1 valandą buvo veikiamos įvairiais endocitozės inhibitoriais: nistatinu (Nys), chlorpromazinu (Chlor), nokodazolu (Nok) arba 5-(N-etil-N-izopropil) amiloridu (EIPA). Šie inhibitoriai buvo paruošti pilnoje DMEM terpėje. Po inkubacijos inhibitoriais, ląstelės tris kartus plaunamos šviežia pilna ląstelių auginimo terpe. Tuomet ląstelės buvo veikiamos pilna DMEM terpe su 0.04 mg/mL I-APND bei inkubuojamos 3 valandas. Po inkubacijos, ląstelės vėl tris kartus plaunamos PBS, tripsinizuojamos ir centrifuguojamos 200 g 7 minutes. Ląstelės resuspenduojamos 500 µL PBS, suskaičiuojamas ląstelių skaičius ir endocitozės slopinimas įvertintamas matuojant susikaupusių I-APND ląstelėse emisiją naudojant FLS920 spektrometrą, esant 980 nm sužadinimui.

Be to, I-APND kaupimasis ląstelėse po poveikio inhibitoriais buvo stebimas naudojant konfokalinį mikroskopą. Tiek MDA-MB-231, tiek MCF-7 ląstelės buvo sėjamos į 8 šulinėlių plokšteles su išimamais šulinėliais. Ląstelių tankis $3x10^4$ ląstelių į šulinėlį. Tuomet ląstelės buvo inkubuojamos su I-APND inkubatoriuje. Po šio inkubavimo ląstelės 1 valandą buvo veikiamos endocitozės inhibitoriais (Nys, Chlor, Noc arba EIPA). Tada ląstelių terpė, kurioje buvo inhibitorių, buvo pakeista pilna DMEM terpe, turinčia 100 µg/mL I-APND. Ląstelės buvo inkubuojamos su I-APND 3 valandas. Po inkubacijos ląstelės buvo fiksuojamos ir dažomos, kaip aprašyta anksčiau.

2.10. Statistinė analizė

Visi duomenys buvo pateikti kaip vidutinės vertės su atitinkamu standartiniu nuokrypiu, kai imties dydis (n) 3–6, išskyrus I-APND kaupimosi dinamikos rezultatus, kurių imties dydis buvo 9. Statistinis reikšmingumas buvo nustatytas atliekant Stjudento t-testą 95% pasikliovimo lygiu. Kuomet p reikšmė mažesnė nei 0,05, rezultatai buvo laikomi statistiškai reikšmingais.

3. REZULTATAI

3.1. Apkonvertuojančių nanodalelių charakteristikų tyrimai

Iš literatūros yra žinoma, kad APND emisijos intensyvumas skiriasi priklausomai nuo paviršiaus dangalo (Liras ir kt., 2014). Tačiau yra straipsnių, kuriuose teigiama, kad APND, turinčių teigiamą, neigiamą arba neutralų paviršiaus krūvį, emisijos intensyvumas nepasikeitė (Palo ir kt., 2018). Dėl to, buvo atlikti spektroskopiniai APND tyrimai, norint ištirti, kokią įtaką APND emisijai turi šiame darbe naudoti dangalai.

Šiame darbe naudotos APND buvo žadinamos 980 nm bangos ilgio lazeriu. Rezultate, dėl apkonversijos reiškinio, gauname APND emisiją nuo UV iki NIR srities (nuo 350 nm iki 850 nm). Emisijos spektruose galima išskirti šešias pagrindines smailes ties 345, 360, 450, 481, 646 ir 793 nm, kurios atitinka elektroninius tulio jonų šuolius. Dvi iš šių smailių, 345 ir 360 nm, yra UV srityje, o viena 793 nm yra NIR srityje. Tad šios APND yra tinkamos tiek diagnostikai, tiek terapijai. APND emisija NIR srityje (esant 800 nm) yra tinkama giluminių navikų diagnostikai, nes 793 nm spinduliuotė yra biologinio optinio skaidrumo lange (750–950 nm) (Skripka ir kt., 2019). Emisija UV srityje gali būti naudojama fotodinaminei terapijai, jei UV sugeriantis fotosensibilizatorius yra konjuguotas su APND (Z. Zhang ir kt., 2020).

I-APND emisijos pokyčio, priklausomai nuo paviršiaus modifikacijos beveik nėepastebėta. Emisijos spektruose matyti stipriausia emisija pasižyminti smailė ties 793 nm. II-APND atveju matomas skirtumas tarp skirtingai dengtų APND emisijos spektrų. Ypač nedidele emisija pasižymėjo b-APND. Tokie rezultatai gali būti grindžiami emisijos gesinimu dėl vandens molekulių sąveikos su APND (K. Zheng ir kt., 2019). Įprastai APND emisijos gesinimą sumažina amfifilinės arba hidrofobinės polimerinės dangos (Steponavičiūtė ir kt., 2020). Lyginant dengtas ir nedengtas APND, didesnis emisijos intensyvumas aptinkamas dėl dangalo „apsaugos“ nuo vandens molekulių (Steponavičiūtė ir kt., 2021).

3.2. APND hidrodinaminio dydžio ir zeta potencialo tyrimai

APND hidrodinaminiai dydžio matavimų rezultatai parodė, kad I-APND hidrodinaminis skersmuo yra apie 46 nm, 56 nm ir 85 nm, o, zeta potencialo reikšmės buvo -25,1 mV, -10,7 mV ir -44,4 mV. atitinkamai cAPND, pAPND ir sAPND atvejais. II-APND dydis buvo apie 45–90 nm, kai ir zeta potencialo

vertės buvo 27,9 mV, -1,6 mV ir -14,3 mV atitinkamai b-APND, 25-APND ir 75-APND.

3.3. APND koloidinio stabilumo tyrimai

APND koloidinio stabilumo tyrimai buvo atlikti įvairiose vandeninėse terpėse: dejonizuotame arba DV, ląstelių auginimo terpėje DMEM su ir be 10% FBS, ir PBS. I-APND, koncentracija 1 mg/mL, II-APND koncentracija 0,1 mg/mL. Tyrimai atlikti 9 dienas.

APND koloidinis stabilumas buvo matuojamas kaip emisijos intensyvumo pokyčiai ties 793 nm emisijos smaile laike 9 dienas. I-APND stabilumo matavimų rezultatai parodo, kad FBS stabilizuoja APND (DMEM su FBS atveju), lyginant tik PBS arba DMEM atveju. I-APND stabilumo pokyčiai gali būti ankstyvas BV susidarymo aplink daleles požymis. II-APND elgiasi šiek tiek kitaip. Po savaitės vis dar buvo galima aptikti 75-APND emisiją. Tuo tarpu kitos dengimą turinčios APND aglomeravosi ir nusėdo. Šie rezultatai gali būti dėl silpnos elektrostatinės sąveikos tarp APND. II-APND stabilumo tyrimų rezultatai DMEM terpėje su FBS yra panašūs į I-APND atvejį. Šie rezultatai įrodo BV formavimąsi ir APND stabilizavimąsi dispersijoje (Moore ir kt., 2015). Tačiau polimeru padengti II-APND atspindi ilgalaikį tiksliai tobulą koloidinį stabilumą, kurį galima paaiškinti kaip baltymų kiekio sumažėjimą APND paviršiuje dėl PEG kiekio, esančio APND paviršiaus modifikacijoje. Verta paminėti, kad PEG sumažina baltymų ant paviršiaus perteklių, adsorbciją, užkertant kelią ND sedimentacijai (Sahoo ir kt., 2007).

3.4. APND biosuderinamumo tyrimai

Prieš kiekvieną ląstelių eksperimentą labai svarbu išsiaiškinti, ar APND yra biologiškai suderinamos. Šiam tyrimui buvo pasirinktos dvi žmogaus adenokarcinomos ląstelių linijos MDA-MB-231 ir MCF-7. Ląstelių gyvybingumo tyrimai buvo atlikti pasitelkus tris metodikas: I-APND atveju LDH ir automatinį gyvybingų ląstelių skaičiavimą, naudojant ADAM-MC ląstelių skaičiuoklį. II-APND ląstelių gyvybingumas buvo tiriamas XTT kolorimetriniu tyrimu.

Tyrimų rezultatai parodė, kad skirtingą paviršiaus modifikaciją turinčios I-APND neturėjo statiškai reikšmingo poveikio tiriamų ląstelių gyvybingumui taikant abu anksčiau išvardintus tyrimų metodus. Tačiau rezultatai su II-APND atskleidė, kad MDA-MB-231 ląstelėms APND turėjo nežymų poveikį (gyvybingumas sumažėjo iki 70–80%) po 24 valandų

inkubacijos su II-APND. Tačiau tokiomis pačiomis sąlygomis reikšmingo poveikio MCF-7 ląstelių gyvybingumui nepastebėta. Pagal ISO standartą Nr. 10993-5, jei ląstelių gyvybingumas po poveikio ND nukrenta žemiau 70 %, tokios ND turėtų būti laikomos toksiškos ląstelėms. Abu suderinamumo tyrimai parodė APND tinkamumą tolimesniems tyrimams.

Literatūroje galima rasti gaunamų rezultatų skirtumų tarp *in vitro* ir *in vivo* biosuderinamumo tyrimų. Pavyzdžiui, yra straipsnių, kuriuose buvo parodyta, kad ilgesnis polimeru dengtų $NaYF_4$:Yb^{3+}, Er^{3+} APND poveikis žmogaus kepenų ląstelių karcinomos ląstelėms (HepG2) gali žymiai sumažinti ląstelių gyvybingumą po 48 valandų poveikio, nors po 24 valandų inkubacijos pokyčių neaptikta (C. Wang et al. , 2020). Tyrimas su be oleino rūgšties, oleino rūgštimi modifikuotų ir lipidais dengtų $LiYF_4$:Yb, Tm APND atskleidė nedidelį, tačiau statistiškai reikšmingą žmogaus plaučių vėžio ląstelių A549 gyvybingumo sumažėjimą po ilgesnės inkubacijos ND (72 valandų) nei po 24 valandų inkubacijos su APND (Rojas-Gutierrez ir kt., 2019). Be to, iš literatūros žinoma, kad citotoksiškumas priklauso nuo APND paviršiaus dangos. Pavyzdžiui, Sun ir kt. darbe parodyta, kad citratu dengtos $NaLuF_4$:Yb,Tm APND nežymiai (iki 90 %) sumažina ląstelių gyvybingumą žmogaus nosiaryklės epidermio karcinomos ląstelių linijoje, KB, esant didžiausiai tirtai 1000 μg/mL koncentracijai (Sun ir kt., 2013). Kitame Liu ir kolegų tyrime buvo tirta silicio dioksidu dengtų $NaYF_4$:Tm/Yb/Gd APND įtaka MCF-7 ląstelėms. Ląsteliniams tyrimams buvo naudojama APND koncentracija nuo 62,5 μg/mL iki 250 μg/mL. Tyrimo metu pastebėtas 20 % gyvybingumo sumažėjimas, lyginant su kontroline grupe (J. Liu ir kt., 2012). Taip pat yra žinoma, kad jei APND nėra stabilios biologinėje terpėje, jos negali būti naudojamos *in vivo* eksperimentams. Kartais APND gali būti biologiškai suderinamos su vėžinėmis ar sveikomis ląstelėmis, bet nesuderinamos su makrofagais. Toks skirtumas buvo parodytas Wysokińskos tyrime (Wysokińska ir kt., 2019). $NaGdF_4$: Yb^{3+}, Er^{3+} parodė neigiamą poveikį makrofagų gyvybingumui. APND poveikis ląstelėms po 48 valandų, kuomet APND koncentracija buvo pasirinkta 5–25 μg/mL, turėjo itin didžiulę įtaką. Ląstelių gyvybingumas sumažėjo beveik 80 %, lyginant su kontroliniais duomenimis.

3.5. Ląstelių inkubavimas su APND ir ląstelinio kaupimosi tyrimai

Norint sėkmingai taikyti APND *in vivo*, būtinai reikia atsižvelgti ir stengtis išvengti kliūčių, su kuriomis APND „susiduria“ *in vivo*: trumpu cirkuliacijos kraujotakoje laiku, APND sąveika su fagocitinėmis ląstelėmis, ir „neatkeliavimu“ į tikslinę vietą. Tuo tarpu, kalbant apie *in vitro* tyrimus, čia

susiduriama su iššūkiais kaip: APND citotoksiškumas ląstelėms; baltymų, esančių terpėje, sąveika su APND (adsorbcija ant APND paviršiaus), bei APND-baltymo komplekso sąveikos galimas nebuvimas su ląsteline membrana bei nepatekimu į ląsteles. Šiuos tris aspektus galima būtų įvardyti kaip kliūtis, kurias reiktų įveikti prieš atliekant tyrimus su ląstelėmis. Šiame poskyryje dėmesys bus skiriamas APND kaupimuisi ląstelėse, priklausomai nuo paviršiaus padengimo, įvairiose vėžinėse ląstelėse kaip MDA-MB-231 ir MCF-7.

I-APND kaupimosi dinamika vėžinėse ląstelėse buvo tiriama skirtingais laikais: po 0.5, 1, 3, 6, 9 ir 24 valandų. Tyrime naudoti du metodai: APND emisija ląstelėse matuojama fluorimetru, o ląstelės ties kiekvienu inkubacijos laiku vaizdinamos pasitelkiant lazerinės skenuojančios konfokalinės mikroskopijos (LSKM) metodą. Ląstelėse susikaupusių APND emisijos intensyvumas atvaizduojamas kiekvienu tyrimo laiko momentu kaip emisijos intensyvumas vienai ląstelei. APND kaupimasi kreivė tarsi panaši į mikroorganizmų augimo kreivę. APND kaupimosi dinamikos kreivėje galima išskirti kelias fazes (Damalakienė ir kt., 2013): augimo, eksponentinę (iki 9 val.) ir soties fazę ties 24 val. Lyginant APND kaupimąsi abiejose vėžio ląstelių linijose, pastebėta, kad kaupimasis priklauso nuo ląstelių linijos ir APND padengimo. cAPND labiausiai kaupiasi MDA-MB-231 ląstelėse lyginant su APND, dengtomis fosfolipidais ir SiO_2, o mažiausias kaupimasis buvo pAPND atveju. MCF-7 ląstelėse kaupimasis yra penkis kartus mažesnis nei MDA-MB-231 ląstelėse. Labiausiai MCF-7 ląstelės kaupia sAPND, cAPND bei sAPND itin panašiu greičiu. Literatūroje galima rasti, kad ND patekimas ir kaupimosi ląstelėse dinamika priklauso nuo ND paviršiaus krūvio, paviršiaus dangalo, ND dydžio, koncentracijos, ND inkubacijos laiko, ląstelių linijos (Albanese ir kt., 2012; Damalakienė ir kt. , 2013). Geriausia ND forma ir dydis kaupimuisi $LiYF_4:Yb^{3+}$, Tm^{3+} yra kuomet APND panašios į deimantą (arba lazdelės formos) ir yra maždaug 50 nm dydžio (Rojas-Gutierrez ir kt., 2019). Tačiau, yra tyrimų, teigiančių priešingai. Pavyzdžiui, sferinės $NaYbF_4$ APND gali būti kaupiamos greičiau nei lazdelės formos analogai (B. Chen ir kt., 2021).

Iš I-APND kaupimosi dinamikos kreivių matyti, kad sotis pasiekiama maždaug po 24 valandų ląstelių inkubacijos su APND. Norint atlikti kokybinę analizę, ląstelės buvo veikiamos:

1) I-APND 1, 3, 6 ir 24 valandas,

2) II-APND 24 valandas, nudažytos, fiksuotos ir vaizdinamos LSKM.

Jei lyginti I-APND ir II-APND kaupimąsi vizualiai, akivaizdu, kad kaupimasis priklauso nuo ląstelių linijos ir APND paviršiaus modifikacijos. MCF-7 ląstelės mažiau kaupia APND, lyginant su MDA-MB-231 ląstelėmis.

Yra žinoma, kad MDA-MB-231 ląstelės yra vėžinės kamieninės ląstelės ir yra agresyvesnės. Be to, LSKM vaizdai yra kokybinė analizė, kuri papildo kiekybinius analizės duomenis (kaupimosi dinamikos kreives).

Po 1 valandos I-APND pradeda kauptis citoplazmoje, vezikulinėse struktūrose, panašiose į endosomas. Ilginant inkubacijos trukmę, pūslelių kiekis ląstelėse didėja. Vezikulėse esančių APND kiekis tiesiogiai koreliuoja su APND emisijos signalu. Programiškai perklojant dažytų branduolių bei citoskeleto fluorescenciją ir APND emisiją, tampa akivaizdu, kad APND yra citoplazmoje, o ne branduolio viduje. Kaip matyti iš paveikslėlių, tendencija yra panaši į I-APND kaupimosi dinamikos grafikuose. Iš gautų rezultatų matyti, kad b-APND bei 25-APND gerai kaupiasi abiejose vėžinių ląstelių linijose. Tuo tarpu, I-APND kaupimosi rezultatai lyginant su I-APND vaizdinimo duomenimis rodo p-APND didžiausią kaupimąsi MDA-MB-231 ląstelėse lyginant su MCF-7 ląstelėmis.

Atlikus vaizdinimo eksperimentus, kartais yra sudėtinga nusakyti kurioje plokštumoje APND ląstelėse yra susikaupusios: ląstelės viršuje, viduje ar ląstelės apačioje. Norint atsakyti į šį klausimą buvo atlikti optiniai pjūviai z kryptimi konfokalinės mikroskopijos mikroskopu bei atliktos 3D vizualizacijos. Iš gautų rezultatų akivaizdu, kad APND agregatai kaupiasi tik virš b-APND, o kitais dangalais dengtos APND geriau kaupiamos ląstelių ir daugiausiai randamos ląstelių viduje.

Literatūroje pastebima, kad po 24 valandų inkubacijos laikotarpio su ND, ND linkę lokalizuotis lizosomose (Sousa De Almeida ir kt., 2021). Tikimasi, kad po poveikio ND, ND lokalizuosis endocitinėse pūslelėse, kurios vėliau susilieja su ankstyvomis endosomomis/ fagosomomis ir galiausiai su lizosomomis (Bourquin ir kt., 2018). Tačiau ND kaupimasis neapsiriboja vien lizosomomis, jas taip pat gali pasisavinti vėlyvosios endosomos arba daugiapūsleliniai kūneliai (Damalakienė ir kt., 2013). Norint eksperimentiškai nustatyti II-APND „likimą“ krūties vėžio ląstelėse, buvo atlikta kolokalizacijos analizė naudojant LysoTracker fluorescencinį dažą. Šis dažas leidžia žymėti ir sekti organeles, turinčias rūgštinį pH ląstelėse, suteikiant vertingos informacijos apie tai, ar II-APND patenka į ląsteles per endocitozę ir pasiekia lizosomas. Gauti rezultatai parodė, kad II-APND kolokalizacija su lizosomomis skiriasi tarp vėžinių ląstelių linijų. Pirsono koreliacijos koeficiento analizė (PKK), rodanti kolokalizaciją tarp II-APND ir lizosomų, buvo apskaičiuota abiems ląstelių linijoms. Jei PKK reikšmė yra tarp 0.5 ir 1,0, vadinasi, yra stipri koreliacija, jei reikšmė mažesnė nei 0,5, yra dalinė kolokalizacija. PKK vertės b-APND, 25-APND arba 75-APND atvejais buvo:

1) MDA-MB-231 ląstelių linijoje atitinkamai $0,46 \pm 0,03$, $0,51 \pm 0,10$ ir $0,36 \pm 0,05$, kas įrodo dalinę kolokalizaciją;

2) MCF-7 ląstelių linijose reikšmės buvo atitinkamai 0,04 ± 0,02, 0,23 ± 0,02 ir 0,05 ± 0,01, kas įrodo minimalią arba nereikšmingą kolokalizaciją.

Palyginus dvi ląstelių linijas, akivaizdu, kad MDA-MB-231 ląstelės pasižymi didesne proliferacija nei MCF-7 ląstelės, kurios įprastai auga kolonijomis, kas gali trukdyti veiksmingai pristatyti APND į šias ląsteles. Be to, APND kaupimosi skirtumai gali atsirasti dėl skirtingų BV, susidariusių aplink ND. Literatūros duomenimis, „PEGilintos“ ND ilgiau išlieka kraujotakos sistemoje, nes PEG atstumia daugumą kraujyje esančių baltymų, o BV susidaro mažesnis (Pelaz ir kt., 2015). Šio tyrimo atveju 25-APND yra labai „PEGilintos“, todėl BV gali susidaryti mažesnis nei 75-APND paviršiuje, vadinasi, ND kaupimosi greitis yra didesnis. b-APND tyrimuose buvo naudojama tik kaip kontrolė, ir jos negali būti naudojamos tolimesniemsms tyrimams, dėl nepakankamo koloidinio stabilumo ir agregacijos ląstelių biologinėje terpėje.

3.6. Endocitozės kelių įvertinimas

Siekiant labiau suprasti APND kaupimosi kelius vėžinėse ląstelėse, buvo atliktas išsamus APND kaupimosi šiose ląstelėse tyrimas. Šis tyrimas apėmė endocitozės inhibitorių, kurie slopina specifinius endocitinius mechanizmus, poveikį vėžinėms ląstelėms. Šiam tyrimui buvo naudojami keli endocitozės inhibitoriai:

- nistatinas (Nys) – nuo kaveolino priklausomos endocitozės (CVME) inhibitorius;
- chlorpromazinas (Chlor) – nuo klatrino priklausomos endocitozės (CME) inhibitorius;
- nokodazolas (Noc) – mikrovamzdelių susidarymo/išpakavimo inhibitorius;
- 5-(N-etil-N-izopropil)-amiloridas (EIPA) – makropinocitozės inhibitorius.

Prieš atliekant inhibitorių poveikį ląstelėms, buvo atliktas skirtingų inhibitorių koncentracijų poveikis ląstelių gyvybingumui tyrimas. Gauti rezultatai atskleidė tinkamas koncentracijas ląstelėms, todėl abi vėžinių ląstelių linijos buvo veikiamos tomis pačiomis koncentracijomis, „draugiškomis“ ląstelėms.

Abi ląstelių linijos (MDA-MB-231 ir MCF-7) buvo inkubuojamos su inhibitoriais 1 valandą, vėliau 3 valandas buvo veikiamos I-APND. Norint sužinoti, kokio tipo endocitozės būdu I-APND patenka į ląsteles (nuo

energijos priklausomos ar nepriklausomos) buvo atliktas tyrimas nuo energijos priklausomai enodicitozei įvertinti labai žemoje 4 °C temperatūroje.

Iš gautų rezultatų matyti, kad endocitozės slopinimui akivaizdžiai įtakos turi ir APND paviršiaus modifikikacijos, ir ląstelių linija. MDA-MB-231 ląstelėse Nys žymiai slopino pAPND įsisavinimą, todėl santykinis kaupimasis sumažėjo 45%, lyginant su kontrole. Tačiau Nys parodė minimalų cAPND (79%) ir sAPND (97%) kaupimosi slopinimą. Poveikis Noc slopino cAPND (23 %), sAPND (41 %) kaupimąsi ir mažiausiai slopino pAPND (78 %) kaupimąsi. Panašiai kaip ir Noc, Chlor taip pat sumažino cAPND kaupimosi dinamikos greitį iki 47%, o sAPND ir pAPND atvejais neturėjo įtakos, lyginant su kontroliniais duomenimis. EIPA turėjo slopinamąjį poveikį tik sAPND kaupimuisi, sumažindamas jį iki 29 %. MCF-7 ląstelių linijos atveju poveikis Nys sumažino cAPND ir sAPND kaupimosi efektyvumą atitinkamai 61% ir 67%. Dėl Noc slopinimo pAPND ir sAPND įsisavinimas sumažėjo iki 83%, tuo tarpu Noc neturėjo įtakos cAPND įsisavinimui MCF-7 ląstelėse. Poveikis Chlor padidino cAPND ir pAPND įsisavinimą, tačiau šiek tiek sumažino sAPND kaupimąsi (74%). EIPA šiek tiek sumažino cAPND (88 %) ir pAPND (91 %) patekimą į ląsteles, o sAPND kaupimasis sumažėjo iki 50%.

APND ląstelių internalizacijos kelias paprastai priklauso nuo specifinių baltymų ir atitinkamų ląstelės membranos receptorių sąveikos (Behzadi ir kt., 2017). Akivaizdu, kad abiejose vėžinių ląstelių linijose yra reikšmingų APND kaupimosi skirtumų po poveikio inhibitoriais. Stebėjimai rodo, kad cAPND patenka į MDA-MB-231 ląsteles pirmiausia nuo CME. Įvairiose ląstelių linijose karboksi grupėmis dengtos ND, kurių dydis yra nuo 40 iki 200 nm, dažniausiai yra kaupiamos nuo CME, įskaitant MDA-MB-231 ir MCF-7 ląsteles (Chaves ir kt., 2017). Kita vertus, buvo nustatyta, kad pAPND patenka į MDA-MB-231 ląsteles per CVME, kuri sutampa su Rojas-Gutierrez ir kolegų tyrimų rezultatais (Rojas-Gutierrez ir kt., 2019), rodančiais, kad lipidais padengtos APND, kurių matmenys yra 92 nm išilgai pagrindinės (ilgosios) ašies ir 53 nm išilgai trumposios ašies, naudoja CVME ND patekimui. Be to, tie patys autoriai taip pat nurodo ir priešingus rezultatus, kuriuose lipidais dengtos APND patenka į ląsteles per CME. Vadinasi, gali būti keli tų pačių APND patekimo į ląsteles būdai. Išvados apie sAPND kaupimąsi

MDA-MB-231 ir MCF-7 ląstelėse sutampa su ankstesniais Francia ir kt. duomenimis, kur buvo patvirtinta, kad SiO_2 dengtos ND, kurių hidrodinaminis dydis yra 50 nm, patenka į HeLa ląsteles makropinocitozės būdu (Francia ir kt., 2019).

Visi šiame tyrime naudojami inhibitoriai turėjo silpnesnį poveikį APND endocitozės keliams MCF-7 ląstelių linijoje lyginant su MDA-MB-231

ląstelėmis. Šis neatitikimas gali būti siejamas su MCF-7 ląstelių tendencija formuoti kolonijas, vadinasi, inhibitoriai galėjo veikti tik išorinį kolonijos sluoksnį. MCF-7 ląstelių atveju CME ir makropinocitozė yra atitinkamai cAPND ir sAPND patekimo į ląsteles keliai.

3.7. Baltyminio vainiko sąsaja su endocitiniais keliais

BV sudėties skirtumai vaidina lemiamą vaidmenį ND kaupimosi ir transportavimo keliuose (Docter ir kt., 2015; Fleischer ir Payne, 2014; Qin ir kt., 2020). Aplink I-APND susidariusių BV sudėties proteominę analizę atliko dr. Marija Ger Vilniaus universiteto Biochemijos institute. Pirmiausia, buvo tiriamas bendras baltymų kiekis BV, adsorbuotas ant I-APND paviršiaus įvairiais laiko intervalais iki 24 valandų inkubacijos DMEM su FBS. Tyrimas buvo atliktas pasitelkiant gelio elektroforezės metodą.

Gauti rezultatai parodė, kad APND dispergavus terpėje, kurioje gausu baltymų, ir po 24 val. inkubacijos, ant sAPND paviršiaus prisijungusių baltymų kiekis yra didesnis penkis kartus lyginant su cAPND ar ant pAPND paviršiaus esančių baltymų kiekiais. Be to, baltymų elektroforezės analizė atskleidžia, kad kiekvienas skirtingai padengtų APND tipas turi specifinį baltymų rinkinį, susietą su jo paviršiumi.

Atlikus skysčių chromatografijos masės spektrometrijos analizę, siekiant identifikuoti baltymus, esančius ant APND paviršiaus, nustatyta: ant cAPND paviršiaus buvo aptikti 67 baltymai, pAPND – 63 baltymai, sAPND – 86 baltymai. Baltymų analizė parodė, kad gausiausi baltymai, rasti ant cAPND buvo serumo albuminas, α-2-HS-glikoproteinas ir α-1-antiproteinazė. Panašiai pAPND pasižymėjo dideliu serumo albumino ir α-2-HS-glikoproteino kiekiu kartu su apolipoproteinu A-I. Kita vertus, sAPND baltymai atitiko skirtingą baltymų profilį, jame rasta serumo albumino,
α-2-makroglobulino (A2M) ir V krešėjimo faktoriaus (F5). Šie rezultatai pabrėžia skirtingas skirtingai padengtų I-APND baltymų kompozicijas.

Proteominė analizė buvo atlikta skirtingais laiko momentais, ypač po 1 ir 3 valandų, kuomet APND kaupimosi dinamika stabilizuojasi. Buvo nustatyta, kad cAPND BV pasižymi didele ekspresija du baltymai, trombospondinas-I (THBS1) ir su adenililciklaze susijęs baltymas 1 (CAP1). Nustatyta, kad pAPND atveju šeši baltymai gali prisidėti prie ND kaupimosi ląstelėse skirtumų. Kaip minėta anksčiau, sAPND pasižymėjo didesne baltymų adsorbcija ant paviršiaus, o tai gali būti siejama su didesniu paviršiaus plotu ir neigiamu paviršiaus krūviu, lyginant su kitais APND paviršiaus padengimais. Iš viso rasta apie 51 skirtingo kiekio baltymų tiek

sAPND, tiek pAPND po 1 valandos inkubacijos terpėje su serumu, bei 44 skirtingi baltymai rasti tiek po 1, tiek po 3 valandų. Tarp šių baltymų 46 pasižymėjo didele ekspresija sAPND BV po 1 valandos inkubacijos, o 39 baltymai buvo nuolat ekspresuojami abiem laiko momentais. Be to, naudojant Enrichr įrankį BV rasta baltymų, dalyvaujančių kraujo krešėjime, ir komplemento sistemos susidaryme sAPND BV atveju. Baltymai, būdingi kiekvienam BV, kaip CAP1 ir THBS1 cAPND atveju, F5 ir ApoA1 – pAPND, o A2M ir F5 – sAPND atvejais, yra laikomi labiausiai tikėtinais kandidatais, atsakingais už pastebėtus skirtingų tipų dengtų APND ląstelių kaupimosi skirtumus.

4. IŠVADOS

I) $LiYF_4:Yb^{3+},Tm^{3+}$ APND, padengtų citratu, DOPC:PEG-DOPE fosfolipidais, SiO_2 (I-APND) ir polimerais kaip P_9MAA-25 ir P_9MAA-75 (II-APND), spektroskopiniai tyrimai parodė, kad serumo baltymais praturtinta ląstelių augimo terpė, stabilizuoja APND. Šis stabilumas priskiriamas baltymų vainikui (BV), susidariusiam aplink kiekvieną APND, esant serumo baltymų ląstelių augimo terpėje.

II) APND kaupimosi ląstelėse dinamika priklauso nuo APND paviršiaus modifikacijų. cAPND geriausiai kaupiasi MDA-MB-231 ląstelėse. Ši patekimo į ląsteles dinamika yra dėl cAPND dydžo ir BV, susidariusio aplink šias ND.

III) Naudojant du nepriklausomus citotoksiškumo (LDH tyrimą) ir gyvybingumo (automatinį ląstelių skaičiavimo metodą) įvertinimo metodus, nebuvo nustatytas neigiamas APND poveikis nė vienai vėžinių ląstelių linijai.

IV) Ląstelių paviršiaus proteomos tyrimai atskleidė, kad specifinė baltymų ekspresija vėžinių ląstelių plazminėje membranoje turi įtakos APND kaupimosi ląstelėse greičiui. MDA-MB-231 paviršiuje yra daugiausia integrinų šeimos baltymų, kurie yra atsakingi už nuo klatrino priklausomos endocitozės kelią. cAPND BV turi THBS1 baltymą, kuris sąveikauja su integrinais, dėl to cAPND kaupimos dinamika yra didžiausia MDA-MB-231 ląstelių linijoje.

V) BV dydis ir sudėtis turi įtakos APND endocitozei. sAPND, kurių BV turi penkis kartus daugiau baltymų, palyginti su pAPND arba cAPND, pasižymi baltymais, kaip A2M ir F5, dėl kurių abiejose vėžio ląstelių linijose sAPND patenka per makropinocitozės kelią. cAPND pasižymi mažiausiu dydžiu ir savo BV turi CAP1 ir THBS1 baltymų, atsakingų už nuo klatrino priklausomos endocitozės kelią MDA-MB-231 ląstelių linijoje. MCF-7 ląstelių atveju cAPND patenka per nuo kaveolino priklausomos endocitozės mechanizmą. pAPND BV yra ApoA1 ir F5, kurių dėka pAPND į abejas ląstelių linijas aptenka per nuo kaveolino priklausomą endocitozės kelią.

VI) PEG kiekio APND paviršiaus modifikacijose kiekio įtakos APND koloidiniam stabilumui ir kaupimuisi ląstelėse tyrimai parodė, kad PEG tankis APND paviršiuje turi įtakos tiek APND koloidiniam stabilumui, tiek II-APND kaupimuisi vėžinėse ląstelėse. II-APND koloidiškai stabilios terpėje, kurioje gausu serumo baltymų. Didelį kiekį PEG turinčios APND, tokios kaip 25-APND kaupiasi abiejose vėžinių ląstelių linijose didesniu greičiu nei mažesnį PEG kiekį turinčios APND (75-APND).

8. REFERENCES/LITERATŪROS SĄRAŠAS

Albanese, A., Tang, P. S., & Chan, W. C. W. (2012). The effect of nanoparticle size, shape, and surface chemistry on biological systems. *Annual Review of Biomedical Engineering*, *14*, 1–16.

Al-Hajj, M., Wicha, M. S., Benito-Hernandez, A., Morrison, S. J., & Clarke, M. F. (2003). Prospective identification of tumorigenic breast cancer cells. *Proceedings of the National Academy of Sciences of the United States of America*, *100*(7), 3983–3988.

Andresen, E., Würth, C., Prinz, C., Michaelis, M., & Resch-Genger, U. (2020). Time-resolved luminescence spectroscopy for monitoring the stability and dissolution behaviour of upconverting nanocrystals with different surface coatings. *Nanoscale*, *12*(23), 12589–12601.

Aoyama, M., Hata, K., Higashisaka, K., Nagano, K., Yoshioka, Y., & Tsutsumi, Y. (2016). Clusterin in the protein corona plays a key role in the stealth effect of nanoparticles against phagocytes. *Biochemical and Biophysical Research Communications*, *480*(4), 690–695.

Arppe, R., Hyppänen, I., Perälä, N., Peltomaa, R., Kaiser, M., Würth, C., Christ, S., Resch-Genger, U., Schäferling, M., & Soukka, T. (2015). Quenching of the upconversion luminescence of $NaYF_4$:Yb^3 ,Er^{3+} and $NaYF_4$:Yb^{3+},Tm^{3+} nanophosphors by water: the role of the sensitizer Yb^{3+} in non-radiative relaxation. *Nanoscale*, *7*(27), 11746–11757.

Auzel, F. (2004). Upconversion and Anti-Stokes processes with f and d Ions in solids. *Chemical Reviews*, *104*(1), 139–173.

Behzadi, S., Serpooshan, V., Tao, W., Hamaly, M. A., Alkawareek, M. Y., Dreaden, E. C., Brown, D., Alkilany, A. M., Farokhzad, O. C., & Mahmoudi, M. (2017). Cellular uptake of nanoparticles: journey inside the cell. *Chemical Society Reviews*, *46*(14), 4218–4244.

Beyazit, S., Ambrosini, S., Marchyk, N., Palo, E., Kale, V., Soukka, T., Tse Sum Bui, B., & Haupt, K. (2014). Versatile synthetic strategy for coating upconverting nanoparticles with polymer shells through localized photopolymerization by using the particles as internal light sources. *Angewandte Chemie-International Edition*, *53*(34), 8919–8923.

Bloembergen, N. (1959). Solid state infrared quantum counters. *Physical Reviews Letters*, *2*, 84–85.

Borth, W. (1992). α2 macroglobulin, a multifunctional binding protein with targeting characteristics. *The FASEB Journal*, *6*(15), 3345–3353.

Bourquin, J., Milosevic, A., Hauser, D., Lehner, R., Blank, F., Petri-Fink, A., Rothen-Rutishauser, B., Bourquin, J., Milosevic, A., Hauser, D., Lehner, R., Petri-Fink, A., Rothen-Rutishauser, B., & Blank, F. (2018).

Biodistribution, clearance, and long-term fate of clinically relevant nanomaterials. *Advanced Materials*, *30*(19), 1704307.

Bres, E. E., & Faissner, A. (2019). Low density receptor-related protein 1 interactions with the extracellular matrix: More than meets the eye. *Frontiers in Cell and Developmental Biology*, *7*(MAR), 436452.

Cai, R., & Chen, C. (2019). The crown and the scepter: roles of the protein corona in nanomedicine. *Advanced Materials*, *31*(45), 1805740.

Cailleau, R., Olive, M., & Cruciger, Q. V. J. (1978). Long-term human breast carcinoma cell lines of metastatic origin: preliminary characterization. *In Vitro*, *14*(11), 911–915.

Capriotti, A. L., Caracciolo, G., Caruso, G., Foglia, P., Pozzi, D., Samperi, R., & Lagana, A. (2011). Differential analysis of "protein corona" profile adsorbed onto different nonviral gene delivery systems. *Analytical Biochemistry*, *419*(2), 180–189.

Caracciolo, G., Palchetti, S., Digiacomo, L., Chiozzi, R. Z. Z., Capriotti, A. L., Amenitsch, H., Tentori, P. M., Palmieri, V., Papi, M., Cardarelli, F., Pozzi, D., & Laganà, A. (2018). Human Biomolecular Corona of Liposomal Doxorubicin: The Overlooked Factor in Anticancer Drug Delivery. *ACS Applied Materials and Interfaces*, *10*(27), 22951–22962.

Chaves, N. L., Estrela-Lopis, I., Böttner, J., Lopes, C., Guido, B. C., De Sousa, A. R., & Báo, S. N. (2017). Exploring cellular uptake of iron oxide nanoparticles associated with rhodium citrate in breast cancer cells. *International Journal of Nanomedicine*, *12*, 5511–5523.

Chávez-García, D., Juarez-Moreno, K., Campos, C. H., Tejeda, E. M., Alderete, J. B., & Hirata, G. A. (2018). Cytotoxicity, genotoxicity and uptake detection of folic acid-functionalized green upconversion nanoparticles Y_2O_3/Er^{3+}, Yb^{3+} as biolabels for cancer cells. *Journal of Materials Science*, *53*(9), 6665–6680.

Chen, B., Wang, Y., Guo, Y., Shi, P., & Wang, F. (2021). $NaYbF_4@NaYF_4$ nanoparticles: controlled shell growth and shape-dependent cellular uptake. *ACS Applied Materials & Interfaces*, *13*(2), 2327–2335.

Chen, G., Qiu, H., Prasad, P. N., & Chen, X. (2014). Upconversion nanoparticles: design, nanochemistry, and applications in theranostics. *Chemical Reviews*, *114*(10), 5161–5214.

Correard, F., Maximova, K., Estève, M. A., Villard, C., Roy, M., Al-Kattan, A., Sentis, M., Gingras, M., Kabashin, A. V., & Braguer, D. (2014). Gold nanoparticles prepared by laser ablation in aqueous biocompatible solutions: Assessment of safety and biological identity for nanomedicine applications. *International Journal of Nanomedicine*, *9*, 5415–5430.

Cox, A., Andreozzi, P., Dal Magro, R., Fiordaliso, F., Corbelli, A., Talamini, L., Chinello, C., Raimondo, F., Magni, F., Tringali, M., Krol, S., Silva, P. J., Stellacci, F., Masserini, M., & Re, F. (2018). Evolution of nanoparticle protein corona across the blood−brain barrier. *ACS Nano*, *12*(7), 7292–7300.

Damalakiene, L., Karabanovas, V., Bagdonas, S., Valius, M., & Rotomskis, R. (2013). Intracellular distribution of nontargeted quantum dots after natural uptake and microinjection. *International Journal of Nanomedicine*, *8*, 555–568.

Dawson, K. A., & Yan, Y. (2021). Current understanding of biological identity at the nanoscale and future prospects. *Nature Nanotechnology*, *16*(3), 229–242.

Dekkers, S., Oomen, A. G., Bleeker, E. A. J., Vandebriel, R. J., Micheletti, C., Cabellos, J., Janer, G., Fuentes, N., Vázquez-Campos, S., Borges, T., Silva, M. J., Prina-Mello, A., Movia, D., Nesslany, F., Ribeiro, A. R., Leite, P. E., Groenewold, M., Cassee, F. R., Sips, A. J. A. M., … Wijnhoven, S. W. P. (2016). Towards a nanospecific approach for risk assessment. *Regulatory Toxicology and Pharmacology*, *80*, 46–59.

Digiacomo, L., Cardarelli, F., Pozzi, D., Palchetti, S., Digman, M. A., Gratton, E., Capriotti, A. L., Mahmoudi, M., & Caracciolo, G. (2017). An apolipoprotein-enriched biomolecular corona switches the cellular uptake mechanism and trafficking pathway of lipid nanoparticles. *Nanoscale*, *9*(44), 17254–17262.

Docter, D., Westmeier, D., Markiewicz, M., Stolte, S., Knauer, S. K., & Stauber, R. H. (2015). The nanoparticle biomolecule corona: lessons learned - challenge accepted? *Chemical Society Reviews*, *44*(17), 6094–6121.

Dong, H., Sun, L. D., & Yan, C. H. (2015). Energy transfer in lanthanide upconversion studies for extended optical applications. *Chemical Society Reviews*, *44*(6), 1608–1634.

Dreaden, E. C., Austin, L. A., MacKey, M. A., & El-Sayed, M. A. (2012). Size matters: gold nanoparticles in targeted cancer drug delivery. *Therapeutic Delivery*, *3*(4), 457–478.

Duong, H. T. T., Chen, Y., Tawfik, S. A., Wen, S., Parviz, M., Shimoni, O., & Ab, D. J. (2018). Systematic investigation of functional ligands for colloidal stable upconversion nanoparticles. *RSC Advances*, *8*(9), 4842–4849.

Fan, D., Cao, Y., Cao, M., Wang, Y., Cao, Y., & Gong, T. (2023). Nanomedicine in cancer therapy. *Signal Transduction and Targeted Therapy*, *8*(1), 1–34.

Farka, Z., Mickert, M. J., Hlaváček, A., Skládal, P., & Gorris, H. H. (2017). Single molecule upconversion-linked immunosorbent assay with extended dynamic range for the sensitive detection of diagnostic biomarkers. *Analytical Chemistry*, *89*(21), 11825–11830.

Farka, Z., Mickert, M. J., Mikušová, Z., Hlaváček, A., Bouchalová, P., Xu, W., Bouchal, P., Skládal, P., & Gorris, H. H. (2020). Surface design of photon-upconversion nanoparticles for high-contrast immunocytochemistry. *Nanoscale*, *12*(15), 8303–8313.

Fleischer, C. C., & Payne, C. K. (2014). Nanoparticle-cell interactions: molecular structure of the protein corona and cellular outcomes. *Accounts of Chemical Research*, *47*(8), 2651–2659.

Foroozandeh, P., & Aziz, A. A. (2018). Insight into Cellular Uptake and Intracellular Trafficking of Nanoparticles. *Nanoscale Research Letters*, *13*(1), 1–12.

Francia, V., Yang, K., Deville, S., Reker-Smit, C., Nelissen, I., & Salvati, A. (2019). Corona composition can affect the mechanisms cells use to internalize nanoparticles. *ACS Nano*, *13*(10), 11107–11121.

Gangadharan, B., Ing, M., Delignat, S., Peyron, I., Teyssandier, M., Kaveri, S. V., & Lacroix-Desmazes, S. (2017). The C1 and C2 domains of blood coagulation factor VIII mediate its endocytosis by dendritic cells. *Haematologica*, *102*(2), 271.

Giaquinto, A. N., Sung, H., Miller, K. D., Kramer, J. L., Newman, L. A., Minihan, A., Jemal, A., & Siegel, R. L. (2022). Breast Cancer Statistics 2022. *CA-A Cancer Journal for Clinicians*, *72*(6), 524–541.

Gillet, J. P., Varma, S., & Gottesman, M. M. (2013). The Clinical Relevance of Cancer Cell Lines. *JNCI: Journal of the National Cancer Institute*, *105*(7), 452–458.

Gnach, A., & Bednarkiewicz, A. (2012). Lanthanide-doped up-converting nanoparticles: merits and challenges. *Nano Today*, *7*(6), 532–563.

Gnach, A., Lipinski, T., Bednarkiewicz, A., Rybka, J., & Capobianco, J. A. (2015). Upconverting nanoparticles: assessing the toxicity. *Chemical Society Reviews*, *44*(6), 1561–1584.

Grodzinski, P., Kircher, M., Goldberg, M., & Gabizon, A. (2019). Integrating nanotechnology into cancer care. *ACS Nano*, *13*(7), 7370–7376.

Gu, B., & Zhang, Q. (2018). Recent advances on functionalized upconversion nanoparticles for detection of small molecules and ions in biosystems. *Advanced Science*, *5*(3), 1700609.

Guller, A. E., Generalova, A. N., Petersen, E. V., Nechaev, A. V., Trusova, I. A., Landyshev, N. N., Nadort, A., Grebenik, E. A., Deyev, S. M., Shekhter, A. B., & Zvyagin, A. V. (2015). Cytotoxicity and non-specific

cellular uptake of bare and surface-modified upconversion nanoparticles in human skin cells. *Nano Research, 8*(5), 1546–1562.

Haase, M., & Schäfer, H. (2011). Upconverting Nanoparticles Angewandte. *Angewandte Chemie, 50*(26), 5808–5829.

Heuser, J., & Kirchhausen, T. (1985). Deep-etch views of clathrin sssemblies. *Journal of Ultrastructure Research, 92*, 1–27.

Hirai, T., Orikoshi, T., & Komasawa, I. (2002). Preparation of Y_2O_3:Yb,Er infrared-to-visible conversion phosphor fine particles using an emulsion liquid membrane system. *Chemistry of Materials*, *14*(8), 3576–3583.

Hlaváček, A., Sedlmeier, A., Skládal, P., & Gorris, H. H. (2014). Electrophoretic characterization and purification of silica-coated photon-upconverting nanoparticles and their bioconjugates. *ACS Applied Materials and Interfaces*, *6*(9), 6930–6935.

Holliday, D. L., & Speirs, V. (2011). Choosing the right cell line for breast cancer research. *Breast Cancer Research*, *13*(4), No. 215.

Hoshyar, N., Gray, S., Han, H., & Bao, G. (2016). The effect of nanoparticle size on in vivo pharmacokinetics and cellular interaction. *Nanomedicine*, *11*(6), 673.

Hubberstey, A. V., & Mottillo, E. P. (2002). Cyclase-associated proteins: CAPacity for linking signal transduction and actin polymerization. *The FASEB Journal*, *16*(6), 487–499.

Idris, N. M., Gnanasammandhan, M. K., Zhang, J., Ho, P. C., Mahendran, R., & Zhang, Y. (2012). In vivo photodynamic therapy using upconversion nanoparticles as remote-controlled nanotransducers. *Nature Medicine*, *18*(10), 1580–1585.

Jalani, G., Tam, V., Vetrone, F., & Cerruti, M. (2018). Seeing, targeting and delivering with upconverting nanoparticles. *Journal of the American Chemical Society*, *140*(35), 10923–10931.

Jiang, X., Cao, C., Feng, W., & Li, F. (2016). Nd^{3+}-doped $LiYF_4$ nanocrystals for bio-imaging in the second near-infrared window. *Journal of Materials Chemistry B*, *4*(1), 87–95.

Kang, D., Jeon, E., Kim, S., & Lee, J. (2020). Lanthanide-doped upconversion nanomaterials: recent advances and applications. *BioChip Journal*, *14*, 124–135.

Khabir, Z., Guller, A. E., Rozova, V. S., Liang, L., Lai, Y. J., Goldys, E. M., Hu, H., Vickery, K., & Zvyagin, A. V. (2019). Tracing upconversion nanoparticle penetration in human skin. *Colloids and Surfaces B: Biointerfaces*, *184*, 110480.

Kobayashi, H., Ogawa, M., Alford, R., Choyke, P. L., & Urano, Y. (2010). New strategies for fluorescent probe design in medical diagnostic imaging. *Chemical Reviews*, *110*(5), 2620–2640.

Lambot, N., Lybaert, P., Boom, A., Delogne-Desnoeck, J., Vanbellinghen, A. M., Graff, G., Lebrun, P., & Meuris, S. (2006). Evidence for a Clathrin-Mediated Recycling of Albumin in Human Term Placenta. *Biology of Reproduction*, *75*(1), 90–97.

Lei, Z., Ling, X., Mei, Q., Fu, S., Zhang, J., Zhang, Y., Lei, Z., Zhang, Y., Ling, X., Mei, Q., Fu, S., & Zhang, J. (2020). An excitation navigating energy migration of lanthanide ions in upconversion nanoparticles. *Advanced Materials*, *32*(9), No. 1906225.

Lesniak, A., Campbell, A., Monopoli, M. P., Lynch, I., Salvati, A., & Dawson, K. A. (2010). Serum heat inactivation affects protein corona composition and nanoparticle uptake. *Biomaterials*, *31*(36), 9511–9518.

Lesniak, A., Fenaroli, F., Monopoli, M. P., Åberg, C., Dawson, K. A., & Salvati, A. (2012). Effects of the presence or absence of a protein corona on silica nanoparticle uptake and impact on cells. *ACS Nano*, *6*(7), 5845–5857.

Li, L. Le, Zhang, R., Yin, L., Zheng, K., Qin, W., Selvin, P. R., & Lu, Y. (2012). Biomimetic surface engineering of lanthanide-doped upconversion nanoparticles as versatile bioprobes. *Angewandte Chemie International Edition*, *51*(25), 6121–6125.

Li, Z., Liang, T., Lv, S., Zhuang, Q., & Liu, Z. (2015). A rationally designed upconversion nanoprobe for in vivo detection of hydroxyl radical. *Journal of the American Chemical Society*, *137*(34), 11179–11185.

Liras, M., González-Béjar, M., Peinado, E., Francés-Soriano, L., Pérez-Prieto, J., Quijada-Garrido, I., & García, O. (2014). Thin amphiphilic polymer-capped upconversion nanoparticles: Enhanced emission and thermoresponsive properties. *Chemistry of Materials*, *26*(13), 4014–4022.

Liu, J., Bu, W., Zhang, S., Chen, F., Xing, H., Pan, L., Zhou, L., Peng, W., & Shi, J. (2012). Controlled synthesis of uniform and monodisperse upconversion core/mesoporous silica shell nanocomposites for bimodal imaging. *Chemistry - A European Journal*, *18*(8), 2335–2341.

Liu, Q., Feng, W., Yang, T., Yi, T., & Li, F. (2013). Upconversion luminescence imaging of cells and small animals. *Nature Protocols*, *8*(10), 2033–2044.

Liu, Y. L., Chou, C. K., Kim, M., Vasisht, R., Kuo, Y. A., Ang, P., Liu, C., Perillo, E. P., Chen, Y. A., Blocher, K., Horng, H., Chen, Y. I., Nguyen, D. T., Yankeelov, T. E., Hung, M. C., Dunn, A. K., & Yeh, H. C. (2019).

Assessing metastatic potential of breast cancer cells based on EGFR dynamics. *Scientific Reports*, *9*(1), 1–13.

Liu, Z., Zhan, X., Yang, M., Yang, Q., Xu, X., Lan, F., Wu, Y., & Gu, Z. (2016). A magnetic-dependent protein corona of tailor-made superparamagnetic iron oxides alters their biological behaviors. *Nanoscale*, *8*(14), 7544–7555.

Mahmoudi, M. (2021). The need for robust characterization of nanomaterials for nanomedicine applications. *Nature Communications*, *12*(1), 1–5.

Maiorano, G., Sabella, S., Sorce, B., Brunetti, V., Malvindi, M. A., Cingolani, R., & Pompa, P. P. (2010). Effects of cell culture media on the dynamic formation of protein-nanoparticle complexes and influence on the cellular response. *ACS Nano*, *4*(12), 7481–7491.

Märkl, S., Schroter, A., & Hirsch, T. (2020). Small and bright water-protected upconversion nanoparticles with long-time stability in complex, aqueous media by phospholipid membrane coating. *Nano Letters*, *20*(12), 8620–8625.

Means, N., Elechalawar, C. K., Chen, W. R., Bhattacharya, R., & Mukherjee, P. (2022). Revealing macropinocytosis using nanoparticles. *Molecular Aspects of Medicine*, *83*.

Mettenbrink, E. M., Yang, W., & Wilhelm, S. (2022). Bioimaging with upconversion nanoparticles. *Advanced Photonics Research*, *3*(12).

Mikhailenko, I., Krylov, D., Argraves, K. M. T., Roberts, D. D., Liau, G., & Strickland, D. K. (1997). Cellular internalization and degradation of thrombospondin-1 is mediated by the amino-terminal heparin binding domain (HBD). High affinity interaction of dimeric HBD with the low density lipoprotein receptor-related protein. *Journal of Biological Chemistry*, *272*(10), 6784–6791.

Moore, T. L., Rodriguez-Lorenzo, L., Hirsch, V., Balog, S., Urban, D., Jud, C., Rothen-Rutishauser, B., Lattuada, M., & Petri-Fink, A. (2015). Nanoparticle colloidal stability in cell culture media and impact on cellular interactions. *Chemical Society Reviews*, *44*(17), 6287–6305.

Mosquera, J., García I., Henriksen-Lacey, M., Martínez-Calvo M., Dhanjani M., Mascareñas, J. L., & Liz-Marzán, L. M. (2020). Reversible control of protein corona formation on gold nanoparticles using host−guest interactions. *ACS Nano*, *14*(5), 5382–5391.

Motta, G., & Tersariol, I. L. S. (2017). Modulation of the Plasma Kallikrein-Kinin System Proteins Performed by Heparan Sulfate Proteoglycans. *Frontiers in Physiology*, *8*, No. 481.

Mousavi, A. S., Malerød, L., Berg, T., & Kjeken, R. (2004). Clathrin-dependent endocytosis. *Biochemical Journal*, *377*, 1–16.

Murphy-Ullrich, J. E. (2022). Thrombospondin-1 Signaling Through the Calreticulin/LDL Receptor Related Protein 1 Axis: Functions and Possible Roles in Glaucoma. *Frontiers in Cell and Developmental Biology*, *10*, 898772.

Nabi, I. R., & Le, P. U. (2003). Mini-review caveolae/raft-dependent endocytosis. *The Journal of Cell Biology* , *161*(4), 673–677.

Nam, S. H., Bae, Y. M., Park, Y. Il, Kim, J. H., Kim, H. M., Choi, J. S., Lee, K. T., Hyeon, T., & Suh, Y. D. (2011). Long-term real-time tracking of lanthanide ion doped upconverting nanoparticles in living cells. *Angewandte Chemie - International Edition*, *123*, 6217–6221.

Nguyen, V. H., & Lee, B. J. (2017). Protein corona: a new approach for nanomedicine design. *International Journal of Nanomedicine*, *12*, 3137–3151.

Ogden, C. A., DeCathelineau, A., Hoffmann, P. R., Bratton, D., Fadok, B., Ghebrehiwet, V. A., & Henson, P. M. (2001). C1q and Mannose Binding Lectin Engagement of Cell Surface Calreticulin and Cd91 Initiates Macropinocytosis and Uptake of Apoptotic Cells. *Journal of Experimental Medicine*, *194*(6), 781–796.

Oliveira, H., Bednarkiewicz, A., Falk, A., Fröhlich, E., Lisjak, D., Prina-Mello, A., Resch, S., Schimpel, C., Vrček, I. V., Wysokińska, E., & Gorris, H. H. (2019). Critical Considerations on the Clinical Translation of Upconversion Nanoparticles (UCNPs): Recommendations from the European Upconversion Network (COST Action CM1403). *Advanced Healthcare Materials*, *8*(1), No. 1801233.

Palo, E., Lahtinen, S., Päkkilä, H., Salomäki, M., Soukka, T., & Lastusaari, M. (2018). Effective shielding of $NaYF_4$:Yb^{3+},Er^{3+} upconverting nanoparticles in aqueous environments using layer-by-layer assembly. *Langmuir*, *34*(26), 7759–7766.

Paul, N. R., Jacquemet, G., & Caswell, P. T. (2015). Endocytic Trafficking of Integrins in Cell Migration. *Current Biology*, *25*(22), R1092–R1105.

Pelaz, B., del Pino, P., Maffre, P., Hartmann, R., Gallego, M., Rivera-Ferná ndez, S., de la Fuente, J. M., Ulrich Nienhaus, G., & Parak, W. J. (2015). Surface functionalization of nanoparticles with polyethylene glycol: effects on protein adsorption and cellular uptake. *ACS Nano*, *9*(7), 6996–7008.

Pisani, C., Gaillard, J. C., Dorandeu, C., Charnay, C., Guari, Y., Chopineau, J., Devoisselle, J. M., Armengaud, J., & Prat, O. (2017). Experimental separation steps influence the protein content of corona around mesoporous silica nanoparticles. *Nanoscale*, *9*(18), 5769–5772.

Poláchová, V., Pastucha, M., Mikušová, Z., Mickert, M. J., Hlaváček, A., Gorris, H. H., Skládal, P., & Farka, Z. (2019). Click-conjugated photon-upconversion nanoparticles in an immunoassay for honeybee pathogen Melissococcus plutonius. *Nanoscale*, *11*(17), 8343–8351.

Polo, S., & Di Fiore, P. P. (2006). Endocytosis conducts the cell signaling orchestra. *Cell*, *124*(5), 897–900.

Qin, M., Zhang, J., Li, M., Yang, D., Liu, D., Song, S., Fu, J., Zhang, H., Dai, W., Wang, X., Wang, Y., He, B., & Zhang, Q. (2020). Proteomic analysis of intracellular protein corona of nanoparticles elucidates nano-trafficking network and nano-bio interactions. *Theranostics*, *10*(3), 1213–1229.

Qiu, Y., Liu, Y., Wang, L., Xu, L., Bai, R., Ji, Y., Wu, X., Zhao, Y., Li, Y., & Chen, C. (2010). Surface chemistry and aspect ratio mediated cellular uptake of Au nanorods. *Biomaterials*, *31*(30), 7606–7619.

Rao, L., Meng, Q. F., Bu, L. L., Cai, B., Huang, Q., Sun, Z. J., Zhang, W. F., Li, A., Guo, S. S., Liu, W., Wang, T. H., & Zhao, X. Z. (2017). Erythrocyte membrane-coated upconversion nanoparticles with minimal protein adsorption for enhanced tumor imaging. *ACS Applied Materials and Interfaces*, *9*(3), 2159–2168.

Ritz, S., Schöttler, S., Kotman, N., Baier, G., Musyanovych, A., Kuharev, J., Landfester, K., Schild, H., Jahn, O., Tenzer, S., & Mailänder, V. (2015). Protein Corona of Nanoparticles: Distinct Proteins Regulate the Cellular Uptake. *Biomacromolecules*, *16*(4), 1311–1321.

Rodriguez Burbano, D. C., Naccache, R., & Capobianco, J. A. (2015). Near-IR triggered photon upconversion: imaging, detection, and therapy. In *Handbook on the Physics and Chemistry of Rare Earths*.

Rojas-Gutierrez, P. A., Bekah, D., Seuntjens, J., DeWolf, C. E., & Capobianco, J. A. (2019). Cellular uptake, cytotoxicity and trafficking of supported lipid bilayer coated lanthanide upconverting nanoparticles in alveolar lung cancer cells. *ACS Applied Bio Materials*, *2*(10), 4257–4536.

Roy, K., Patel, Y. S., Kanwar, R. K., Rajkhowa, R., Wang, X., & Kanwar, J. R. (2016). Biodegradable Eri silk nanoparticles as a delivery vehicle for bovine lactoferrin against MDA-MB-231 and MCF-7 breast cancer cells. *International Journal of Nanomedicine*, *11*, 25–44.

Saha, K., Rahimi, M., Yazdani, M., Kim, S. T., Moyano, D. F., Hou, S., Das, R., Mout, R., Rezaee, F., Mahmoudi, M., & Rotello, V. M. (2016). Regulation of Macrophage Recognition through the Interplay of Nanoparticle Surface Functionality and Protein Corona. *ACS Nano*, *10*(4), 4421–4430.

Sahoo, B., Goswami, M., Nag, S., & Maiti, S. (2007). Spontaneous formation of a protein corona prevents the loss of quantum dot fluorescence in physiological buffers. *Chemical Physics Letters*, *445*(4–6), 217–220.

Schäffler, M., Sousa, F., Wenk, A., Sitia, L., Hirn, S., Schleh, C., Haberl, N., Violatto, M., Canovi, M., Andreozzi, P., Salmona, M., Bigini, P., Kreyling, W. G., & Krol, S. (2014). Blood protein coating of gold nanoparticles as potential tool for organ targeting. *Biomaterials*, *35*(10), 3455–3466.

Schöttler, S., Becker, G., Winzen, S., Steinbach, T., Mohr, K., Landfester, K., Mailänder, V., & Wurm, F. R. (2016). Protein adsorption is required for stealth effect of poly(ethylene glycol)- and poly(phosphoester)-coated nanocarriers. *Nature Nanotechnology*, *11*(4), 372–377.

Sid, B., Sartelet, H., Bellon, G., El Btaouri, H., Rath, G., Delorme, N., Haye, B., & Martiny, L. (2004). Thrombospondin 1: A multifunctional protein implicated in the regulation of tumor growth. *Critical Reviews in Oncology/Hematology*, *49*(3), 245–258.

Sikora, B., Kowalik, P., Mikulski, J., Fronc, K., Kamińska, I., Szewczyk, M., Konopka, A., Zajdel, K., Minikayev, R., Sobczak, K., Zaleszczyk, W., Borodziuk, A., Rybusiński, J., Szczytko, J., Sienkiewicz, A., Wojciechowski, T., Stępień, P., Frontczak-Baniewicz, M., Łapiński, M., … Elbaum, D. (2017). Mammalian cell defence mechanisms against the cytotoxicity of $NaYF_4$:(Er,Yb,Gd) nanoparticles. *Nanoscale*, *9*(37), 14259–14271.

Skripka, A., Karabanovas, V., Jarockyte, G., Marin, R., Tam, V., Cerruti, M., Rotomskis, R., & Vetrone, F. (2019). Decoupling theranostics with rare earth doped nanoparticles. *Advanced Functional Materials*, *29*(12), No. 1807105.

Soenen, S. J., Manshian, B. B., Abdelmonem, A. M., Montenegro, J. M., Tan, S., Balcaen, L., Vanhaecke, F., Brisson, A. R., Parak, W. J., De Smedt, S. C., & Braeckmans, K. (2014). The cellular interactions of PEGylated gold nanoparticles: Effect of PEGylation on cellular uptake and cytotoxicity. *Particle and Particle Systems Characterization*, *31*(7), 794–800.

Soule, H. D., Vazquez, J., Long, A., Albert, S., & Brennan, M. (1973). A human cell line from a pleural effusion derived from a breast carcinoma. *Journal of The National Cancer Institute*, *51*(5), 1409–1416.

Sousa De Almeida, M., Susnik, E., Drasler, B., Taladriz-Blanco, P., Petri-Fink Ab, A., & Rothen-Rutishauser, B. (2021). Understanding nanoparticle endocytosis to improve targeting strategies in nanomedicine. *Chemical Society Reviews*, *50*(9), 5397–5434.

Steponaviciute, M., Klimkevicius, V., & Makuska, R. (2020). Synthesis and stability against oxidation of random brush copolymers carrying PEO side chains and catechol moieties. *Materials Today Communications*, *25*, No. 101262.

Steponaviciute, M., Klimkevicius, V., & Makuska, R. (2021). Synthesis and properties of cationic gradient brush copolymers carrying PEO side chains and catechol moieties. *Macromolecular Chemistry and Physics*, *222*(4), No. 2000364.

Steponkiene, S., Dapkute, D., & Rotomskis, R. (2015). Accumulation and distribution of non-targeted and anti-CD44-conjugated quantum dots in distinct phenotypes of breast cancer. *Journal of Nanomedicine & Nanotechnology*, *06*(06), No. 1000341.

Sun, Y., Peng, J., Feng, W., & Li, F. (2013). Upconversion Nanophosphors $NaLuF_4$: Yb,Tm for lymphatic imaging in vivo by real-time upconversion luminescence imaging under ambient light and high-resolution X-ray CT. *Theranostics*, *3*(5), 346–353.

Sun, Y., Zhang, W., Wang, B., Xu, X., Chou, J., Shimoni, O., Ung, A. T., & Jin, D. (2018). A supramolecular self-assembly strategy for upconversion nanoparticle bioconjugation. *Chemical Communications*, *54*(31), 3851–3854.

Sung, H., Ferlay, J., Siegel, R. L., Laversanne, M., Soerjomataram, I., Jemal, A., & Bray, F. (2021). Global cancer statistics 2020: GLOBOCAN estimates of incidence and mortality worldwide for 36 cancers in 185 countries. *CA-A Cancer Journal for Clinicians*, *71*(3), 209–249.

Thiele, L., Diederichs, J. E., Reszka, R., Merkle, H. P., & Walter, E. (2003). Competitive adsorption of serum proteins at microparticles affects phagocytosis by dendritic cells. *Biomaterials*, *24*(8), 1409–1418.

Tian, J., Zeng, X., Xie, X., Han, S., Liew, O. W., Chen, Y. T., Wang, L., & Liu, X. (2015). Intracellular adenosine triphosphate deprivation through lanthanide-doped nanoparticles. *Journal of the American Chemical Society*, *137*(20), 6550–6558.

Tonigold, M., Simon, J., Estupiñán, D., Kokkinopoulou, M., Reinholz, J., Kintzel, U., Kaltbeitzel, A., Renz, P., Domogalla, M. P., Steinbrink, K., Lieberwirth, I., Crespy, D., Landfester, K., & Mailänder, V. (2018). Pre-adsorption of antibodies enables targeting of nanocarriers despite a biomolecular corona. *Nature Nanotechnology*, *13*(9), 862–869.

Toy, R., Peiris, P. M., Ghaghada, K. B., & Karathanasis, E. (2014). Shaping cancer nanomedicine: the effect of particle shape on the *in vivo* journey of nanoparticles. *Nanomedicine*, *9*(1), 121–134.

Voronovic, E., Skripka, A., Jarockyte, G., Ger, M., Kuciauskas, D., Kaupinis, A., Valius, M., Rotomskis, R., Vetrone, F., & Karabanovas, V. (2021). Uptake of Upconverting Nanoparticles by Breast Cancer Cells: Surface Coating versus the Protein Corona. *ACS Applied Materials and Interfaces*, *13*(33), 39076–39087.

Walczyk, D., Bombelli, F. B., Monopoli, M. P., Lynch, I., & Dawson, K. A. (2010). What the cell "sees" in bionanoscience. *Journal of the American Chemical Society*, *132*(16), 5761–5768.

Wang, C., He, M., Chen, B., & Hu, B. (2020). Study on cytotoxicity, cellular uptake and elimination of rare-earth-doped upconversion nanoparticles in human hepatocellular carcinoma cells. *Ecotoxicology and Environmental Safety*, *203*, 110951.

Wang, K., Zhang, Y., Wang, J., Yuan, A., Sun, M., Wu, J., & Hu, Y. (2016). Self-assembled IR780-loaded transferrin nanoparticles as an imaging, targeting and PDT/PTT agent for cancer therapy. *Scientific Reports* , *6*(1), 1–11.

Wang, M., Abbineni, G., Clevenger, A., Mao, C., & Xu, S. (2011). Upconversion nanoparticles: synthesis, surface modification and biological applications. *Nanomedicine: Nanotechnology, Biology and Medicine*, *7*(6), 710–729.

Wang, W., Gaus, K., Tilley, R. D., & Gooding, J. J. (2019). The impact of nanoparticle shape on cellular internalisation and transport: what do the different analysis methods tell us? *Materials Horizons*, *6*(8), 1538–1547.

Wang, X., Yakovliev, A., Ohulchanskyy, T. Y., Wu, L., Zeng, S., Han, X., Qu, J., & Chen, G. (2018). Efficient erbium-sensitized core/shell nanocrystals for short wave infrared bioimaging. *Advanced Optical Materials*, *6*(20), No. 1800690.

Wei, Y., Liu, Y., He, Y., & Wang, Y. (2021). Mitochondria and lysosome-targetable fluorescent probes for hydrogen peroxide. *Journal of Materials Chemistry B*, *9*(4), 908–920.

Wilhelm, S., Kaiser, M., Würth, C., Heiland, J., Carrillo-Carrion, C., Muhr, V., Wolfbeis, O. S., Parak, W. J., Resch-Genger, U., & Hirsch, T. (2015). Water dispersible upconverting nanoparticles: Effects of surface modification on their luminescence and colloidal stability. *Nanoscale*, *7*(4), 1403–1410.

Wilhelm, S., Tavares, A. J., Dai, Q., Ohta, S., Audet, J., Dvorak, H. F., & Chan, W. C. W. (2016). Analysis of nanoparticle delivery to tumours. *Nature Reviews Materials*, *1*(5), 1–12.

Wolfram, J., Yang, Y., Shen, J., Moten, A., Chen, C., Shen, H., Ferrari, M., & Zhao, Y. (2014). The nano-plasma interface: Implications of the protein corona. *Colloids and Surfaces B: Biointerfaces*, *124*, 17–24.

Wu, S., Han, G., Milliron, D. J., Aloni, S., Altoe, V., Talapin, D. V., Cohen, B. E., & Schuck, P. J. (2009). Non-blinking and photostable upconverted luminescence from single lanthanide-doped nanocrystals. *Proceedings of the National Academy of Sciences*, *106*(27), 10917–10921.

Wu, W., Pu, Y., & Shi, J. (2022). Nanomedicine-enabled chemotherapy-based synergetic cancer treatments. *Journal of Nanobiotechnology*, *20*(1), No. 4.

Wysokińska, E., Cichos, J., Kowalczyk, A., Karbowiak, M., Strzadała, L., Bednarkiewicz, A., & Kałas, W. (2019). Toxicity mechanism of low doses of $NaGdF_4$:Yb^{3+}, Er^{3+} upconverting nanoparticles in activated macrophage cell lines. *Biomolecules*, *9*(1), No. 14.

Wysokińska, E., Cichos, J., Zioło, E., Bednarkiewicz, A., Strzadała, L., Karbowiak, M., Hreniak, D., & Kałas, W. (2016). Cytotoxic interactions of bare and coated $NaGdF_4$:Yb^{3+}:Er^{3+} nanoparticles with macrophage and fibroblast cells. *Toxicology in Vitro* , *32*, 16–25.

Xue, X., Huang, Y., Bo, R., Jia, B., Wu, H., Yuan, Y., Wang, Z., Ma, Z., Jing, D., Xu, X., Yu, W., Lin, T. yin, & Li, Y. (2018). Trojan Horse nanotheranostics with dual transformability and multifunctionality for highly effective cancer treatment. *Nature Communications*, *9*, No. 3653.

Yamazaki, Y., Zhao, N., Caulfield, T. R., Liu, C. C., & Bu, G. (2019). Apolipoprotein E and Alzheimer disease: pathobiology and targeting strategies. *Nature Reviews Neurology*, *15*(9), 501–518.

Yan, Y., Gause, K. T., Kamphuis, M. M. J., Ang, C., Brien-simpson, N. M. O., Lenzo, J. C., Reynolds, E. C., Nice, E. C., & Caruso, F. (2013). Differential Roles of the Protein Corona in the Cellular Uptake of Nanoporous Polymer Particles by Monocyte and and Macrophage Cell Lines. *ACS Nano*, *12*, 10960–10970.

Yang, Z., Wang, X., Liang, G., Yang, A., & Li, J. (2022). Photocontrolled chondrogenic differentiation and long-term tracking of mesenchymal stem cells in vivo by upconversion nanoparticles. *Journal of Materials Chemistry B*, *10*(4), 518–536.

Yao, J., Huang, C., Liu, C., & Yang, M. (2020). Upconversion luminescence nanomaterials: A versatile platform for imaging, sensing, and therapy. *Talanta*, *208*, No. 120157.

Zhang, W., Meckes, B., & Mirkin, C. A. (2019). Spherical nucleic acids with tailored and active protein coronae. *ACS Central Science*, *5*(12), 1983–1990.

Zhang, Z., Rahmat, J. N., Mahendran, R., Zhang, Y., Zhang, Z., Rahmat, J. N., Zhang, Y., & Mahendran, R. (2020). Controllable assembly of upconversion nanoparticles enhanced tumor cell penetration and killing efficiency. *Advanced Science*, *7*(24), No. 2001831.

Zheng, J., Wu, Y., Xing, D., & Zhang, T. (2020). Synchronous detection of glutathione/hydrogen peroxide for monitoring redox status *in vivo* with a ratiometric upconverting nanoprobe. *Nano Research*, *12*(4), 19.

Zheng, K., Loh, K. Y., Wang, Y., Chen, Q., Fan, J., Jung, T., Nam, S. H., Suh, Y. D., & Liu, X. (2019). Recent advances in upconversion nanocrystals: Expanding the kaleidoscopic toolbox for emerging applications. *Nano Today*, *29*, No. 100797.

Zhou, B., Shi, B., Jin, D., & Liu, X. (2015). Controlling upconversion nanocrystals for emerging applications. *Nature Nanotechnology*, *10*(11), 924–936.

Zhou, L., Wang, R., Yao, C., Li, X., Wang, C., Zhang, X., Xu, C., Zeng, A., Zhao, D., & Zhang, F. (2015). Single-band upconversion nanoprobes for multiplexed simultaneous in situ molecular mapping of cancer biomarkers. *Nature Communications* , *6*(1), 1–12.

Zhou, Y., & Dai, Z. (2018). New strategies in the design of nanomedicines to oppose uptake by the mononuclear phagocyte system and enhance cancer therapeutic efficacy. *Chemistry-An Asian Journal*, *13*(22), 3333–3340.

Ziegler, Y. S., Moresco, J. J., Tu, P. G., Yates, J. R., & Nardulli, A. M. (2014). Plasma membrane proteomics of human breast cancer cell lines identifies potential targets for breast cancer diagnosis and treatment. *PLoS ONE*, *9*(7), No. e102341.

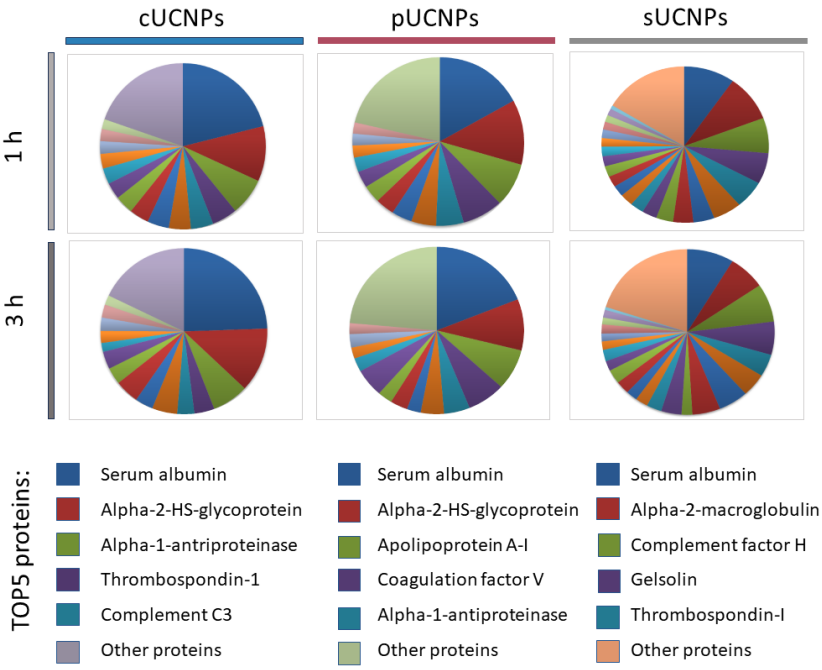

Figure S1. *The proportions of the most abundant proteins in the protein corona (PC) of cUCNPs and pUCNPs were analyzed after 1 or 3 hours of incubation in DMEM with FBS. The highlighted titles in the graph represent the relative abundance of the most abundant proteins on the surface of cUCNPs and pUCNPs compared to each other.*

ACKNOWLEDGEMENT

Life is interesting in that it seems like only four years are given for a Ph.D. studies, but how much can be experienced and learned in it. During these four years of my Ph.D., I became a lecturer, experienced the Covid lockdown, got married, wrote and published my first book, volunteered, overcame my fear of swimming and learned to swim, and traveled to 15 countries and... wrote my dissertation. As much as I have read other people's dissertations, I have seen that no one ever thanks themselves. So, first of all, selfishly (and maybe for the first time in history?), I would like to thank myself for daring to accept the challenge of a doctoral student and to try the path of a Ph.D. student.

Of course, I would not have written and completed this work without my best guide ever, supervisor Prof. Habil. Dr. Ričardas Rotomskis. Thank You for the opportunity to practice, work and travel on the path of a Ph.D student. Sometimes it seemed that I came with silly questions, but I always got the right answers in the professor's office. I would also like to thank the consultant Dr. Vitalijus Karabanovas, who performed no less work than the supervisor, and one could say equal. He provided extremely valuable suggestions and recommendations, and always answered all my questions. I would also like to thank the entire team of the Biomedical Physics Laboratory for the warm climate and the opportunity to be myself, because I felt like at home all these years at work.

And indeed, four years have passed so quickly that it's hard to even realize that I am here on the end of the road with a finally written dissertation. A dissertation would not be possible if it were not for a scientific publication. For them, I would like to thank all the co-authors of the publications, and especially Dr. Artiom Skripka - for many valuable comments, and much, much, much help in writing the first article in my life. Dr. Vaidas Klimkevičius, for equally valuable comments and extremely professional cooperation.

I would also like to thank my family. Since I am only child, I will not thank my brothers and sisters, but I would especially like to thank my mother and father for encouraging me to take up this difficult work and always supporting me on this difficult path. I would also like to say a big thank You to my beloved husband Aurelijus for supporting me all this way and believing in me. Also to my life's BFF Živilė, who accompanied me towards the finish of my dissertation and supported me with her presence and smile.

How is a dissertation without the honorable Reviewers. When You read these lines, I would like to say a big thank You for agreeing to be them, for

daring to accept the challenge and for taking Your precious time to appreciate this work.

And finally, I would like to thank the Committee / Defense Panel that will be with me during the defense of this thesis. And to everyone else whom I have met along the way of my life and had the opportunity to gain support, experience and knowledge. Thank You very very much!

LIST OF PUBLICATIONS

This thesis is based on the following papers that are included in Web of Science platform:

1) E. Voronovic, A. Skripka, G. Jarockyte, M. Ger, D. Kuciauskas, A. Kaupinis, M. Valius, R. Rotomskis, F. Vetrone, V. Karabanovas. Uptake of Upconverting Nanoparticles by Breast Cancer Cells: Surface Coating versus the Protein Corona. *ACS Applied Materials and Interfaces,* 13 (33): 39076-39087 (2021). DOI: 10.1021/acsami.1c10618

2) V. Klimkevicius, E. Voronovic, G. Jarockyte, A. Skripka, F. Vetrone, R. Rotomskis, A. Katelnikovas, V. Karabanovas. Polymer brush coated upconverting nanoparticles with improved colloidal stability and cellular labeling. *Journal of Material Chemistry B,* 10 (4), 625-636 (2022). DOI: 10.1039/D1TB01644J

RESEARCH RESULTS COMMUNICATION AT CONFERENCES

Oral presentations on dissertation topic:

Voronovič, E. Nanoparticles‘ surface impact on their accumulation in cancer cells. NanoBSR symposium. June 14-17th, 2022, Tällberg, Sweden.

Voronovic, E., Steponkiene, S., Jarockyte, G., Dapkute, D., Karabanovas, V., Rotomskis, R. The Accumulation of Upconverting Nanoparticles in Different Subtypes of Breast Cancer Cells. 8th International Conference on Nanomedicine, Drug Delivery, and Tissue Engineering (NDDTE 2023). March 23-25th, 2023, Lisbon, Portugal.

Poster presentations on dissertation topic:

Godlevskaja, K., **Voronovič, E.,** Jarockytė, G., Skripka, A., Vetrone, F., Karabanovas, V., Rotomskis, R. Žmogaus kraujo plazmos įtaka aukštynkeitėms nanodalelėms: koloidinio stabilumo ir biosuderinamumo tyrimas in vitro. 43-oji Lietuvos nacionalinė fizikos konferencija (LNFK-43). 2019 m. spalio 3-5 d. Kaunas, Lietuva. Tezių knyga 124 p.

Voronovič, E., Skripka, A., Jarockytė, G., Ger, M., Kučiauskas, D., Kaupinis, A., Valius, M., Vetrone, F., Rotomkis, R., Karabanovas, V. Baltymų vainiko įtaka apkonvertuojančių nanodalelių kaupimuis ląstelėse.

44-oji Lietuvos nacionalinė fizikos konferencija (LNFK-44). 2021 m. spalio 6-8 d. Vilnius, Lietuva. Abstract book page 126.

Voronovic, E., Skripka, A., Jarockyte, G., Ger, M., Kaupinis, A., Dalius Kuciauskas, D., Valius, M., Vetrone, F., Rotomskis, R., Karabanovas, V. Every particle with a crown: protein corona guided accumulation of upconverting nanoparticles in cancer cells. Spectral shaping for biomedical and energy applications 2022 (SHIFT-2022). Tenerife, Spain. Abstract Book page 156.

Poster presentations are indirectly related to the topic of the dissertation:

Kazlauskė, E., Steponkienė, S., Karabanovas, V., Rotomskis, R. Kvantinio taško ir fotosensibilizatoriaus-chlorino e6 komplekso stabilumo tyrimai ląstelių auginimo terpėse. 45-oji Lietuvos nacionalinė fizikos konferencija, Vilnius, 2023 m. spalio 25-27 d.

Steponkiene, S., Dapkute, D., **Voronovic, E.**, Jarockyte, J., Daugelaite, A. M., Skripka, A., Karabanovas, V. Nanoparticle-loaded Mesenchymal Stem Cells for Tumor-tropic Delivery of Theranostic Agents. European Foundation for Clinical Nanomedicine (CLINAM), Basel, Switzerland, October 8-11, 2023.

Mlynska, A., Butkute, A., **Voronovic, E.**, Karabanovas, V., Steponkiene, S. Nanotechnologies for targeting the tumor microenvironment in the colorectal cancer. European Foundation for Clinical Nanomedicine (CLINAM), Basel, Switzerland, October 8-11, 2023.

Peciukaityte, E., **Voronovic, E.,** Butkute, A., Mlynska, A., Steponkiene, S., Karabanovas, V., Rotomskis, R. Accumulation of Quantum Dots and Chlorin e6 Complex in Distinct Phenotypes of Human Colon Cancer Cells. 3rd Baltic Biophysics Conference 2022 (BBC-2022). October 6-7 th, 2022. Vilnius, Lietuva. Tezių knyga 89 p.

OTHER PUBLICATIONS

Books:

Voronovič Evelina. Kaip sėkmingai parengti Biotechnologijos studijų krypties baigiamąjį darbą. Vilniaus Gedimino technikos universitetas, 2023. DOI: 10.20334/2023-014-S

Kazlauskė Evelina. Final Thesis Manual in The Field of Biotechnology. Vilniaus Gedimino technikos universitetas, 2024.
DOI: 10.20334/2024-005-S

CURRICULUM VITAE

Evelina Kazlauskė (formerly Evelina Voronovič)

Work & Education	
2021 - Present	**Lecturer** Department of Chemistry and Bioengineering Vilnius Gediminas Technical University Vilnius, Lithuania
2019 - Present	**Junior Research Fellow** Biomedical Physics Laboratory National Cancer Institute Vilnius, Lithuania
2019 - 2023	**Biophysics, PhD student** Vilnius University
2018 - 2021	**Assistant** Department of Chemistry and Bioengineering Vilnius Gediminas Technical University Vilnius, Lithuania
2017 - 2019	**Biophysicist** Biomedical Physics Laboratory, National Cancer Institute, Vilnius, Lithuania
2016 - 2018	**Nanobiotechnology, MSc** Vilnius Gediminas Technical University Vilnius, Lithuania
2012 - 2016	**Bioengineering, BSc** Vilnius Gediminas Technical University Vilnius, Lithuania
Internships	
February 16-18th, 2022	**SupBiotech**, Paris, France *Erasmus+ staff mobility*

September 16-18th, 2019	**Umeå University**, Umeå, Sweden *Erasmus+ staff mobility*
July - September 2017	**Leibniz Institute of Photonic Technology,** Jena, Germany Topic: Formation and Characterization of silicon nanostructures *Erasmus+ internship*
June - August 2015	**University of Applied Sciences Upper Austria**, Wels, Austria Topic: Algae cultivation *Erasmus+ internship*
June - September 2014	**Malmö University,** Faculty of Health and Society, Malmö, Sweden Topic: Synthesis and characterization of graphene-AgNPs composite *Erasmus+ internship*
Grants	
October 2023	Research Council of Lithuania **fund for study results** of 2023
February 2023	Research Council of Lithuania **fund for doctoral student trips** in the first half of 2023 (agreement no. S-DAK-23-2)
April 2022 – March 2025	Research Council of Lithuania grant on project: "**Mesenchymal stem cells as vehicles for targeted delivery of theranostic nanoparticles into aggressive type of cancer cells**" No. S-MIP-22-31 National Cancer Institute Vilnius, Lithuania
March – April 2015	Research Council of Lithuania grant on project: "**Influence of arginine on the solubility of recombinant protein biosynthesized by *E. coli in*****

	vivo Vilnius Gediminas Technical University Vilnius, Lithuania
Certificate	
January 2021	**Certificate** obtained at Laboratory Animals Science course, allowing to independently plan and conduct experiments involving experimental animals in compliance with Directive 2010/63/EU of the European Parliament and the Council.
Awards	
Spring semester, 2023	VU Life Sciences Center **one-time targeted scholarship** for ongoing scientific activities
Autumn semester, 2022	VU Life Sciences Center **one-time targeted scholarship** for ongoing scientific activities
Spring semester, 2021	VU Life Sciences Center **named scholarship** for active scientific activity
February, 2020	Award for the best teacher in the Department of Chemistry and Bioengineering, Vilnius Gediminas Technical University
April, 2019	Award for the best teacher in the Department of Chemistry and Bioengineering, Vilnius Gediminas Technical University
July, 2019	**1st place, Gold Poster Award** *Investigation of Protein Corona Formed on Upconverting Nanoparticles* 5th Internation Conference "Current Trends in Cancer Theranostics" Trakai, Lithuania
October, 2018	**2nd place, the Best Poster Award** *Upconverting Nanoparticles' Colloidal Stability and Impact of their Surface Modification on the Cellular Accumulation* 4th-5th Baltic Biophysics Conference Kaunas, Lithuania

June, 2017	**2nd place, Silver Poster Award** *Upconverting Nanoparticles Covered with Different Coatings: Optical Properties, Stability and Accumulation in Cancer Cells* 3rd International Conference "Current Trends in Cancer Theranostics" Pakruojis, Lithuania
March, 2017	**1st place, The Best Oral Presentation on Interdisciplinary Research** *Toxicity and Accumulation of Upconverting Nanoparticles in Cancer Cells* 60th International Conference of Physics and Natural Sciences "Open Readings 2017" Vilnius, Lithuania
June, 2016	Laureate of the project **"VGTU graduates: 100 perspectives 2016"** Vilnius, Lithuania
Membership, coordination	
April, 2023	Moderator of the student conference „Naujoji mokslininkų karta" organised by Research Council of Lithuania
2022	Organizing committee member of 3rd Baltic Biophysics Conference held in Vilnius, Lithuania
2020 and 2021	Coordinator of the best master thesis competition (organised by Lithuanian Society of Young Researchers and Ministry of Foreign Affairs of The Republic of Lithuania)
2020-2021	Member of the council of Lithuanian Society of Young Researchers
2020 - present	Member of Lithuanian Society of Young Researchers

Vilniaus universiteto leidykla
Saulėtekio al. 9, III rūmai, LT-10222 Vilnius
El. p. info@leidykla.vu.lt, www.leidykla.vu.lt
bookshop.vu.lt, journals.vu.lt
Tiražas 15 egz.